SELF-SIMILAR EVOLUTION OF ULTRAFAST PULSES IN SOLID-STATE LASER RESONATORS

A Dissertation

Presented to the Faculty of the Graduate School

of Cornell University

in Partial Fulfillment of the Requirements for the Degree of

Doctor of Philosophy

by

Victor G. Bucklew

August 2014

SELF-SIMILAR EVOLUTION OF ULTRAFAST PULSES IN SOLID-STATE LASER RESONATORS

Victor G. Bucklew, Ph.D.

Cornell University 2014

This work formulates, theorizes, and presents a novel method of modelocking ultrafast sources with short gain media. By appropriately balancing the complex interplay of elements within the laser cavity, a passive self-similar pulse solution can be obtained which can support one to two orders of magnitude more energy than other pulse evolutions in an analogous system before encountering wave-breaking. A purely analytical model which describes this pulse evolution is presented, and the results are shown to match simulation and explain the connection between this evolution in the solid state, and the analogue evolution in fiber laser systems. Several methods for realizing this pulse evolution experimentally are detailed and shown to be feasible through numerical simulation. Additionally, theoretical and numerical work is presented which describe a self similar evolution in passive fiber with increasing nonlinearity. Lastly, numerical experiments are presented which detail the feasibility of a nonlinear-dispersive self similar evolution in a fiber laser.

BIOGRAPHICAL SKETCH

Victor G. Bucklew was born and raised in Madison, Wisconsin where he completed his B.S. in Physics in 2008 from the University of Wisconsin-Madison. While completing his studies he spent time working on LIDAR related research topics and cultivated a fascination with optics and the propagation of light. This interest led him to pursue his graduate studies in Electrical Engineering with an emphasis on lasers at Cornell University where he earned a M.S. in Electrical Engineering in 2012.

This document is dedicated to Cary Hunkel and James Bucklew, two of the best parents in the world.

ACKNOWLEDGEMENTS

The author would like to thank his advisor Professor Clifford Pollock for granting him the academic freedom to pursue specific research interests, while at the same time providing a wise, grounding, and practical guiding hand. The author is also extremely grateful for the academic support and kindness which Professor Frank Wise and Professor Michal Lipson offered during his time at Cornell. The author would like to thank Meghnaa Tallapragada for her ardent love of beluga whales. Your love of these creatures continues to inspire me. The author would also like to acknowledge his former lab mates and friends Bryan Hicks and Bryant Wysocki for their support and friendship. The author is indebted to William Renninger and would like to thank him for providing help and encouragement throughout the duration of his program. The author would also like to thank Logan Wright, Erin Lamb, Yuxing Tang, and other members of the Wise research group for stimulating and fruitful conversations. He would also like to thank Crash, Kurt Bunnelle, Felice Klein, and Elizabeth McClean for their friendship and encouragement.

TABLE OF CONTENTS

LIST OF TABLES

LIST OF FIGURES

CHAPTER 1

INTRODUCTION

1.1 Applications of High Energy Ultrafast Pulses

High energy femtosecond pulses are vital tools for many basic research, industrial, and medical applications. Recent progress in biomedical imaging, which has extended two photon microscopy techniques to higher orders, has been able to precisely and non-invasively image sub-cortical structures within mice specimen [21], and offers promise of extending the technology to humans. This technology is largely determined by the ultrafast laser sources driving the imaging processes [50]. The development of femtosecond laser sources has provided important advances for the field of ophthalmology by enabling high precision femtosecond ocular surgeries for correcting vision and for removing cataracts [43, 26, 34]. Femtosecond micro-machining is also becoming increasingly more popular in industrial procedures requiring precise, efficient sources. For many applications, microJoules of pulse energy is necessary. In micro-machining, when a high energy picosecond pulse is absorbed by a material, heat diffusion quickly spreads the absorbed energy of the pulse on the temporal order of the exciting pulse. This creates both an inefficiency in the machining process, as well as uncertainty in machining precision, as energy is no longer confined within the mode area of the pulse. By employing high energy femtosecond pulses, the efficiency and precision of the system can be greatly enhanced, by cutting on a time scale shorter than thermal diffusion. A recent demonstration applying femtosecond micro machining techniques to patterning fuel injectors in vehicles has proven to be more efficient, as well as better for gas mileage.

Another interesting application of high energy femtosecond pulses is with high harmonic generation. In this process, a high energy mid-IR femtosecond pulse train is used as a driving field to ionize an electron from its atom, and then accelerate it. When the electron recombines with the atom, it emits radiation coherent with the exciting field, generating a portion of usable energy at X-ray and UV wavelengths [19, 16, 13].

The demonstration of the above technologies have largely hinged on corresponding breakthroughs in ultrafast laser science. The main thrusts of ultrafast laser physics seem to follow three similar trends: to increase pulse energy, to reduce pulse duration, and to make systems more compact, stable, and easily implementable. Important demonstrations within each of these thrusts have historically been a result of researchers turning their attention back to the underlying physics of nonlinear pulse formation and propagation. This work is oriented in much the same way, and is centered around understanding how different nonlinear pulse evolutions can help address these three thrusts.

1.2 Ultrafast Pulse Formation and Propagation in Laser Cavities

The formation and propagation of an ultrafast laser pulse within a resonator is a complicated affair. The process critically depends on the complex interplay between the wealth of linear and nonlinear phenomena within the cavity. Not only does the collective influence of the individual effects of gain, spectral filtering from the gain medium, group velocity dispersion (GVD) and higher order dispersion, self phase modulation (SPM), saturable absorption, and linear loss

need to be accounted for to accurately model such a system, but a spatially dependent accounting of all of these effects must also be considered. Furthermore, the periodic boundary conditions required for laser stability in the steady state, imposes the further restriction that the dissipative affects, which include both linear and nonlinear phenomena, must balance each other each round trip, as well as the conservative affects, which also include the influence of nonlinear and linear affects.

In one sense this seems like an overwhelming affair. However, in another sense, the number of different linear and nonlinear phenomena which a pulse encounters within an ultrafast resonator, provides a playground of sorts for understanding nonlinear pulse evolutions. Additionally, the complexity of the system provides the necessary degrees of freedom and flexibility for scientists to develop and meet the diverse requirements of pulses required by various research and industrial applications.

The nonlinear Schrodinger equation (NLSE) provides a useful starting point for understanding pulse propagation. The NLSE models how the amplitude of the temporal envelope of an ultrafast pulse, A(z,t), will respond to the conservative effects of self phase modulation and group velocity dispersion as the pulse propagates a distance z through a transparent dielectric medium. The NLSE can be written as

$$\frac{\partial A(z,t)}{\partial z} = \left[i\gamma(z)|A(z,t)|^2 - \frac{i}{2}\beta(z)\frac{\partial^2}{\partial t^2} \right] A(z,t). \tag{1.1}$$

Here, $\gamma(z)$ represents the self phase modulation parameter and is given by $\frac{2k_0 n_2}{\pi w(z)^2}$ where k_0 is the spatial frequency about line center, n_2 is the nonlinear index

of refraction, and $w(z)$ is the spot size of the laser pulse as a function of position z. $\beta(z)$ is the group velocity dispersion parameter and is defined by, $\frac{\partial^2 k(\omega)}{\partial \omega^2}$, where k is the frequency dependent spatial frequency and the partial derivative is with respect to frequency ω.

Eq (1.1) tells us that as a pulse propagates through a dielectric media, its envelope will change as a result of the phase accrued from group velocity dispersion and self phase modulation. An interesting example when this is not the case is with soliton pulse propagation [17]. In certain circumstances, when the pulse energy and peak power of A(z,t) is carefully chosen, the phases from GVD and SPM can cancel and compensate each other at each position within the dielectric medium except for a constant phase shift, which results in a pulse envelope which remains constant as it propagates.

In order to model pulse propagation within a laser resonator, dissipative affects must also be included in the equation. Adding the affects of saturable frequency dependent gain, loss, and saturable absorption to Eq (1.1), the change in the envelope of the ultrafast pulse is expressed as,

$$\frac{\partial A(z,t)}{\partial z} = \left[\frac{g_0(z)/2}{1 + \frac{E_p}{E_{sat}}} (1 + \frac{1}{\omega_c^2} \frac{\partial^2}{\partial t^2}) - \frac{i}{2} \beta(z) \frac{\partial^2}{\partial t^2} + i\gamma(z)|A(z,t)|^2 - Q_{ideal}(|A(z,t)|^2) - l(z) \right] A(z,t). \tag{1.2}$$

Here, g_0 denotes the unsaturated gain coefficient and E_p is the intra-cavity pulse energy. The saturation energy of the gain medium is expressed as E_{sat}. ω_c is the frequency furthest from line center ω_0 which still provides gain to the resonator and accounts for the frequency dependent nature of laser emission. As already discussed, $\beta(z)$ and $\gamma(z)$ represent the group velocity dispersion and

self phase modulation, respectively. $Q_{ideal}(|A(t)|^2) = \frac{q_0}{1+|A(t)|^2/P_{sat}}$ represents the saturable absorber (SA) profile, where q_0 is related to the modulation depth of the absorber and P_{sat} is the saturation power of the absorber.

Although the choice to not include higher order dispersion and nonlinearity within Eq (1.2) is somewhat arbitrary, under most conditions, when the pulse width is greater than approximately 30 fs and the net group velocity dispersion is not zero, the effects of higher order dispersion and nonlinearity are negligible. Eq (1.2) provides an analytical model which will be referenced throughout the rest of this work for understanding pulse propagation and formation in a variety of different lasers and environments.

1.3 Limitations to Generating High Energy Pulses

Now that an understanding of the importance of generating high energy pulses has been established, along with a discussion of the basic analytical building blocks of ultrafast pulse propagation, a discussion of the limitations of ultrafast pulse propagation is made. Attempts to directly scale the energy of ultrafast pulses within laser resonators have all been confronted with the issue of optical wave breaking. Much like a large water wave approaching a beach shore, an optical wave of high intensity also breaks upon itself. The amount of energy which can be accreted under such a pulse before it breaks depends on the evolution of the pulse; Different pulse evolutions, or solutions to Eq (1.2), distribute and tolerate the nonlinear phase shifts from SPM differently.

A useful metric for quantifying the amount of nonlinear phase which different pulse evolutions can handle before wave breaking is the B-integral where

$B = \int_{z=0}^{L} k_0 n_2 I(z) dz$, which is simply the accumulated nonlinear phase which an ultrafast pulse accrues during propagation of a length L of a dielectric medium with nonlinear index n_2. The maximum value of nonlinear phase which a pulse can handle before breaking upon itself, and thus the maximum intensity which a specific nonlinear evolution can be scaled to, can be expressed by the B-integral. Assuming that the pulse is spatially and temporally collimated, this upper limit to the B-integral for a specific evolution can be written as, as $\phi_{nl} = k_0 n_2 I_{peak} L$, which is oftentimes referred to as the critical nonlinear phase. I_{peak} is the peak intensity of the ultrafast pulse.

Attempts to scale the energy of ultrafast pulses have looked to either direct or indirect scaling methods. Indirect scaling refers to externally amplifying a low or moderate energy pulse formed within a laser resonator to obtain higher energies than the pulse evolution within the resonator would normally allow. Such methods have been very successful, and pulses amplified within these systems may be scaled to almost arbitrary energy levels. However, the cost of indirect energy scaling is that the overall system also scales in bulkiness, cost, and complexity, which oftentimes makes such systems impractical for certain commercial applications. Furthermore, the noise within such systems is greater than the noise within a system with feedback (such as a laser) so oftentimes, the output pulses obtained from indirect scaling methods are unsuited for applications requiring quiet sources. The intrinsic potential inherent to a certain class of laser, is oftentimes also compromised with external amplification. For example, fiber lasers, by virtue of the versatility and flexibility of fiber, can be made very compact, portable, and resilient. External amplifiers composed of additional pump sources and bulk optics take away this very natural advantage. Externally amplifying ultrafast solid state laser systems, which oftentimes possess

very large gain bandwidths and large emission cross sections, are not making full utility of the properties of the gain medium if the pulse evolution within the resonator cannot not take full advantage of these properties before encountering wave breaking. The same logical conclusion can be applied to semiconductor laser systems which can naturally be made efficient, high power, and compact.

The second method of energy scaling, referred to as direct energy scaling, concentrates on how to scale the pulse energy directly inside a laser resonator. As just discussed, methods of increasing pulse energy without adding bulky, expensive optics outside of the cavity is attractive from the point of view of commercial application as well as from the viewpoint of extracting the natural benefits which each class of laser inherently possesses. However, such methods require turning attention back to the resonator where the pulse originally forms, requiring one to reexamine the physics of Eq (1.2) with the purpose of developing pulse evolutions which are capable of supporting higher energy pulses without wave breaking. This work reports on research efforts aimed towards formulating, extending, and understanding pulse evolutions which show promise of directly generating high energy ultrafast pulses from resonators with short gain medium.

1.4 Historical Development of Ultrafast Pulse Evolutions in Lasers

Before proceeding to a discussion of the particular pulse evolution which the majority of this work addresses (the passive self similar pulse), a summary of the historical development of several key pulse evolutions will be made. The re-

lationship between pulse energy E and pulse width T is an important characteristic to be aware of for a given pulse evolution. Such a relationship, oftentimes called an energy area theorem, provides a quick analytic tool for understanding how different elements of the laser resonator expressed by Eq (1.2) affect the physical characteristics of an ultrafast pulse. Such relationships tell the designer how the laser pulse handles and distributes increases in energy, and as such, gives the designer a starting point for understanding how a certain evolution might handle optical wave breaking.

1.4.1 Soliton

As discussed in the first section, fundamental soliton pulses are formed by a balance between normal (anomalous) group velocity dispersion and a self focussing (de-focussing) nonlinearity. Here, the relationship between GVD and SPM for a soliton pulse has been derived and expressed as [17],

$$ET = 2\frac{|\beta|}{\gamma} \tag{1.3}$$

As can be seen, the area theorem predicts that as the energy of a soliton pulse increases, the pulse width necessarily will decrease for a fixed relationship between group velocity dispersion and self phase modulation. In any real laser cavity there are dissipative effects such as saturable absorption, gain, and loss, so a soliton explanation of pulse evolution (which only depends on only conservative effects) is not strictly true. However, 'soliton' solutions do essentially form in laser resonators where the effects of the dissipative processes on pulse formation are greatly overshadowed by the balancing of the phase terms

resulting from the conservative terms. Such a laser can generally tolerate only very small nonlinear phase shifts, generally much less than π ($\phi_{nl} << \pi$) before breaking [48].

1.4.2 Chirped Soliton

In 1991, Haus derived an average cavity solution to laser cavity which included dissipative effects and which provided insight into the influence of both the sign and magnitude of group velocity dispersion (GVD) in ultrafast pulse formation [18]. The chirped hyperbolic secant shaped solutions, formed with a frequency dependent gain and a completely unsaturated saturable absorber, described by a first order Taylor expansion of an ideal saturable absorber, are oftentimes called solitons due to similarities with the optical solitons of the nonlinear Schrodinger equation (NLSE). These solutions included the dissipative effects which the previously mentioned soliton laser did not account for. The energy area theorem of a chirped soliton evolution can be written as,

$$ET = \frac{3(\beta^2\omega^2 + 4)}{2\omega(2\gamma + \beta\alpha_1\omega_c)^2}(3\beta\gamma\omega_c - 6\alpha_1 \pm \sqrt{4(2\beta^2\omega_c^2 + 9)\alpha_1^2 - 4\beta\gamma\omega_c\alpha_1 + \gamma^2(9\beta^2\omega_c^2 + 32)}). \tag{1.4}$$

Here, α is the coefficient describing the strength of the first order Taylor expanded, unsaturated, saturable absorber. Again, we see that for a fixed relationship between resonator elements, that the pulse energy E and pulse width T maintain an inverse relationship. The chirped solitons described in this section are a specialized type of dissipative soliton, which is discussed below.

1.4.3 Dispersion Managed Soliton

Haus' theory demonstrated that the temporal width of a pulse subject to a self focussing (defocussing) nonlinearity could be minimized by choosing the net dispersion of the resonator to be both small and anomalous (normal). As laser gain media generally have normal dispersion about their center wavelengths and self focussing nonlinearities, the normal dispersion must be compensated by the addition of an element providing anomalous dispersion. The affect of a positionally dependent dispersion function on a pulse in the steady state is to induce a temporal dynamic, oftentimes described by the term 'breathing', into the temporal width of the pulse as it travels through a round trip in the resonator. As his original theory did not account for this, he derived an additional steady state solution of mode locking which described the phenomenon of pulse breathing [36]. These solutions, called dispersion managed solitons (DMS), have Gaussian shaped field amplitudes and are formed by gain filtering and completely unsaturated saturable absorbers. Besides allowing for short pulse temporal pulses, this evolution was also significant in that the breathing aspect of the solution provided an averaging effect for nonlinear phase accumulation. This means that if we had two equivalent resonators (besides the dispersion map), a DMS with minimum pulse duration the same as the constant pulse duration of a soliton laser, would have a smaller nonlinear phase accumulation than the equivalent soliton laser. Not surprisingly, DMS were able to tolerate higher values of ϕ_{NL} than their soliton counterparts before wave breaking (¡π) [48]. This is a clear example of how a different pulse evolution can often be used to push pulse energies to higher values before encountering optical wave breaking.

The energy area theorem of these pulses can be written as,

$$ET^3 = \sqrt{\pi}\sqrt{\frac{(1/\omega^2) + 4\beta^2}{\alpha_1^2 + \gamma^2}} \tag{1.5}$$

1.4.4 Dissipative Soliton

As the demand for simultaneously high energy and temporally short pulses grew, the ability of solitons and dispersion managed solitons to meet these needs were challenged, especially in fiber laser systems. The energy area theorems of both solutions showed that as the intra-cavity temporal width decreased, the pulse energy and peak power had to simultaneously increase. Consequently, because the chirp functions of both solutions were not purely linear, the phenomenon of wave-breaking ultimately became a limiting factor in energy scaling. Solutions aimed at navigating the problem of wave-breaking looked to both the sign and magnitude of the net cavity dispersion. With increasingly larger amounts of net normal dispersion, the pulse duration could be increased, allowing more energy to accrete under the pulse envelope before reaching critical peak powers. The resultant temporally broad pulses could, to a degree, be de-chirped outside of the resonator to achieve shorter temporal durations than otherwise possible with such energies in the dispersion managed or chirped soliton pulse regimes.

Lasers relying on increasing the net normal dispersion within a resonator to scale the energy of a pulse, of which a variety of numerical and analytical work has been conducted, are often grouped into two categories; chirped pulse oscillators (CPO) in the context of solid state lasers [30, 29, 31] (See full works of Kalashnikov) and all-normal dispersion (ANDi) lasers in the context of fiber

lasers [38, 12, 49]. Although the formulation of the master equation used to model the pulse evolution vary from work to work, both chirped pulse oscillators and ANDi lasers rely on the dissipative processes of spectral filtering and saturable absorption to stabilize the pulse evolution. As such, these pulses are often collectively labeled as dissipative solitons. There are several analytical descriptions of energy area theorems for dissipative solitons. Two insightful results were derived by Renninger et al in the context of fiber lasers [38] and Kalshnikov et al in the context of solid state lasers [32, 28]. These lasers can often tolerate nonlinear phase shifts ϕ_{NL} up to 10π [48].

1.4.5 Self Similar Pulse

So far, all of the theories which have been discussed describe pulse solutions which do not have purely linear chirp. Because the chirp function is not purely linear, the ability of chirped pulse lasers to efficiently de-chirp a high energy temporally broad pulse is met with varying limitation. Consequently, the original problem of energy scaling while maintaining ultrafast pulse widths, is not strictly resolved. A solution to this observation, first realized experimentally in 2004 by Ilday et al, came in the form of self similar pulse evolution [24]. Self similar optical pulses are spatially asymptotic parabolic solutions to the NLSE with gain and were first described analytically and numerically in the context of fiber amplifiers [14, 2].

Ilday et al. generalized the concept to a fiber laser resonator, experimentally demonstrating the design considerations which needed to be met in order to achieve a self consistent steady state self similar pulse within a laser resonator.

The pulse intensity of the solution was nearly parabolic and the chirp function nearly perfectly linear. Self similar evolution has so far provided the shortest pulse durations to date in fiber lasers [10], demonstrating the importance of the shape of the chirp function in ultrafast systems. Work aimed at providing analytical descriptions of amplifier self similar pulses, which are oftentimes called similaritons, has been attempted, but due to the dynamic positional nature of self similar pulses in the steady state, work has been so far been constrained to semi-analytical theory and numerical simulation [3, 25].

After the realization of self similar pulses in fiber lasers, numerical simulation further generalized the concept to solid state laser systems by Ilday et al in the case of active self similar pulses [22], and by the author in the case of passive self similar pulses [6]. Furthermore, the author demonstrated the first analytical treatment of a passive self similar pulse evolution [7], identifying the design considerations which must be met to generate high energy pulses of short temporal duration in lasers with short gain media, as well as deriving an energy area theorem which accounts for self similar energy scaling in both fiber and solid state laser systems. The expression of this theorem, which will be derived in detail later in the work, can be written as,

$$\frac{E}{T^3} = \frac{4(g - l - l_{ns})^2}{\beta\gamma} \tag{1.6}$$

where l_{ns} denotes the non-saturable loss coefficient of the saturable absorber, g represents the saturated gain coefficient, and l represents the loss coefficient of the resonator. Depending on the type of self similar pulse, and the class of laser it is propagating within, self similar pulses can have peak nonlinear phase shifts as small as a soliton, or as large as a DM soliton [7].

1.5 Connecting Pulse Evolutions in Fiber Lasers to Oscillators with short gain media

Now that an understanding of several key pulse evolutions has been established, we see that an understanding of the physical basis behind a pulse evolution is useful in addressing its potential for ultrafast direct energy scalability. As we saw in the previous chapter, developments in pulse evolutions often arose from researchers hitting a wall in energy scaling with an already understood evolution. However, solid state, semiconductor, and fiber lasers have all developed in slightly different directions. For example, the self similar evolution has only been realized in fiber laser systems. This fact is not surprising: Fiber lasers have extremely large round trip gain, and can tolerate very high levels of loss which makes construction comparatively easier. Compared to solid state and semiconductor class lasers, and optical parametric oscillators, fiber lasers also possess orders of magnitude higher nonlinearities for a given peak power, due to both mode confinement and length of dielectric media in the cavity with significant self focussing nonlinearity.

Historically, for a soliton pulse evolution, this meant that fiber lasers were much more limited in output energy than solid state systems, and therefore could not realistically compete. However, due almost entirely to the discovery and intelligent formulation of new pulse evolutions, which were capable of handling larger and larger nonlinear phase shifts, fiber lasers have surpassed solid state lasers in many key performance traits. Indeed, the motivation for generalizing the pulse evolutions which have reached a relative state of maturity in fiber laser systems to other classes of lasers in which the evolutions have

remained largely unexplored, is desirable.

Although the often order of magnitudes difference in group delay dispersion (GDD), nonlinear phase shifts, and steady state round trip gain, at first sight make it seem that such a generalization would be implausible, it is important to remember that the physical mechanisms behind pulse formation is the same in all classes of lasers and resonators. The difference lies only in the magnitudes of the elements which comprise the cavity. Thus, if one can understand the physical mechanisms or routes behind the formation of a certain type of pulse, one would expect that designing a laser cavity around it would not be unrealistic.

In Chapter 2, a conceptual description of how to generalize the passive self similar solution of fiber lasers to solid state lasers is presented. Numerical simulation is then presented which confirms that the concept is valid. In Chapter 3, a theoretical framework for understanding passive self similar evolution in both solid state and fiber laser systems is derived, and key results are confirmed through numerical simulation. Chapter 4 is focussed around how to experimentally realize the nonlinear pulse evolution presented in Chapters 2 and 3, and several practical experimental designs are presented and tested through numerical simulation. Chapter 5 includes a discussion of how the passive self similar pulse could also be realized in an optical parametric oscillator, and derives a basic theoretical model which supports this claim. The theoretical model is once again tested against numerical simulation and found to be valid. Chapter 6 is a response to Chapter 4 and the difficulty of experimentally realizing the conditions under which a passive self similar pulse may form in a solid state laser in a low energy limit. It derives a novel self similar pulse solution which offers

promise for helping to navigate these difficulties, and confirms the theoretical model through numerical simulation. Chapter 7 presents simulations which describe a new type of nonlinear pulse evolution in an ultrafast fiber laser. This evolution offers promise for producing high energy, strongly linearly chirped pulses with bandwidths larger than the gain medium of the laser.

CHAPTER 2

SELF SIMILARITY IN SOLID STATE LASER SYSTEMS

The understanding of amplifier self similar evolution has played an important role in the development of ultrafast fiber lasers. Self similar and dissipative soliton evolutions have consistently vied for the titles of shortest and most energetic pulse out of a fiber laser. Recognizing that these self similar pulses now compete with typical outputs from dispersion managed solid state lasers (which generally possess orders of magnitude smaller values of nonlinear phase shifts), tells us that if a self similar evolution could be realized in the solid state, important advances in directly energy scaling of solid state laser systems would be enabled. This chapter will explore the feasibility of such an endeavor. First, the chapter will review the development of self similar pulses in fiber amplifiers and lasers. Second, with the understanding gained from this review, the chapter will formulate a mechanism by which self similar pulses in short gain media laser systems can be achieved. Third, the chapter will test this theory against numerical simulation to verify the proposed method. Finally, through simulation, this work will identify the requirements on saturable absorption and output coupling which must be practically met in order to experimentally realize such a self similar pulse evolution.

2.0.1 Self Similar Pulses in Fiber Amplifiers

Self similarity is a principle which is encountered throughout the physical sciences and mathematics. Self similarity refers to the property of a system such that at least one divisible unit of the system possesses characteristics which are

also found within the system as a whole. Thus, it is called self similar. Many fractal sets are self similar under magnification. If you look at a specific region of a self similar fractal set under magnification, you see that the magnified image looks similar (if not identical) to the unmagnified image.

Self similar pulses within the field of ultrafast optics were first proposed and understood in the context of fiber amplifiers, and are oftentimes called amplifier similaritons. The amplifier similariton is a pulse with a parabolic temporal intensity profile which grow exponentially in both bandwidth and pulse width as it traverse regions of positive nonlinearity, normal GVD, and constant gain. Mathematically, this pulse is a spatially asymptotic solution to the Nonlinear Schrodinger Equation (NLSE) with gain. Eq (2.1) describes the environment within which the amplifier self similar pulse can form.

$$\frac{\partial A(t,z)}{\partial z} = [-\frac{j}{2}\beta\frac{\partial^2}{\partial t^2} + j\gamma|A(t,z)|^2 + \frac{g}{2}A(t,z)]A(t,z) \tag{2.1}$$

In Eq 2.1, g is the saturated, frequency *independent* gain. Fermann, et al, [14, 2] show through symmetry reduction techniques, that in the absence of bandwidth limitations in the gain medium and for $\gamma\beta > 0$, Eq (2.1) possesses a spatially asymptotic temporally parabolic solution in the limit $z \to \infty$ of the form,

$$A(t,z) = A_0(z)[1 - [\frac{t}{t_p(z)}]^2]^{1/2} exp[j\phi(t,z)] \tag{2.2}$$

for $|t| < t_p(z)$ and A(t,z)=0 elsewhere [14]. $t_p(z)$ is the pulse width at location z in the gain medium.

The amplitude $A_0(z)$ and pulse width $t_p(z)$ grow exponentially according to the following,

$$A_0(z) = \frac{1}{2}(gE_{in})^{1/3}(\gamma_0\beta/2)^{-1/6}\exp(gz/3) \tag{2.3}$$

$$t_p(z) = 3(g)^{-2/3}(\gamma_0\beta/2)^{1/3}E_{in}^{1/3}\exp(gz/3) \tag{2.4}$$

$$\phi(z,t) = \phi_0 + \frac{3\gamma_0}{2g}A_0^2(z) - \frac{g}{6\beta}t^2 \tag{2.5}$$

The phase profile $\phi(t,z)$ of the asymptotic nonlinear attracting solution is quadratic and the resultant chirp $-\frac{\partial\phi(t,z)}{\partial t}$ is purely linear. The pulse amplitude is scaled, and its pulse width and bandwidth increase, but it remains parabolic and hence linearly chirped. This is an essential observation. The collective influence of gain, GVD, and self phase modulation (SPM) act to broaden both spectral and temporal widths, while maintaing an overall linear chirp. Since the pulse is temporally broad, the peak power of a self similar pulse remains low, allowing tremendous amounts of optical energy to accrete under the pulse waveform before reaching critical peak powers. The linearity of the chirp and the large spectral bandwidth allow the pulse to undergo large nonlinear phase shifts before encountering wave breaking and also allow the pulse to be compressed to its transform limit outside of the gain medium, allowing for directly generable high energy and ultrafast pulses.

Another key insight from self similar fiber amplifiers comes in the recognition that the asymptotic solution given in Eqs (2.3-2.5) is a nonlinearly attracting solution. That is, the injection of an arbitrary seed pulse (in shape, energy, temporal width, etc) would eventually result in that seed pulse attracting towards the parabolic solution detailed in Eq (2.1). Of course, this is only true provided that the gain could remain constant for a long enough distance, that the bandwidth did not encounter any restrictions, and that the pulse en route to the self similar solution did not encounter wave breaking. However, practically

speaking, there are seed pulses which do attract near to the asymptotic solution quicker than others.

In Ref [14], numerical examples which show the relationship between the initial pulse width and energy, and the length of fiber needed to reach the asymptotic solution, are shown. In general, the shorter the initial pulse width, the larger the initial intensity is, and the larger the overall nonlinearity. Under normal conditions, pulses with higher nonlinearity generate bandwidth more quickly than pulses with lower nonlinearity, and can more quickly 'breathe 'into the desired solution, which requires temporally and spectrally reshaping of the pulse. Of course, if the nonlinearity is too large, the pulse cannot near close enough to the asymptotic solution, before it generates so much bandwidth and nonlinear phase that it breaks apart. So two things are required for an efficient attraction. First, the pulse needs an environment which allows it to easily grow in bandwidth and temporal width. Two, this breathing environment must not push the pulse so quickly that it cannot fall into and stabilize itself within the nonlinear attraction region.

2.0.2 Self Similar Pulses in Fiber Lasers

A self similar pulse evolution in a laser would be extremely useful for direct energy scaling. Many of the issues relating to optical wave breaking could be avoided if the temporal shape of the pulse is parabolic. With such a pulse solution, nonlinear phase is generated by SPM with a linear chirp, and then spread linearly by GVD. This means that for a perfectly parabolic pulse, in a system without spectral filtering, pulse frequencies could never overtake each other,

and the pulse could never break. Furthermore, even a pulse which is not perfectly parabolic but which still displays some of the properties of the self similar evolution, there are clear advantages. Because the amplifier self similar pulse broadens temporally as it evolves, the peak power grows at a slower rate than it would with pulses formed under different nonlinear environments with the same energy. This is a boon for direct energy scaling, as much more energy can be accreted under a quasi - self similar before reaching critical peak powers than a pulse propagating with a different evolution. Additionally, the temporally broad self similar pulse has a linear temporal chirp, meaning that it can be easily and compactly de-chirped to its time bandwidth product outside of the laser resonator.

Since the first experimental demonstrations of self similar fiber lasers [23] research efforts have confirmed that the pulse evolution is indeed useful in direct energy scaling and concluded that there are two types of self similar evolutions which can take place within a laser resonator; active and passive. The active, or 'amplifier similariton', forms as a result of the local nonlinear attraction felt within the gain medium, much like a self similar pulse propagating within an optical amplifier. The other elements within the cavity are important in creating a self consistent steady state round trip solution where the pulse width, bandwidth, pulse shape, and energy are reproducible after each round trip but, the elements are not directly responsible for the formation of the self similar pulse. This means that the attraction to the self similar pulse is the spatially asymptotic nonlinear attracting solution of the NLSE with gain, and thus occurs only within the gain medium. The other elements in the cavity just serve to reverse the changes undergone by the pulse within the gain medium, so that on the next round trip the same self similar evolution, categorized in part by a monotonic

increase in temporal and spectral width, can take place in the gain fiber.

The second type of evolution, called the 'passive similariton', is the result of a nonlinear attraction formed by the collective influence of all of the elements within the resonator. The order in which these elements occur in the resonator does not matter as the nonlinear attractor results from an average effect of all of the cavity elements and not just a local attraction isolated within a specific spatial location in the resonator.

The long gain media in fiber lasers create an environment where a circulating pulse experiences a large potential or capacity to breathe as it propagates. This potential is largely due to the magnitudes of gain, SPM, and GDD, which accompany the long length gain medium. This is not surprising when we consider that SPM generally generates additional frequency components and that normal GDD generally, depending on the chirp of the pulse, spreads these frequency components temporally. The effect of such a large breathing capacity is that the pulse has the potential to dramatically change its evolution (shape, spectral width, temporal width) during one round trip in the steady state. This means that in the steady state, the self similar pulse in fiber has the opportunity to evolve from a pulse which is far from a self similar pulse into a pulse which displays the desired traits of self similarity. Indeed, fiber lasers are capable of supporting two completely different independent pulse evolutions in different parts of the resonator [37]. Such a demonstration would not be possible except for clever cavity design and the intrinsic capacity to breathe which pulses propagating through long length nonlinear media possess.

As already mentioned, the large capacity for pulses in fiber lasers to breathe was used to design self similar fiber lasers. Spectral filters, dispersive delay

lines, and large modulation depth saturable absorbers, have all been used to prepare a pulse for a self similar evolution within the gain medium, or within a passive segment of nonlinear fiber. As will be discussed next, the capacity to breathe is generally much less in lasers with short gain media so the approach required to generate and sustain self similar pulses in the steady state will be different.

2.1 Proposed Concept for Generalizing Result to Solid State Lasers

If one were to apply to the solid state the methods and cavity designs necessary for generating self similar pulses in fiber, the designer would require strong breathing, and the ability to tolerate large loss. For solid state laser systems, group delay dispersion is generally around a hundred times smaller than in fiber systems meaning that the bandwidth of the self similar pulse would need to be many times larger in the solid state system in order to achieve a similar breathing ratio. This means that the solid state pulse would require bandwidths which would only be supported by a few gain media, making the approach limited in its application. Furthermore, amplifier similariton evolution is impeded by the presence of spectral filtering within the gain medium. This means that a pulse with a large spectral bandwidth, which would be required for large breathing in the solid state, would at some point encounter a deflection away from the self similar solution, negating the potential benefits such an evolution offers.

This section emphasizes previous work by the author in Ref [6]. This section

theorizes that an alternate route to self similar evolution, which bypasses the necessity of strong breathing, lies in the assumption that the self similar solution in the solid state can be approached over many round trips (instead of a significant attraction to the solution in one round trip). Such a solution would encounter small round trip breathing ratios and would evolve into a self similar solution slowly over many thousands of cavity round trips. Once in the steady state, the solution would remain parabolic throughout a full round trip, and would be supported in that state by cavity design which would prevent further changes. In order to better understand this evolution, and how cavity elements affect it, the terms 'attraction' and 'deflection' will be employed. Consistent with previous usage by Renninger et al. in [40], the M parameter is introduced to quantify the concept of attraction and pulse shape. The M parameter, given by Eq (2.6), is a figure of merit for how close the pulse profile is to a parabola. The field amplitude $A(t)$ of the pulse is compared to $P(t)$, the normalized field amplitude of a parabola with the same peak power and energy as $A(t)$. If $A(t)$ is a perfect parabola, the M parameter is zero. As a reference, a Gaussian pulse has $M = 0.14$, and a Sech^2 pulse has $M = 0.19$. This paper will arbitrarily consider $M < 0.04$ parabolic as pulses in this range very closely replicate an exactly parabolic temporal shape and as such share the useful phase and chirp characteristics of pulses with $M = 0$. Attraction refers to a cavity element reshaping the temporal profile of a pulse so that it is closer to a parabola. While this normally occurs in the gain medium, other cavity elements may attract the pulse as well. Deflection refers to a cavity element reshaping the temporal profile of a pulse so that the pulse is less parabolic after passage through the element. An attractive element results in a positive ΔM, given by $\frac{M_i - M_f}{M_i} \times 100$, while a deflective element results in a negative ΔM, where M_i and M_f represent the temporal

shapes of the pulse before and after the cavity element, respectively.

$$M^2 = \frac{\int [|A(t)|^2 - |P(t)|^2]^2 dt}{\int [|A(t)|^4] dt} \tag{2.6}$$

For a non-parabolic pulse (M larger than 0.04) to evolve close to a self similar solution (M less than 0.04) over many cavity round trips, the elements within the cavity responsible for pulse shaping must initially produce a net attraction towards the self similar solution. To reach a steady state solution, one or more of these cavity elements must change their attractive or deflective tendencies as M decreases so that in one round trip the pulse shape remains invariant. In the steady state, the net affect of the cavity elements must balance either other so that $\sum_k \Delta M_k = 0$ where the sum is taken over the k cavity elements present in the laser resonator.

The attraction created by the combined affect of gain, SPM, and GVD within the gain medium generally decreases as the pulse becomes more parabolic. Intuitively, this makes sense. A pulse that has already converged to the exact analytical solution put forth by Fermann et al in [14] will not see any further attraction. A fundamental limit to the pulse formation arises from the finite gain bandwidth which always causes a deflection by limiting bandwidth growth. The deflection increases as the spectral bandwidth increases which happens as the pulse becomes more parabolic. Thus, as a pulse becomes more and more parabolic, the gain medium reacts with a decreasing attraction until the attraction from gain, SPM, and GVD is slightly overshadowed by the deflection from spectral filtering. The net affect of the entire gain medium for parabolic M values is a small deflection. At this point, other elements within the cavity must offer an attraction towards a parabolic solution so that a round trip, steady state

solution is reached.

In lieu of this point, the manner in which these other elements, namely the saturable absorber and output coupler, influence the pulse in the evolution and steady state phases of the pulse must now be considered. Beginning with the saturable absorber, it is well known that in order to stabilize a pulse from background continuous wave (CW) amplitude noise, a saturable absorber is required. The saturable absorber serves to stabilize the chirped steady state pulse by reversing small increases to its temporal and spectral profiles, and by suppressing the buildup of a CW emission. The power response profile of a saturable absorber can distort the temporal shape of a pulse and therefore must be closely examined. The term 'power response profile' refers to the manner in which the saturable absorber imposes loss on different instantaneous power segments of a pulse and is a crucial concept. A metric α, defined as $\frac{P_{sat}}{P_{peak}} \times 100$ is introduced to describe the temporal shaping characteristics of a saturable absorber. P_{sat} represents the saturation power of the saturable absorber term in Eq (1.2) and P_{peak} represents the peak power of the pulse being evaluated. As the magnitude of α decreases, the response profile of the saturable absorber becomes more rectangular, where the majority of the instantaneous power segments of the pulse see small saturated loss and the only significant pulse shaping occurs in the low intensity wings of the pulse. As previously discussed, for nearly parabolic M values, the net effect of a bandwidth limited gain medium is a slight deflection. Thus, in order to reach a steady state with M values close to zero, the saturable absorber must provide a net attraction. This requirement is supported when we consider that as M decreases, the center of the pulse continues to become more and more parabolic while the low intensity wings take on super-Gaussian temporal profiles [25]. For α values of a few percent, the sat-

urable absorber only induces loss on the low intensity super-Gaussian wings of the pulse resulting in a more parabolic pulse after passage through the element. In this way, the saturable absorber can act as an attractor and a self consistent solution can be reached.

Thus, the proposed solution would be that of an amplifier similariton in its evolution stage, because the evolution is determined by a local nonlinear attraction within the gain medium, and the saturable absorber for low intensity light, is predominantly to act as a deflector. In the steady state however, the pulse evolution would more closely reflect a passive similariton. This is because the gain medium would be providing a net deflection. The deflection resulting from the spectral filtering overshadowing the combined attraction from gain, SPM, and GVD. Furthermore, the saturable absorber is providing an attraction in the steady state. Thus, the proposed solution in the steady state would be a result of the collective influence of all of the cavity elements and not just a result of a local attractor, as is the case as it is evolving to towards the steady state.

Although the role of the saturable absorber and gain medium have now been discussed in the context of the proposed resonator, a subtle point remains which also must be considered. The remaining cavity element not accounted for, the output coupler, also plays a role in the proposed scheme. This is because the pulse evolution to a self similar solution now occurs over many round trips instead over a single round trip in the steady state. Because the asymptotic solution is approached over many cavity round trips, and because the evolution is inextricably linked together in the spectral, temporal, and amplitude domains, the growth of all three (spectral, temporal, amplitude) must occur proportionally. Because the round trip temporal and spectral breathing ratios of the evolv-

ing pulse are purposefully made small in order to allow self similar evolution to occur in lasers with short gain media, the round trip amplitude growth must also be kept low. The primary way to control the steady state saturated gain of the resonator, is to control the output coupling. For lasing to occur, the integrated gain of the resonator must match the integrated loss of the resonator. Thus, keeping the output coupling low means that the amplitude growth of the pulse is also low, which coincides with the desired small temporal and spectral breathing ratios of the pulse.

2.2 Validation of Concept through Numerical Simulation

Now that an outline for what self similar pulse propagation might practically look like in solid state and other relatively short length gain media, it is important that the concepts are rigorously tested and explored through numerical simulation. Following a similar approach as detailed by the author in Ref [6], Eq (1.2) is solved numerically with a standard split step Fourier algorithm. The simulation is seeded with an independent identically-distributed Gaussian noise sequence in the temporal domain and passed through an infinite impulse response (IIR) filter to smooth out sub-femtosecond temporal fluctuations resulting from the temporal step size of the simulation. The IIR filter was designed to allow the seed radiation to be more representative of real cavity noise (i.e. noise fluctuations on the picosecond time scale). A(z,t) denotes the electric field envelope. $g_0(z)$ is the unsaturated gain, a piecewise constant function with value zero outside the gain medium. We have not yet considered the affects of gain noise in our model but do not anticipate significantly different pulse evolutions with gain noise present. $q_0(z)$ is the saturable loss of the saturable absorber

within the domain of the saturable absorber and zero outside the absorber. P_{sat} is the saturation power of the absorber. E_p is the intra-cavity pulse energy, which is updated after every round trip to account for gain saturation. The output coupling in solid state resonators is generally low so that in the steady state the gain does not change significantly within one round trip. ω_c is the FWHM bandwidth of the gain medium. E_{sat} is the saturation energy, normalized to the cavity round trip time. $\beta(z)$ represents the group velocity dispersion parameter and is a piecewise constant function whose value is dependent on the medium the pulse is traveling within. $\gamma(z)$, given by $\frac{2k_0 n_2}{\pi\omega_0^2}$, is also a piecewise constant function which accounts for the accumulation of nonlinear phase. Nonlinear phase accumulation outside the gain medium is assumed negligible. ω_0 is the beam waist spot size of the laser mode within the gain medium and k_0 is the spatial frequency at line center. $l(z)$ is the linear loss and is only nonzero at the output coupler.

2.2.1 Evolving to the Steady State

To numerically examine the pulse evolution, Eq (1.2) is applied to the material and lasing properties of a Cr:ZnSe ring resonator, shown in Fig. 2.1. Cr:ZnSe is a solid state mid-infrared laser with large gain and nonlinearity, making it an ideal candidate on which to test this concept. The SPM coefficient γ within the 4 mm gain medium is .000442 $\frac{1}{m.W}$ and zero elsewhere. As mentioned in Chapter 1, γ is defined by $\gamma = \frac{k_0 n_2}{A_{eff}}$. The spot size inside the gain medium is 58 μm. n_2 is 3.0×10^{-18} $\frac{m^2}{W}$ and the wavelength λ_0 at line center is 2.4 μm. The GVD of the ZnSe host medium at line center is 230 $\frac{fs^2}{mm}$. The unsaturated gain g_0 is 250 $\frac{1}{m}$, an experimentally achievable value when considering both pump power and the limits

of crystal doping densities for Cr:ZnSe systems. E_{sat}, normalized to the 150 MHz cavity repetition rate, is 8.4 nJ. The pulse dynamics explored here are applicable to many solid state lasers with microsecond upper state lifetimes (i.e. Cr:YAG, Ti:Sapph, and Cr:ZnSe). Future work exploring parabolic pulse dynamics in solid state gain media with millisecond upper state lifetimes is underway. The saturable absorber modulation depth, represented by the magnitude of q_0, is varied between 2-7% in the simulations. Here, the modulation depth refers to the modulation percentage of the electric field amplitude of the pulse, not the modulation in the power. The saturation power, P_{sat}, is varied between 2-100% of the pulse peak power. The output coupling is varied between 2-14% and in this case also represents the output coupling percentage of the electric field amplitude. Both the output coupling and modulation depth are defined this way in this chapter and the next (relative to the electric field and not power) due to a nonstandard definition which the plots in this chapter reflect. However, this is simply a matter of semantics; the results remain exactly the same regardless of the definition used to account for linear and nonlinear loss. Thus, to convert the OC percentage given here to power OC percentage, simply square the value presented here. For example, if the output coupling is labelled as 3%, to transform this to a power output coupling, we would choose a 9% output coupler.

Fig. 2.2 depicts the FWHM temporal and spectral widths of the simulated pulse as it evolves to the steady state. The FWHM temporal and spectral widths initially increase monotonically, consistent with the notion that the pulse evolves to a self similar solution over many cavity round trips. After several thousand round trips the pulse reaches equilibrium. Fig. 2.3, depicts the RMS temporal and spectral widths of the steady state pulse as it makes one round trip in the cavity. The RMS values were used in the steady state to more pre-

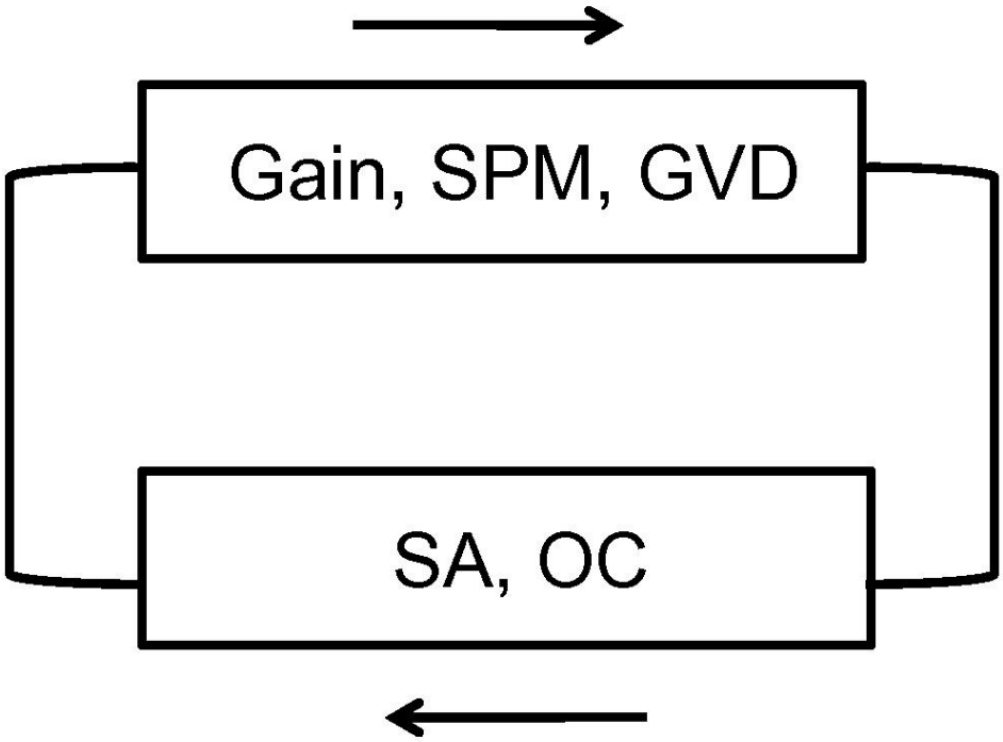

Figure 2.1: Cartoon schematic of the laser. *Gain*: gain medium with finite bandwidth; SPM: self phase modulation; GVD: normal group velocity dispersion; SA: saturable absorber; OC: output coupler

cisely gain information about pulse characteristics (The simulation bandwidth and temporal steps make it difficult to accurately analyze the steady state with FWHM values). In the steady state the pulse barely breathes and is shown to be a self consistent solution which satisfies temporal and spectral boundary conditions. To put the magnitude of the breathing ratios into perspective, self similar fiber lasers often exhibit temporal and spectral breathing ratios of 2-10 in the steady state [37, 40, 41, 24]. Our simulation exhibits a temporal breathing ratio of 1.00088 and a spectral breathing ratio of 1.00080. These ratios, which are very close to unity, support the concept that if the pulse is allowed to evolve to a self similar solution over many cavity round trips, the steady state breathing

ratios will be nearly one, which is ideal for pulses propagating through short gain medium lasers.

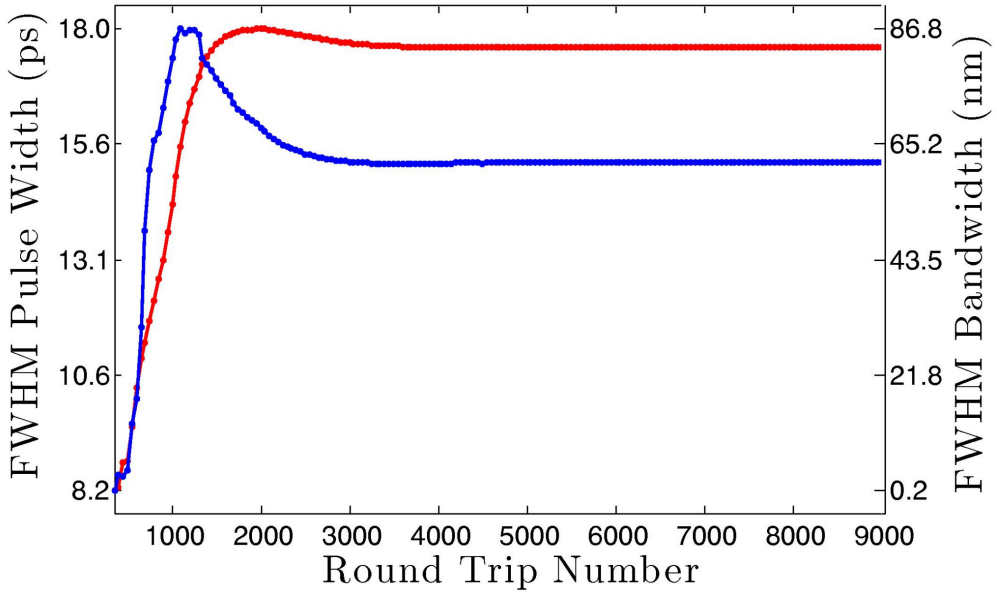

Figure 2.2: The FWHM temporal ***red*** and spectral ***blue*** widths are shown as the pulse evolves to the steady state over many cavity round trips.

From simulation data, we calculate the M parameter of a pulse during its evolution and steady state phases. The M parameter, as previously discussed, is a figure of merit for how close the pulse profile is to a parabola, and sheds light on the path which a pulse takes when evolving towards a steady state solution.

2.2.2 Steady State Pulse Characteristics

As is apparent from Fig. 2.4, the pulse shape is defined by random noise fluctuations for the first 500 round trips as it is stabilized from small CW amplitude fluctuations. In the next 4500 round trips the pulse finds itself in the evolution stage where it is gradually pulled towards the parabolic attractor. Fig. 2.5 de-

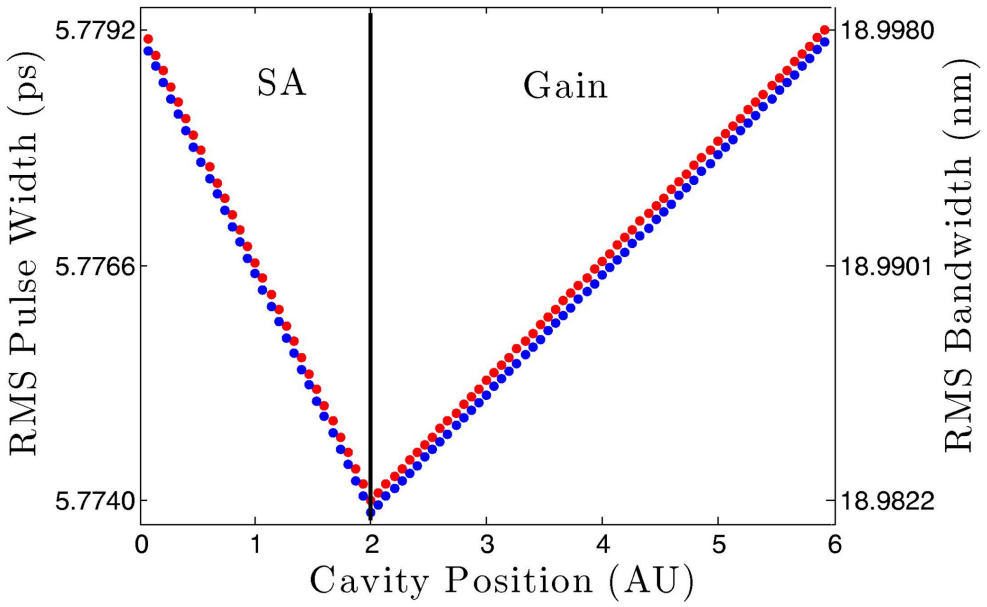

Figure 2.3: The steady state RMS temporal ***red*** and spectral ***blue*** widths of the self similar pulse are shown during one cavity round trip where the pulse passes through both the saturable absorber and gain medium. *SA*: Saturable absorber; *gain*: Gain medium

picts the steady state M parameter as the pulse makes one round trip in the cavity. The steady state, taken at round trip number 9000 of Fig. 2.4, shows that the simulated pulse remains parabolic for the full round trip, confirming that it is neither being strongly attracted nor deflected from the parabolic solution. The fact that the pulse remains parabolic for an entire round trip is contrasted to self similar fiber lasers where the pulse often oscillates between a parabola and a Gaussian [40] or Sech^2 [37] temporal profile in the steady state. The steady state M parameter converges at a value of 0.027. That the pulse never approaches a M parameter value of 0 is due in part to the pulse propagating within a finite gain medium with gain dispersion. Fig. 2.6 depicts the temporal and spectral shape of the simulated pulse, showing that the pulse is in fact temporally parabolic.

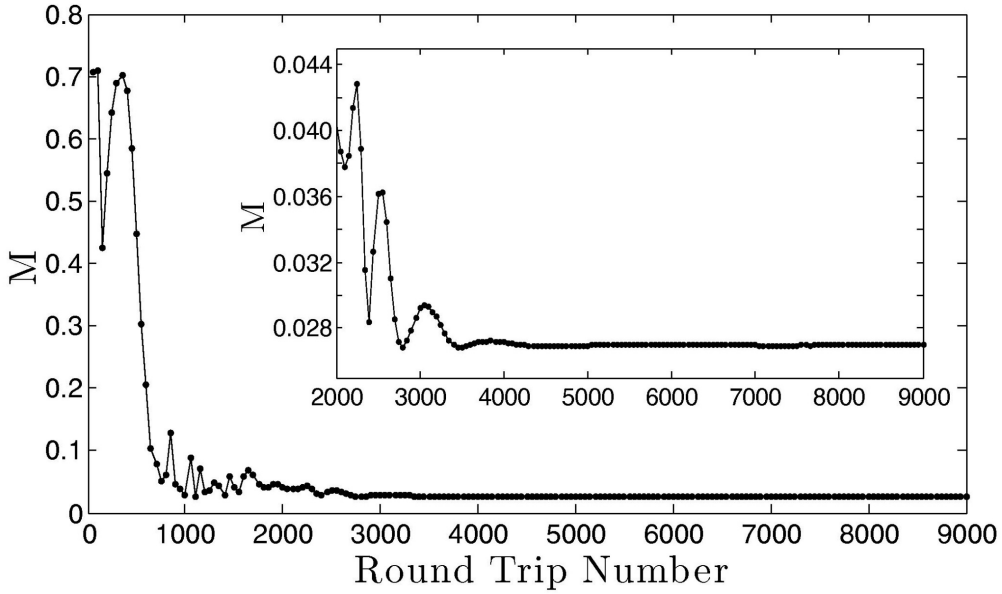

Figure 2.4: The M parameter of a self similar pulse as it evolves to the steady state from noise (main figure) and a snapshot of its evolution as it reaches a steady state pulse shape (inset figure).

2.2.3 Range and Constraints on Self Similar Solution

As seen, the proposed concept for self similar evolution matches quite well with numerical simulation. In order to better map the range of values which the saturable absorber and output coupler must fall within to support such an evolution, as well as to confirm whether the converged pulse is indeed a passive similariton, further numerical experiments are necessary. First, considering whether the pulse is indeed a passive similariton in the steady state, we see that Fig. 2.5 shows that the pulse appears to be slightly deflected from the parabolic solution as it traverses a gain medium with a finite bandwidth. This observation is in agreement with the logic presented in the section explaining the conceptual framework of self similar evolution in the solid state.

Such an observation deserves more attention as it means that the simulated

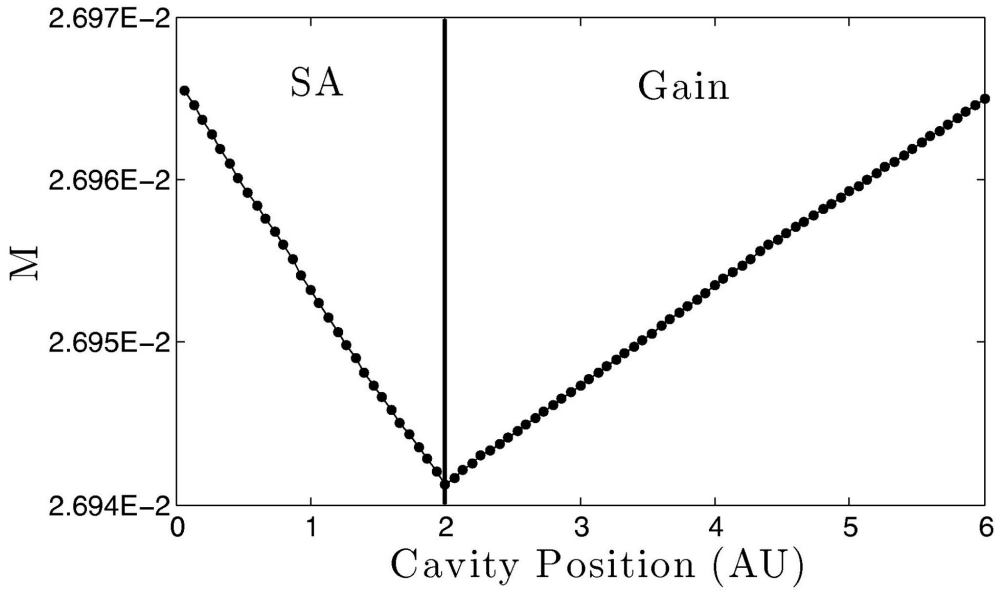

Figure 2.5: The M parameter of the converged self similar pulse during one cavity round trip as the pulse passes through the saturable absorber and gain medium. *SA*: Saturable absorber; *gain*: Gain medium.

solution would in fact be an average cavity, passive similariton, of which an analytical model could be developed around. The ability to generalize the results of these very specific simulations to all classes of lasers with a theoretical model would be very useful. Additionally, the confirmation that the evolution under question is passive self similar would mean that this is a brand new evolution in the solid state. The top graph of Fig 2.7 shows the magnitude and sign of ΔM which the saturable absorber and gain medium produce as the saturable absorber strength α is varied. The bottom graph of Fig 2.7 depicts the M parameter as α is varied. Indeed, as α decreases and the pulse becomes more and more parabolic, ΔM within the gain medium becomes negative and deflective, while ΔM within the saturable absorber becomes positive and attractive. Note that this trend is only observed for parabolic M values (with values below 0.04) formed with α of a couple percent. For the majority of pulse shapes, formed

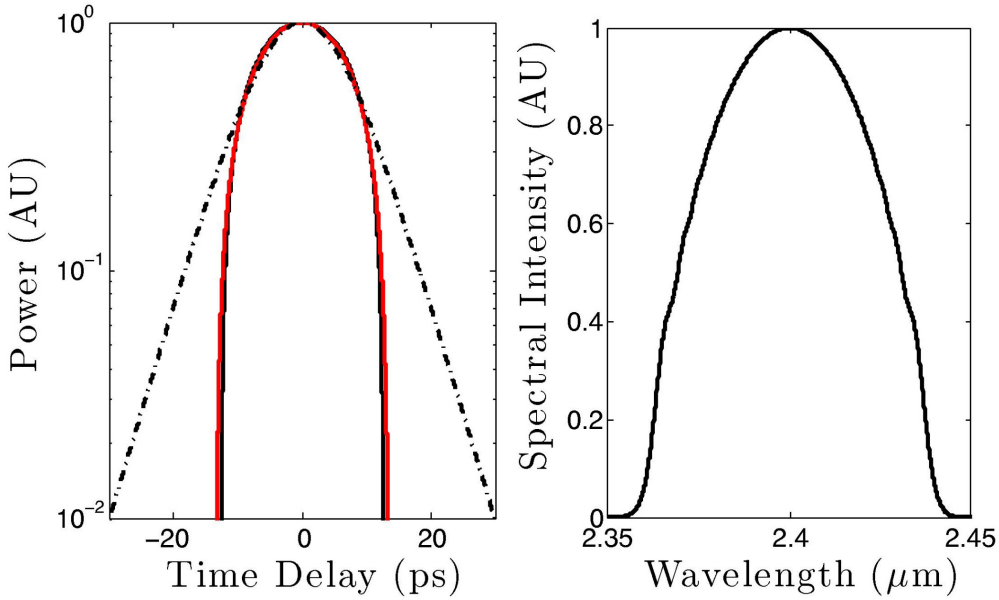

Figure 2.6: Left: Temporal profile of the simulated pulse. ***solid red***: simulated pulse; ***solid black***: parabolic pulse; ***dash dotted black***: sech^2 pulse. Right: Spectrum of the simulated pulse

with larger α values, the gain medium, as one would expect, acts as an attractor. The pulse dynamics in both regimes (parabolic and non parabolic) may be explained by the same concepts of attraction and deflection and the conclusions are consistent.

Now, as a final check, in order to verify that the converged solution has not just been trapped on an upwards bounce of an evolution to the nonlinearly attracting solution within the gain medium (and is thus not an amplifier similariton) [40], simulations were run with and without spectral filtering in the gain medium. Table 2.1 summarizes the results of the converged simulations. Simulation *A* was the control which simulations *B* and *C* were compared to and represents the cavity which has been discussed up until now (a cavity with a finite bandwidth gain medium). Simulation *B* is identical to the control *A* in every respect except that *B* does not include the spectral filtering term which

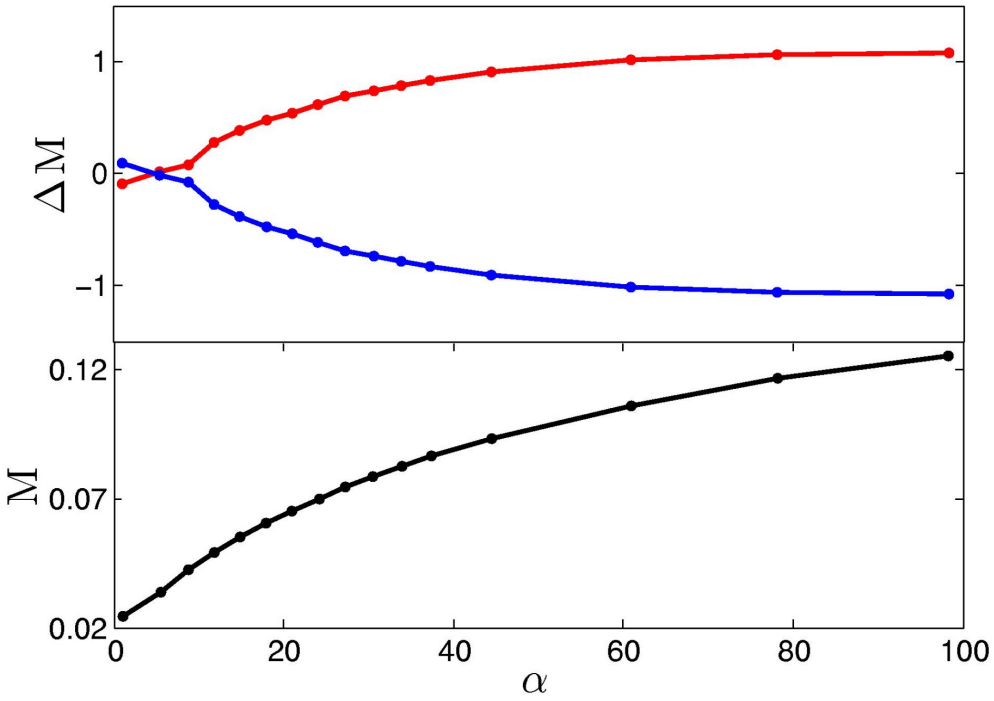

Figure 2.7: Top: ΔM is calculated as a function of the saturable absorber strength α. The ***solid red*** line represents ΔM within the gain medium while the ***solid blue*** line represents the ΔM within the saturable absorber. Bottom: The M parameter is calculated as a function of different α values. q_0 is 7% and the output coupling l is 2%

describes the finite gain bandwidth of the gain medium. Simulation *C* also does not include the spectral filtering term and the strength of the saturable absorber α was adjusted so that the pulse shape in *C* was similar to the pulse shape in the control simulation *A* with a finite bandwidth gain medium.

In *C*, the value of α was adjusted so that the *M* values in *A* and *C* were close to identical. As expected, without spectral filtering within the gain medium, ΔM_{gain} is positive and an attractor while in *A*, with gain filtering, the gain medium acts as a deflector. Because changing α could potentially result in a different evolution to the steady state, thus preventing a conclusion about attraction and deflection with equivalent *M* values, simulation *B* was run. Like

simulation C, simulation B was run without spectral filtering but equivalent to the control A in every other aspect. As Table 2.1 shows, the M parameter of C is much smaller than A. The much smaller M value shows that without gain filtering the pulse can evolve further to the parabolic solution than with gain filtering. This observation suggests that the addition of spectral filtering is causing a deflection of at least similar magnitude to the attraction felt by the gain, SPM, and GVD alone. Coupled with the results of C, we conclude that the affect of spectral filtering within the gain medium is large enough for parabolic M values to produce a net deflection within the gain medium.

B and C also help confirm the proposed pulse shaping dynamics of the saturable absorber. As ΔM_{gain} in B and C is positive, the saturable absorber must be providing a deflection from the parabolic solution to reach a self consistent steady state solution. For a perfectly parabolic pulse (M=0), any value α will result in a deflection. B supports this reasoning; it is almost perfectly parabolic. For a perfect parabola, the deflection will increase as α increases. However, as M increases but still remains parabolic, the absorber can cause either a deflection or attraction depending on the value of α. For M values like in A and C, the center of the pulse is parabolic while the wings are super-Gaussian in structure. An absorber with small α will cause a pulse with a small but nonzero value of M (simulation A) to become more parabolic. The absorber will induce a higher loss on the low intensity non-parabolic wings of the pulse while leaving the center of the pulse relatively unaffected and act as an attractor. As α is increased for equivalent small but still nonzero values of M (simulation C), the saturable absorber begins to induce a variable loss on the center parts of the pulse as well as the super-Gaussian wings and the absorber changes from an attractor into a deflector.

Table 2.1: Pulse Dynamics With and Without Gain Filtering

Simulation	A	B	C
Gain Filter	Yes	No	No
q_0	.07	.07	.07
α	1.12%	1.21%	5.79%
M	0.0245	0.0069	0.0239
ΔM_{gain}	-.096%	.131%	0.302%

To further distinguish this regime of mode locking from other normal dispersion pulse solutions, the self similar pulses in this chapter were compared with known analytical average cavity solutions to Eq (1.2) discussed in Chapter 1. Average cavity solutions, found for $\frac{dA(t,z)}{dz} = 0$, have been derived by assuming very weak to moderate saturation of the saturable absorber term in Eq (1.2). In the limit of very weak saturation, this assumption allows one to rewrite the saturable absorber term $\frac{q_0}{1+|A(t)|^2/P_{sat}}$ in Eq (1.2) as $q_0[1 - |A(t)|^2/P_{sat}]$. Average cavity solutions to this equation are temporally $Sech^2$ in profile (M=0.19) [18]. With the addition of a quintic saturable absorber term, analytical average cavity solutions have also been derived where the solution allows for a variety of different pulse shapes [39]. The M parameter of these pulse shapes range from 0.19 to 0.07 but do not approach the nearly zero M values seen in this chapter. This is not surprising as both the cubic and quintic saturable absorber terms do a poor job of modeling the degree of heavy saturation seen in this chapter (α must approach values of nearly 3000 for the assumption of weak saturation to accurately model Eq (1.2). The spectra of these pulses also do not qualitatively agree with the pulse spectrum in Fig. 3.3, further distinguishing this regime of mode locking from other known normal dispersion average average solutions.

Research which derives an analytical framework for understanding this novel pulse evolution is presented in the following chapter.

As discussed, the saturable absorber power response profile, quantified in part by α is crucial to realizing this new route to self similarity. To experimentally realize such a response profile, a saturable absorbing mirror with a low saturation power could be employed. For systems with a large nonlinear index, simulations suggest that with an appropriately chosen aperture radius, a reasonably small response profile α could also be achieved in the Hard Aperture Kerr Lens mode locking regime.

The saturable absorber must be able to temporally follow the leading and trailing low intensity wings of the pulse in order to effectively trim the temporal and spectral widths of the circulating pulse. Furthermore, the manner in which the saturable absorber trims the temporal and spectral width of the pulse is important. The saturable absorber must have a response time fast enough that it can be lossy for the low intensity wings, but transparent for the high intensity center of the pulse. As the chirped pulse is temporally broad (several ps), the response time of the SA does not need to be ultrafast to adequately stabilize pulses from CW amplitude emissions.

The effect of the output coupler on parabolic pulse formation is also numerically examined, and the results are depicted in Fig. 2.8. The reflectivity of the output coupler controls the magnitude of the steady state saturated gain. For small output coupling the pulse amplitude will not breathe significantly as it travels through the laser gain medium. As the proposed method relies on small steady state amplitude, spectral, and temporal breathing ratios, small output coupling should more readily support self similar formation than an output

coupler with a lower reflectivity. It is important to remember that the output coupling percentage we are talking about here is the amplitude output coupling and not the power output coupling. The two of course have a very simple mathematical relationship, but here we are referencing amplitude output coupling. Fig. 2.8 supports this reasoning showing that small output coupling results in pulses with smaller M parameter values. For each data point in Fig. 2.8 the unsaturated gain was adjusted so that the ratio $\frac{P_{sat}}{P_{peak}} \times 100$ remained constant. This helped decouple the affects of output coupling from the affects of the saturable absorber power response profile on parabolic pulse formation in the laser cavity.

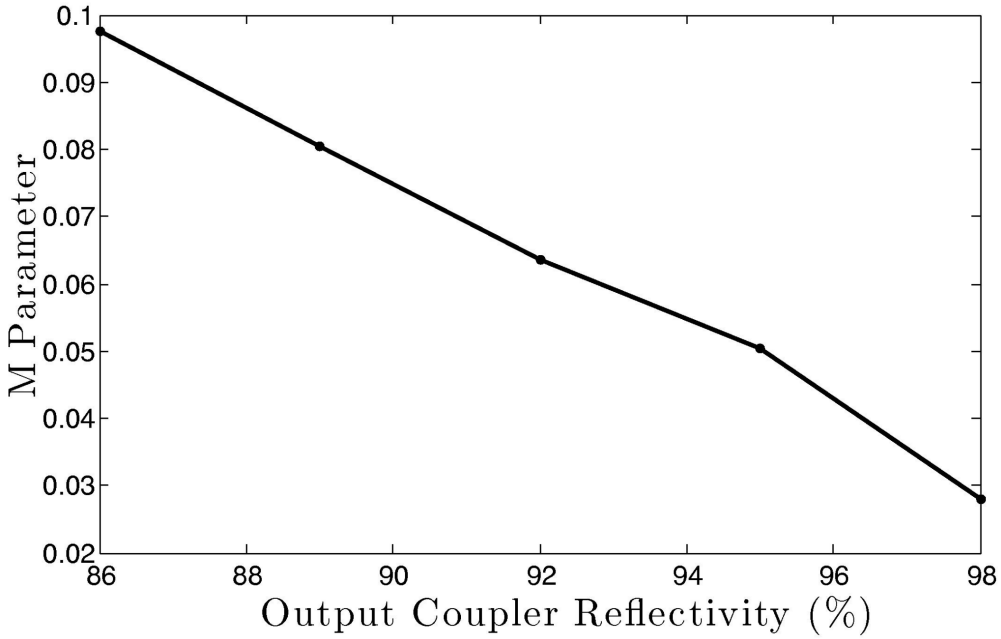

Figure 2.8: The M parameter is calculated as a function of the reflectivity of various output couplers. The power response profile, controlled in part by the magnitude of the value $\frac{P_{sat}}{P_{peak}} \times 100$, was fixed to a value of 1.75 +- 0.16 % for each data point by adjusting the unsaturated gain. q_0 was 5% and P_{sat} was .8kW.

In conclusion, a framework for understanding how a self similar pulse may form and be stabilized in a solid state resonator under practical conditions has

been developed. The conceptual framework has been tested against numerical simulation and found to match well. The mechanisms behind pulse formation, namely, that the self similar pulse evolves slowly to the amplifier similariton asymptotic solution to the NLSE with gain over many thousands of cavity round trips, and then, becomes stabilized in the steady state as a passive similariton has been extensively examined through numerical simulation. The range of values which the output coupler must take in order to sustain a self similar evolution has been identified as well as the range of values which the saturation power of the saturable absorber must take. The following chapter develops an analytical framework for explaining this novel pulse evolution.

CHAPTER 3

THEORETICAL MODEL OF SELF SIMILAR PULSE EVOLUTION

Now that the proposed concept has been tested extensively through numerical simulation, and the initial claim that the steady state pulse would be a passive similariton has been established, a derivation of a purely analytical model for understanding such an evolution can be attempted. This chapter will follow work published by the author in Ref [7] and will, whenever appropriate, expand on the work already conducted. As already discussed, the experimental realization of self-similar fiber lasers played a key role in the development of directly scalable high energy femtosecond sources [23].

Since the initial demonstration, a variety of numerical [6, 22, 23, 42] and semi-analytical approaches [25, 3] have been developed to help describe and optimize such systems. As seen in the previous chapter, numerical simulation can accurately describe positionally-dependent variations in the shape, energy, temporal width, and spectral width of a pulse, but numerical simulation does not readily enable pulse characterization over broad parameter spaces. Semi-analytical theories have been developed to provide insight into pulse formation characteristics but, like numerical simulation, they rely on significant computation time. In general, these approaches have considered pulse propagation in either solid state or fiber laser systems, but not both. Although such distinctions are completely reasonable when trying to understand a system with a method relying on numerical simulation, results obtained in this manner are not immediately applicable to systems other than the one which was simulated.

The underlying principles governing pulse evolution is the same for both solid state and fiber systems. The main difference between the two systems is

the length of the gain medium, and the corresponding orders of magnitude difference in the strength of group delay dispersion, gain, and self phase modulation seen within each class of laser. A purely analytical approach to self similar pulse evolution, analogous to the purely analytical approaches developed in the soliton [17, 52], dissipative soliton [18, 38, 29, 30, 28, 32, 27], and dispersion managed soliton [36] lasers is therefore desired, as these approaches provide an immediate framework for understanding pulse evolution across parameter spaces encompassing many classes of laser systems. The above works describing the variety of different theoretical models of pulse evolution differ from each other in either how an individual work formulates the equation governing mode locking, or in how the work solves the formulated equation.

This chapter reviews the first purely analytical treatment of an average cavity passive self-similar laser derived by the author using some simplifying assumptions. The theoretical solution maintains dependency on free parameters which means that although it is purely analytical, it cannot be labelled as being completely closed-form. The results of the analytical model provide a basis for understanding the mechanisms behind energy scalability in passive self similar lasers as well provide a connection between self similar evolution in fiber and solid state laser systems.

3.1 Average Cavity Analytical Self Similar Model

Analytical models generally reflect 'average' cavity descriptions of pulse evolution [18], of which the passive similariton is an example. An average cavity model is usually based upon the assumption that each element within the laser resonator acts on the pulse simultaneously during each round trip within the

resonator. Closed form analytical models generally reflect these average cavity descriptions of pulse evolution because they usually cannot simultaneously maintain closed form solutions and describe positionally-dependent variations in pulse parameters, as would be required to describe pulse evolution resulting from a local nonlinear attraction. There are average cavity positionally-dependent solutions to laser resonators but these solutions are usually accessible only through numerical simulation [1]. One desirable outcome of an analytical average cavity model is that because pulse propagation does not depend on position within the cavity, an immediate basis for understanding how the system will respond to changes in values of the elements within the resonator is obtained. Insight into energy scalability and other relevant pulse characteristics is immediately achievable. This work constructs such an average cavity description of self-similar pulse formation, from which a purely analytical evaluation of the 'passive', self-similar laser can be made.

3.1.1 Formulating the Master Equation

In order derive an average cavity self similar solution, a master equation describing the key elements responsible for the pulse evolution must be formulated. Ideally, a completely closed form solution to Eq (1.2) could be derived but in practice this is unrealistic. Solutions to nonlinear partial differential equations are notoriously difficult to find. Thus, in order to identify the key cavity elements responsible for describing a passive self similar pulse, the evolution was numerically simulated in a Ti:Sapphire laser using Eq (1.2). There are many fiber and solid state laser systems which could have been chosen for the simulation. However, the choice of a solid state system was made after noting that

generally each element (e.g. GVD, SPM, gain, OC, SA) within one round trip of a solid state resonator causes smaller changes to the complex field amplitude of the circulating pulse than each element within a fiber laser (simply due to the magnitude of each element). For this reason, a solid state system more closely resembles an 'average' cavity analytical model, where all the elements within the resonator act on the pulse simultaneously. The specific choice of a Ti:Sapphire oscillator was made because these lasers have been studied extensively and possess physical properties (e.g. gain bandwidth, upper state lifetime) conducive to ultrafast pulse formation.

The following parameters were chosen for the simulation: The small signal gain ($g_0(z) = 70m^{-1}$) is typical of experiment and not critical. The amplitude output coupling (OC=2%) is purposefully kept low to ensure self-similar formation as detailed in the previous chapter and in Ref [6]. The round trip time (τ_{round} = 10 ns) is also chosen to reflect typical Ti:Sapphire laser systems. The modulation depth of the SA (q_0 = 3%) was chosen by considering realistic experimentally achievable modulation depths as well as numerical computation speed. Numerically larger and smaller modulation depths are still effective in forming pulses. The saturation power ($P_{sat} = \frac{1}{50}P_{peak}$) is chosen to ensure self-similar evolution as detailed in the previous chapter and in Ref [6]). Values of the GVD ($\beta(z)$ =60 fs^2/mm), nonlinear index of refraction ($n_2 = 3\times10^{-20}$ m^2/W), and bandwidth of the gain medium (w_c =2$\pi\times$44 THz) are set by the physical parameters of the gain medium. The SPM coefficient is defined by $\gamma = \frac{2k_0n_2}{\pi w^2}$ where k_0 is the line center spatial frequency, and (w =40μm) is the spot size of the laser mode within the gain medium. The length of the gain medium was set to 10 mm which is common in experiment.

The numerically simulated temporal and spectral intensity profiles of the self similar Ti:Sapphire laser are presented in Fig 3.1. Fig 3.1 shows that the temporal width T of the pulse is 9 ps while the FWHM spectral bandwidth is approximately 5 nm. Despite the fact that the results of Fig 3.1 reflect only one possible cavity configuration, the pulse characteristics seen in Fig 3.1 are observed over large parameter spaces. The parameters most sensitive to passive self-similar evolution in solid state systems are the output coupling, saturation power of the SA, and the bandwidth of the pulse relative to the gain bandwidth. The ranges which the output coupling and the saturation power of the absorber may take to form self-similar pulses in solid state systems is detailed in reference [6]. Generally, the smaller the perturbation to the pulse in the steady state, the more conducive to self-similar formation the evolution will be. Amplitude output coupling less than approximately 5% and peak powers approximately ten times or greater than the saturation power of the absorber are required for passive self similar evolution in solid state systems. For sensitivity on the bandwidth of the pulse, it was found that passive self-similar pulses in solid state lasers were formed when bandwidths were less than 15% of the gain bandwidth. We note that the self-similar pulses simulated in Ti:Sapphire in Ref [22], which had bandwidths approaching the gain bandwidth of Ti:Sapphire, were amplifier similaritons and are not modeled accurately with an average cavity description.

Based on the insight gained from simulation, Eq (1.2) is simplified, noting that bandwidth filtering is inconsequential, and generalized, noting that the role of the saturable absorber is important for passive self-similar evolution. Examining the right-hand trace of Fig 3.1 we see that the pulse has a spectral bandwidth which is less than 3% of the gain bandwidth, barely feeling the affect of

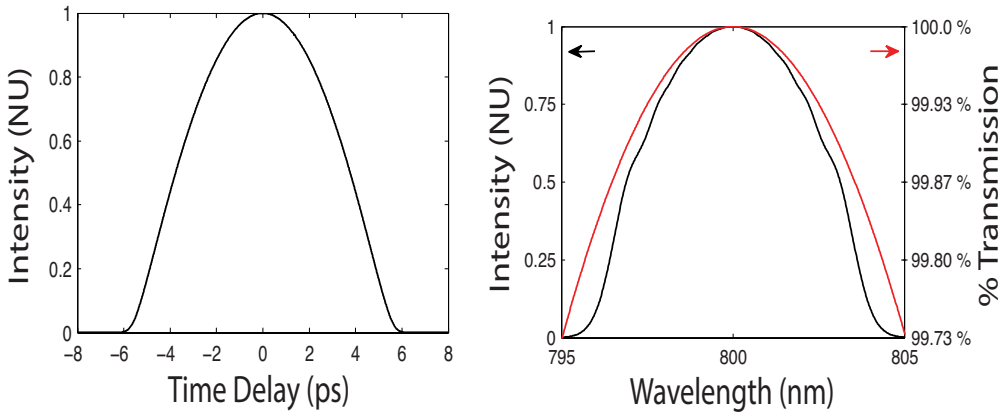

Figure 3.1: **Left**: Temporal profile of a passive self similar pulse in a Ti:Sapphire resonator. **Right**: The spectral intensity of the self similar pulse (black) is shown alongside the frequency dependent percent transmission of the Ti:Sapphire gain medium (red).

spectral filtering from the gain medium. This observation allows us to make the simplifying approximation that the affect of a frequency-dependent saturated gain can be analytically approximated as a constant frequency-independent gain.

Another important consideration in the development of an analytic self similar model is how to describe the saturable absorber. In passive self-similar fiber systems, the SA is expressed as a weakly saturated ideal absorber while for solid state systems, the SA is expressed by a heavily saturated ideal absorber. In order to accommodate such a dynamic range of operation, the term describing the ideal saturable absorber in Eq (1.2) is rewritten in Eq (3.1) with to-be-determined free parameters b_1, c_1, and d_1 which offer more degrees of freedom to the saturable characteristics of the absorber.

In contrast to simulation, which describes positionally-dependent variations in cavity parameters, the theory will assume that each cavity element within Eq

(1.2) acts upon the pulse simultaneously. Such an assumption is generally the only practical way to arrive at a purely analytical description of a system, as the simultaneous treatment of all the elements within the resonator decouples pulse evolution from position in the cavity. For laser systems where each individual element within the cavity does not cause appreciable changes to the pulse characteristics over one round trip, and for laser systems where the pulse solution does not depend on a localized nonlinear attractor, such an assumption is well formulated. The passive self-similar pulse meets both of these requirements as it does not dependent on a localized nonlinear attraction, and as each element within the cavity does not create large changes to the pulse characteristics within one round trip.

Thus, the master equation Eq (1.2) which we have used so far in simulation, is now rewritten as Eq (3.1), in order to model an average cavity description of a self similar laser. In Eq (3.1) each term of the equation is a positionally-independent function (e.g. $\beta(z) \rightarrow \beta$). Furthermore, the generalized expression of the term describing the saturable absorption and the simplifying approximation of a frequency-independent gain were incorporated into Eq (3.1). The resultant equation describing the change to the complex field amplitude of the pulse as a function of position (which for our model should only depend on position by a constant phase shift per round trip) is written as,

$$i\frac{\partial A(z,t)}{\partial z} = \left[\frac{\beta}{2}\frac{\partial^2}{\partial t^2} - \gamma|A(z,t)|^2 - ib_1\frac{|A(z,t)|^2 - c_1}{|A(z,t)|^2 + d_1} + i(g-l)\right]A(z,t) \tag{3.1}$$

where β is the group velocity dispersion, γ is the self phase modulation parameter, g is the saturated gain coefficient, l is the loss, and b_1,c_1, and d_1 represent the to-be-determined variables describing the saturable absorber.

3.1.2 Solving the Formulated Master Equation

Searching for a spatially-stationary solution to Eq (3.1) of the form $A(z,t) = f(t)\exp(i\phi(t) + i\eta z)$. Here, $f(t)$ represents the field amplitude of the pulse, η represents the linear phase shift of the pulse per unit distance, and the temporal phase $\phi(t)$ is modeled as quadratic and of the form $\phi(t) = \alpha t^2$ (self-similar pulses have linear temporal chirp). Eq (3.1) can be divided into its real and imaginary components and expressed as,

$$(-2d_1t^2\alpha^2\beta + d_1\eta)f(t) + (\eta - 2t^2\alpha^2\beta - d_1\gamma)f(t)^3 - \gamma f(t)^5 + \frac{1}{2}d_1\beta f''(t) + \frac{1}{2}\beta f(t)^2 f''(t) = 0 \tag{3.2}$$

$$(ib_1c_1 + id_1g - id_1l + id_1\alpha\beta)f(t) + (ig - ib_1 - il + i\alpha\beta)f(t)^3 + 2id_1t\alpha\beta f'(t) + 2it\alpha\beta f(t)^2 f'(t) = 0 \tag{3.3}$$

where $f'(t)$ and $f''(t)$ denote the respective first and second derivatives of the field amplitude with respect to time.

In Eq (3.2) we note that for laser systems operating in the net normal dispersion regime, the last two terms can be dropped. The magnitude of the squared temporal duration T^2 of such a pulse is much larger than the magnitude of the group velocity dispersion β. This observation is supported by considering the left-hand trace of Fig 3.1 which shows that the temporal width T of the simulated pulse within the resonator is approximately 9 ps. The ratio of the group velocity dispersion (β =60 fs^2/mm) to the squared magnitude pulse duration is then β/T^2 =7.4 $\times 10^{-4} m^{-1}$ which is negligible. Simulation and inspection show that when $\frac{\beta}{T^2} \rightarrow 0$, the last two terms of Eq (3.2) tend to zero much faster than the other terms in Eq (3.2) and may be neglected. The mathematical limit describ-

ing the $\beta f''(t)$ terms of Eq (3.2) can be written as $\lim_{\frac{\beta}{T^2}\to 0} \frac{d^2}{dt^2} f(t) = 0$ which accounts for the nature of these terms when $\frac{\beta}{T^2} \to 0$ [2, 30, 28]. Specific artifacts of this simplifying assumption on the analytical theory are revisited at the conclusion of this work.

With this approximation, Eq (3.2) may be solved for the field amplitude $f(t)$ of the steady state pulse

$$f(t) = \sqrt{\frac{\eta - 2t^2\alpha^2\beta}{\gamma}}. \tag{3.4}$$

Eq (3.4) shows that the intensity profile is parabolic, as expected from simulation. We continue by next determining the coefficients describing the saturable absorber. Substituting the result of Eq (3.4) into Eq (3.3), an equation with dependence on pre-factors t^4, t^2, and 1 is obtained. Grouping together elements with the same temporal pre-factor produces three equations which must each separately equal zero in order to solve Eq (3.3) for all times. By solving these three equations the coefficients b_1, c_1, and d_1 which describe the saturable absorber are determined and expressed as,

$$b_1 = g - l + 3\alpha\beta \tag{3.5}$$

$$c_1 = \frac{2\alpha\beta\eta}{(g - l + 3\alpha\beta)\gamma} \tag{3.6}$$

$$d_1 = 0 \tag{3.7}$$

The saturable absorber coefficients depend on the temporal chirp coefficient α which is still a free parameter. To derive an analytical expression for α, we note that the expression $b_1 \frac{|A(z,t)|^2 - c_1}{|A(z,t)|^2 + d_1}$ describing the saturable absorber must remain greater than zero so that it provides loss at all times. We define the loss

at the peak of the pulse (t= 0) by the variable l_{ns}. Mathematically this statement is equivalent to $b_1 \frac{f(0)^2 - c_1}{f(0)^2 + d_1} = l_{ns}$. Solving this expression for the temporal chirp parameter α we obtain,

$$\alpha = -\frac{g - l - l_{ns}}{\beta}. \tag{3.8}$$

We note that the chirp parameter of Eq (3.8) depends on β and the net gain per unit distance (in this case $g - l - l_{ns}$) the same way which the chirp parameter of a self similar pulse within an infinitely long nonlinear fiber amplifier does [14]. With definitions for both the temporal chirp coefficient α [Eq (3.8)], and the coefficients describing the saturable absorber [Eqns (3.5-3.7)], the expression of the saturable absorber required to form the complex field envelope $A(z,t)$ of the pulse may be written down as

$$b_1 \frac{|A(z,t)|^2 - c_1}{|A(z,t)|^2 + d_1} = \frac{2(g - l - l_{ns})(\eta - \gamma|A(t)|^2)}{\gamma|A(t)|^2} + l_{ns} \tag{3.9}$$

$$A(z,t) = A\sqrt{1 - \frac{t^2}{T^2}}\exp(i\alpha t^2 + i\eta z) \tag{3.10}$$

where the pulse width T is given as $\sqrt{\frac{\eta\beta}{2(g-l-l_{ns})^2}}$ and the amplitude A as $\sqrt{\frac{\eta}{\gamma}}$.

3.2 Derivation of Energy Area Theorem

Using the pulse width T and amplitude A from the average cavity model, we can write down an expression for a theorem which tells us how the pulse energy E=2A^{2}T and width T scale with system parameters. Energy pulse width theorems are useful tools for seeing how resonator elements affect the relationship

between pulse energy and temporal width, as well as for providing insight into the mechanics of energy scalability. From Eq (3.10) the theorem can be expressed as

$$\frac{E}{T^3} = \frac{4(g - l - l_{ns})^2}{\beta\gamma} \tag{3.11}$$

Table 3.1 tabulates important previously derived area theorems for other pulse evolutions listed in the introductory chapter of this work and lists them alongside the area theorem derived in this chapter. In the table α_1 is the strength of the coefficient describing the cubic saturable absorber term, and ω is the bandwidth of the gain medium. Table 3.1 shows that the theorem derived in this work is qualitatively very different from previously derived pulse width theorems. It is well known that the soliton-like solutions of Table 3.1 maintain an inverse relationship between their temporal width and energy for constant system parameters. For the self-similar solution presented in this work, the opposite trend is seen. As the energy E of the self-similar pulse is increased, the chirped temporal width T of the pulse is also increased.

Table 3.1: Area Theorems

Pulse Evolution	Expression
Soliton (NLSE)	$ET = 2\frac{\lvert\beta\rvert}{\gamma}$
DM-Soliton (CGLE)	$ET^3 = \sqrt{\pi}\sqrt{\frac{(1/\omega^2)+4\beta^2}{\alpha_1^2+\gamma^2}}$
Chirped Soliton (CGLE)	$ET = \frac{3(\beta^2\omega^2+4)}{2\omega(2\gamma+\beta\alpha_1\omega)^2}(3\beta\gamma\omega - 6\alpha_1 \pm \sqrt{4(2\beta^2\omega^2+9)\alpha_1^2 - 4\beta\gamma\omega\alpha_1 + \gamma^2(9\beta^2\omega^2+32)})$
Dissipative Soliton (CQGLE)	See reference [39]
Dissipative Soliton (Generalized CGLE)	See reference [32]
Chirped Pulse Oscillator (Generalized CGLE)	See reference [28]
Self Similar (Eq **??**)	$E/T^3 = \frac{4(g-l-l_{ns})^2}{\beta\gamma}$

In comparing the qualitatively different trends of self-similar and soliton-like pulse evolution we can see one of the reasons why the passive self-similar pulse has found success in energy scaling ultrafast fiber systems [24, 8]. As

the peak power of a pulse within an oscillator grows, the nonlinear phase shift which it accrues, also grows. At a critical value of nonlinear phase shift, defined by $\phi_{NL} = n_2 k_0 I_{peak} z$, the pulse eventually breaks. Here, I_{peak} is the peak intensity of the pulse and z is the length of the nonlinear medium. k_0 and n_2 are the line center spatial frequency and nonlinear index. This theorem shows that as energy is scaled to higher values, the rate of increase of the peak power of a self-similar pulse is slower than the rate of increase of the peak power of a soliton-like pulse. This tells us that a self-similar pulse can be scaled to a higher energy than a soliton-like pulse before reaching a specific value of nonlinear phase shift. The shape of the temporal pulse and the specific characteristics of the cavity ultimately determine the maximum value of ϕ_{NL} which a specific pulse solution can incur without wave-breaking. We have observed in simulation that the critical value of nonlinear phase shift for passive self-similar pulses increases with the nonlinear loss of the saturable absorber and can range from near zero to greater than π radians. Experimentally it has been found that self-similar and dissipative soliton solutions in fiber lasers can tolerate nonlinear phase shifts greater than π, while dispersion managed (DM) solitons can tolerate nonlinear phase shifts around π, and soliton pulses can only tolerate nonlinear phase shifts which are $<< \pi$ [48]. In the context of energy scaling this means that self-similar pulses can possess higher energies than soliton-like pulses before reaching a certain value of nonlinear phase shift, and also can sometimes tolerate higher values of nonlinear phase shifts than their soliton-counterparts. Simulations have shown that the linearity of the chirp of the self-similar pulse allows the temporally broad pulses to be de-chirped outside of the resonator by one to close to two orders of magnitude, significantly reducing the temporal width, without loss to the pulse energy.

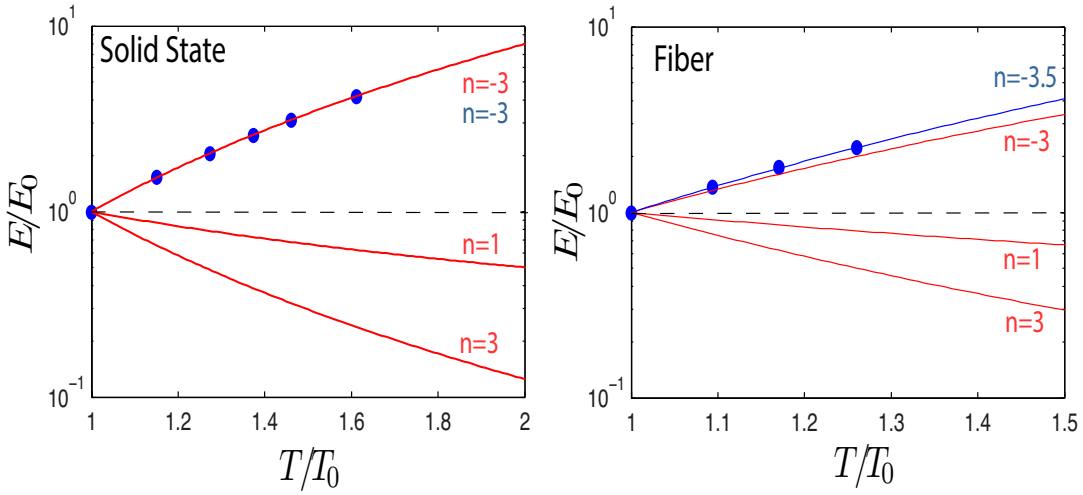

Figure 3.2: The relationship between the energy E and temporal width T of passive self similar pulses, expressed as $E \times T^n = C_0$, is simulated (blue circles), matched to a best fitted energy area theorem with value n (blue line), and compared to the well known area theorems of the DM soliton (n=3), the NLSE soliton (n=1), and the Self-similar model of this paper (n=-3). **Left**: Self-similar solid state laser. **Right**: Self-similar fiber laser

Fig 3.2 shows a plot of energy E versus pulse width T for several different pulse solutions, assuming the energy pulse width theorem is of the form $E \times T^n = C_0$ where n is a variable which denotes the relationship between pulse width and energy, and C_0 is a constant set by the system. Simulations were run for both passive self-similar solid state (Ti:Sapphire) and fiber laser (Yb:fiber) systems to test the theoretical model in two broadly different regimes. Simulation results for each laser type were obtained by keeping the system parameters (i.e. $\beta, \gamma, \omega_c, g-l-l_{ns}$) constant as set by the parameters of the laser gain medium, and experimental design. By adjusting the unsaturated gain coefficient g_0 for each system, a numerical relationship between energy and temporal duration was found. Data points corresponding to numerically simulated self-similar pulses are shown as blue circles, and the best fit value of n which corresponds

to these numerically simulated points are shown on the plot and depicted as a solid blue line. For the solid state system T_0 is 6.2 ps and E_0 is 177.1 nJ and for the fiber system T_0 is 4.7 ps and E_0 is 7.4 nJ.

Fig 3.2 shows that the self-similar theoretical model (n=-3) quantitatively predicts the relationship between energy and temporal width which the simulated self-similar pulses display in both the solid state (n=-3.0) and the fiber (n=-3.5) laser systems. That is, as energy increases, pulse width also increases. Traces of the dispersion managed (DM) soliton area theorem (n=3) and the NLSE soliton area theorem (n=1) are also shown for comparison, highlighting the fact that in increase in energy for these soliton-like pulses results in a decrease in temporal width.

Considering that the theoretical model is an average cavity model which assumes each element within the cavity is acting simultaneously on the pulse, and which does not take into account bandwidth filtering, the excellent quantitative agreement between theory and simulation in two broadly different laser systems is remarkable. Bandwidth filtering was kept in the simulation because we wished to practically test the theoretical model by comparing it against simulation of real laser systems, which contain frequency dependent gain media. However, simulations run without spectral filtering were also performed to show that self similar solutions still formed in the absence of spectral filtering. The theoretical model explains the unique relationship between pulse width and energy which the passive self-similar pulse maintains, which none of the previously derived theorems, except the dissipative soliton laser can even qualitatively account for. The fact that simulation results of a solid state system matched the theoretical model nearly perfectly (n=-3.0) is not surprising con-

sidering that the solid state self similar pulse barely breathes and maintains a parabolic shape throughout the resonator. Such a resonator most accurately models an average cavity model. The passive self similar pulse in a fiber oscillator breathes more than its solid state counterpart and also changes temporal shape throughout a steady state round trip. We believe this fact accounts for the slight discrepancy between theory and simulation for the fiber system (n=-3.5). From our comparison of theory to simulation, we conclude that the theoretical model is a useful tool for developing intuition about passive self-similar pulse evolution and for pinpointing general parameter spaces for simulation and experimental design. Once this intuition has been gathered, an in depth numerical analysis should ultimately be run to determine the precise properties of a given self-similar pulse evolution.

3.3 Verifying the Theoretical Requirements of Saturable Absorber Characteristics

As an additional check of the theoretical model, a comparison between the analytical solution derived for the chirped soliton pulse, and self similar solution derived in this chapter, is made. The closeness between these two evolutions provides a powerful method for checking the predictive capabilities of the theoretical model and, as will be seen in the next section, provides valuable intuition about the connection between passive self similar fiber and solid state class laser systems. The results of theory are compared to the results of simulation for two different pulse evolutions: the passive self-similar pulse and the chirped-soliton pulse formed with net-normal dispersion within a Ti:Sapphire solid state laser

system. For equivalent values of GVD, SPM, gain, and output coupling, the chirped soliton and passive self similar theories only differ from each other in how they model the term describing the saturable absorber. Everything else in the master equations which model the pulse evolution is the same. As discussed in the introductory chapter, a chirped soliton pulse is theorized to form with a saturable absorber which is very weakly saturated, while as seen through simulation and theory a passive self similar pulse is theorized to form with saturable absorber which is heavily saturated, provided that the integrated nonlinear loss of the saturable absorber is small. By changing the saturable characteristics of the absorber from lightly to heavily saturated through numerical simulation, a tool is provided by which to evaluate the predictive capabilities of the derived self-similar theory.

The left trace of Fig 3.3 takes the normalized form of the nonlinear loss function required to generate self-similar pulses in the simulation section (dashed red), and compares it to the theoretically predicted normalized nonlinear loss function (solid red) of Eq (3.9) with the same value of nonlinear loss as that in the normalized simulated function. The analytic (solid blue line) and simulated (dashed blue line) saturable absorber profiles of the normal-dispersion chirped soliton pulse are shown for comparison [18]. As predicted by both theories, Fig 3.3 shows that in solid state systems where the saturable absorber induces a relatively small amount of loss to the system, a very weakly saturated absorber will form a chirped soliton pulse, while a heavily saturated absorber will form a passive self-similar pulse. The middle and right-hand traces of Fig 3.3 compare the analytic temporal and spectral intensity profiles to the simulated temporal and spectral profiles of the pulses formed with either a weakly (chirped soliton) or heavily (passive self similar) saturated absorber.

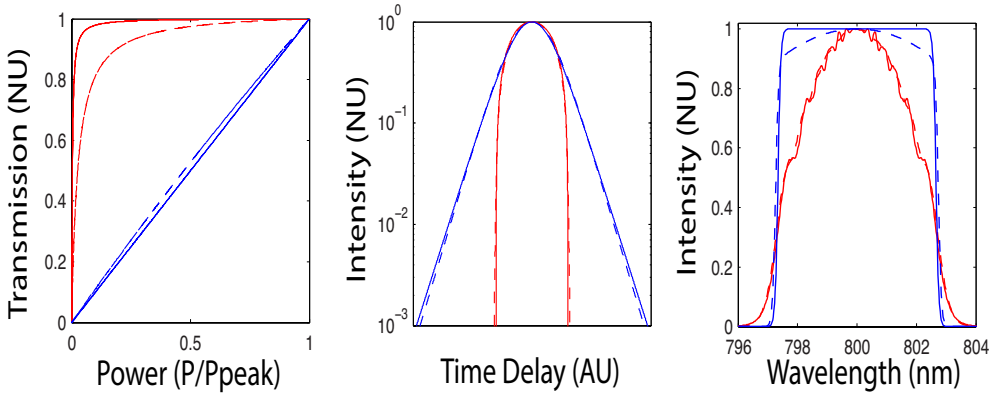

Figure 3.3: **Left**: Normalized transmission of the saturable absorber as a function of normalized power (P/P_{peak}). **Middle**: Logarithmic temporal profile of the pulse. **Right**: Spectral profile of the pulse ***dashed red line***: simulated parabolic profile; ***solid red line***: analytic parabolic profile; ***dashed blue line***: simulated chirped soliton profile; ***solid blue line***: analytical chirped soliton profile.

The functional form of the transmission of the saturable absorber in Eq (3.9) is next examined with different values of the integrated nonlinear loss of the saturable absorber to show how the theoretical model provides a qualitative connection between passive self-similar evolution in both solid state and fiber laser systems. The left-hand trace of Fig 3.4 shows that the analytic theory can describe the saturable absorber characteristics required to form passive self-similar pulses in both solid state and fiber systems. The transmission profile of the saturable absorber in Eq (3.9) is defined as $\exp(-z\times(\frac{2(g-l-l_{ns})(\eta-\gamma|A(t)|^2)}{\gamma|A(t)|^2}+l_{ns}))$. Inspecting this transmission function shows that the manner which the saturable absorber will respond to pulse power will depend mainly on the quantity $(g-l-l_{ns})$, which is the round trip net gain coefficient of the resonator.

The gain and loss of a resonator must be exactly equal in the steady state if we neglect the influence of variations within the cavity which happen on a timescale less than the upper state lifetime of the gain medium. The net gain

coefficient, $(g - l - l_{ns})$ accounts for the gain from the laser medium, the loss from the output coupler, and the constant non-saturable loss which the absorber introduces to the pulse. The only other dissipative process not accounted for within the cavity is the integrated nonlinear loss L_{SA}, of the saturable absorber. This means that $(g-l-l_{ns}) = L_{SA}$ for the gain and loss of the resonator to be equal. The nonlinear loss L_{SA} of a saturable absorber is determined by the modulation depth q_0 and the degree to which it is saturated.

The dashed lines in the left-hand trace of Fig 3.4 depict the simulated normalized transmission profiles of saturable absorbers in two very different self similar systems; the passive self-similar solid state system (red) presented in the simulation section above, and the passive self-similar fiber system simulated in the energy area theorem section. The solid lines of the left-hand trace of Fig 3.4 depict the analytic transmission profiles produced when the integrated losses L_{SA} of the SA in the numerically simulated solid state (red) and fiber (black) systems are substituted into the normalized Eq (3.9) in place of the quantity $z \times (g - l - l_{ns})$. The left-hand trace of Fig 3.4 shows that by changing the integrated nonlinear loss which the simulated normalized transmission profile of the saturable absorber introduces to the pulse L_{SA}, the saturable characteristics of the analytic absorber adapt appropriately to model the corresponding simulated systems. That the model qualitatively reflects the functional response of saturable absorption in two vastly different self-similar systems is remarkable. The reason for normalizing the simulated transmission profiles is due to the non-physical 100% modulation depth of the SA in the analytic theory, which is an artifact of the initial assumption that $\beta/T^2 \rightarrow 0$. Although the modulation depth of the absorber in the analytic theory may not match the modulation depth of simulation and experiment, the manner which the saturable absorber

responds to pulse power, or its normalized shape, can still be compared to simulation.

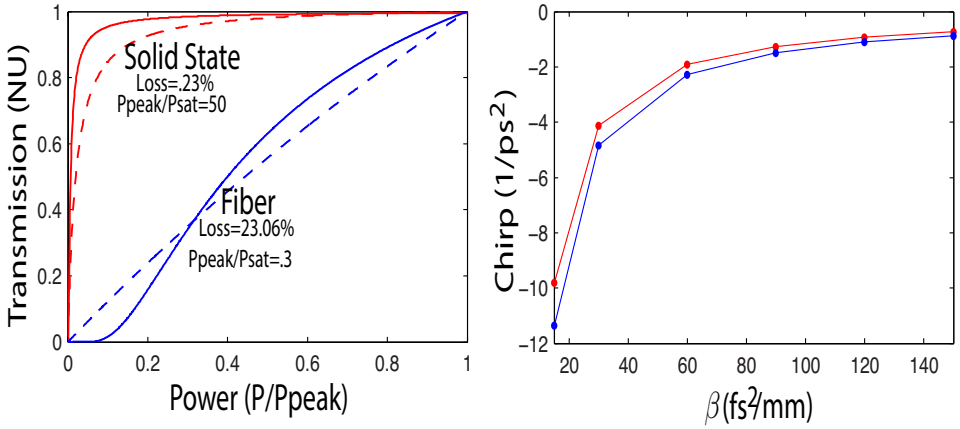

Figure 3.4: **Left**: The normalized *simulated (dashed)* and *analytic (solid)* transmission profiles of the saturable absorber required to produce self similar pulses in *solid state (red)* and *fiber (black)* systems are shown alongside each other. The 'loss' states the integrated loss which the simulated, normalized transmission profiles introduce to the pulse. 'Ppeak/Psat' states the number of times above saturation the absorber in numerical simulation were. **Right**: The analytic chirp parameter α is compared to the chirp parameter from simulation. *solid red line: simulation; solid blue line: analytic.*

It is prudent to note that although both the hyperbolic secant solution in the solid state laser of Fig 3.3 and the passive self-similar solution of the fiber laser in the left trace of Fig 3.4, are formed with weakly saturated absorbers, the total integrated nonlinear loss which the absorbers introduce to the pulse in each scenario, is very different. The theoretical model tells us that the the saturable absorber required to form passive self similar pulses must be heavily saturated if the nonlinear loss is small, or weakly saturated if the nonlinear loss is large. The chirped soliton pulse in the solid state system displays characteristics of being weakly saturated and has a small integrated nonlinear loss. The passive

self similar pulse in the fiber system also displays the characteristics of being weakly saturated but has a much larger integrated nonlinear loss. This means that the integrated loss of the weakly saturated SA (which forms the chirped soliton pulse) in Fig 3.3 does not match the self-similar analytic theory as expected. However, the weakly saturated SA which forms the passive-self similar pulse in fiber in Fig 3.4 does match the self-similar analytic theory. This observation further supports the predictive capabilities of the analytic theory.

Now that it has been seen that both the theory and simulation are in agreement with each other in predicting the nature of the saturable characteristics of the SA, we consider the chirp parameter α given by Eq (3.8). One of the most important practical benefits of self similar evolution is the quadratic temporal phase. Pulses with quadratic temporal phase can be de-chirped to their bandwidth limit outside of the resonator with elements possessing anomalous GVD, thereby allowing for high energy and temporally short (after de-chirping) pulses. For cavity design it is important that the theoretical description of the chirp parameter α reflects the same trends as numeric simulation. The right panel of Fig 3.4 compares the simulated chirp parameter α to the analytic chirp parameter given by Eq (3.8) for different values of cavity group velocity dispersion (GVD). The theoretical chirp parameter matches the simulated chirp parameter nearly perfectly qualitatively. Quantitatively, the simulated chirp parameter is consistently 83 $\pm$2% of the analytical chirp parameter for different values of β and $g - l - lns$. The same qualitatively consistent but slightly different quantitative relationship between the theoretical and simulated models was also found for simulations run without spectral filtering, ruling this out as the cause for the slight discrepancy. It is believed that the reason that the two do not perfectly match is due to the build up dynamics of the pulse and the fact

that the steady state pulse is not a perfect parabola. Future work will explore the relationships between the evolution stage and the steady state phase of the pulse to examine this question in more detail. The important conclusion is that the parameter scales as expected with the group velocity dispersion.

CHAPTER 4

EXPERIMENTAL CONSIDERATIONS FOR GENERATING SELF SIMILAR PULSES IN SOLID STATE LASERS

Now that a conceptual framework has been built up with numerical and analytical tools, a discussion of the practical points which must be considered to generate such an evolution experimentally is made. The main considerations which this chapter addresses are how to experimentally realize a saturable absorber which displays the characteristics of being heavily saturated, as well as potential cavity designs which are able to support the self similar evolution. As seen in the previous two chapters, the response of the saturable absorber is a key mechanism which dictates whether self similar pulse evolution will be the predominant solution within the resonator. This chapter will begin by analyzing different commonly used methods of saturable absorption to see whether they can display the characteristics of being heavily saturated, and will present experimental evidence for certain conclusions. Afterwards, this chapter will show through numerical simulation that both dispersion managed and all normal dispersion passive self similar pulses may be realized, and that the method chosen will depend on the desired characteristics of the output pulse width. Finally, a discussion of experimental difficulties which prevented the author from demonstrating the proposed pulse evolution is made.

4.1 Viability of Different Types of Saturable Absorbers

In the last chapter it was seen that the self similar evolution introduced in this work differs from other pulse evolutions in how the solution models the power

response profile of the saturable absorber. Other pulse evolutions with small values of nonlinear loss require a weakly saturated saturable absorber to initiate and sustain the different forms of soliton mode locking discussed in the introductory chapter and, as such, experimental methods for mode locking these types of lasers have used saturable absorbers which display characteristics of being weakly saturated. This is both because a weakly saturated response is easier to experimentally achieve, and also because the desired soliton solution would not be formed without such a weakly saturated response. In moving towards the regime of heavy saturation it is necessary to revisit the basics of the common methods for producing saturable absorption, and evaluate whether each method is conducive to producing an absorber which can display the characteristics of being heavily saturated.

Before beginning such an investigation it is important to clarify what exactly is required of the saturable absorber in solid state self similar systems. Numerical simulation has determined that the required modulation depth of the absorber will vary depending on the pulse energy circulating within the cavity but, as a general rule of thumb, must be between .5-5%. The degree of saturation of the absorber, resulting in a specific power response profile, can be quantified by considering the ratio of P_{sat} and P_{peak} of an ideal absorber. Such an absorber would require a peak power P_{peak} incident upon it which was 10-50 times greater than the saturation power P_{sat} of the absorber. Another practical consideration is the response time of the saturable absorber. Because the absorber must be able to respond to the low intensity wings of the pulse, which comprise approximately 10% of the temporal duration of the pulse, and because typical pulse durations for solid state systems will range anywhere from 1-15 picoseconds, it follows that the absorber must be able to respond on the approximate temporal

order of 0.1-1.5 picoseconds. With these requirements in mind the commonly used techniques of SESAM mode locking, and hard and soft aperture Kerr lens mode locking, are considered.

4.1.1 Semiconductor Saturable Absorbing Mirrors (SESAMs)

We begin the examination of determining the feasibility of achieving a heavily saturated absorber with an investigation of semiconductor saturable absorbing mirrors (SESAMs). These devices are used frequently throughout the ultrafast community, are relatively easy to fabricate, categorize, and simple to implement in mode locked resonators [33]. The relevant phenomena which we must consider for implementation of SESAMs into passive self similar systems are operating bandwidth, device damage, two photon absorption (TPA), relaxation time, and the ability to display the characteristics of heavy saturation.

Operating Bandwidth

The operating bandwidth of SESAMs can oftentimes be smaller than the gain bandwidth of ultrafast systems, presenting an unwanted spectral filter into the cavity. Additionally, the time bandwidth product of a transform limited self similar pulse is nearly twice that of a transform limited NLSE soliton pulse. This means that for a target pulse width, a self similar pulse will have nearly twice the bandwidth as a soliton pulse with the same temporal width. Generally, this does not present a problem as solid state lasers rarely make use of their entire gain bandwidth. However, many of the highly nonlinear systems where a self similar pulse would be practically very useful, are centered in the

mid IR region of the spectrum, where the gain media have significantly large bandwidths. For example, Cr:ZnSe has a gain bandwidth which spans from 2.1 to 2.8 um. Finding a semiconductor device which can maintain similar device performance over such a broad bandwidth is a challenge.

Graphene based saturable absorbers have attracted attention recently due to their ability to provide a nearly constant degree of linear loss and saturable loss over large spectral regions and serve as mode lockers [4, 44, 46]. Fig 4.2 shows results of an experiment the author conducted to determine the relaxation times in exfoliated few layer graphene (FLG) based saturable absorber samples. The pump probe technique used to measure the relaxation times was the equal pulse correlation (EPC) technique. Details of the EPC technique as well as the report of the experimental set up used in this experiment can be found in Ref [45, 5]. Although the experiments were performed at 800 nm, the time constants of the various relaxation time processes can be generalized to other wavelengths. The time constants were determined to be short enough to be useful for modelocking a self similar pulse evolution. An extremely fast relaxation τ_1 attributed to intraband carrier-carrier thermalization was observed at 15 ± 10 fs followed by slower relaxation attributed to intraband carrier-optical phonon interaction and on the order of, τ_2 = 175 ± 30 fs. A modulation in the absorption depth of 1.4% was observed in the samples from partial saturation due to Pauli blocking [5]

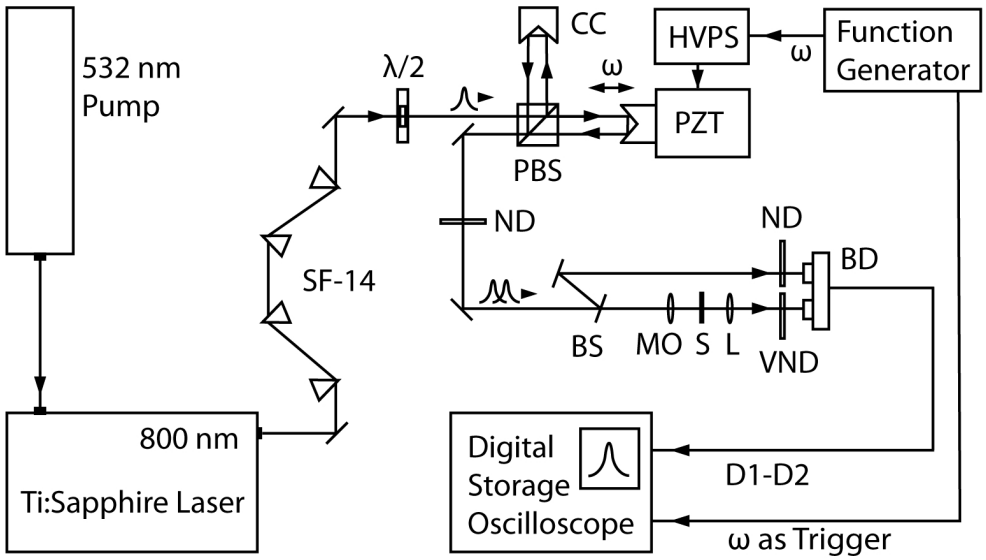

Figure 4.1: A schematic of the experimental setup for the pump probe on FLG experiment is shown.

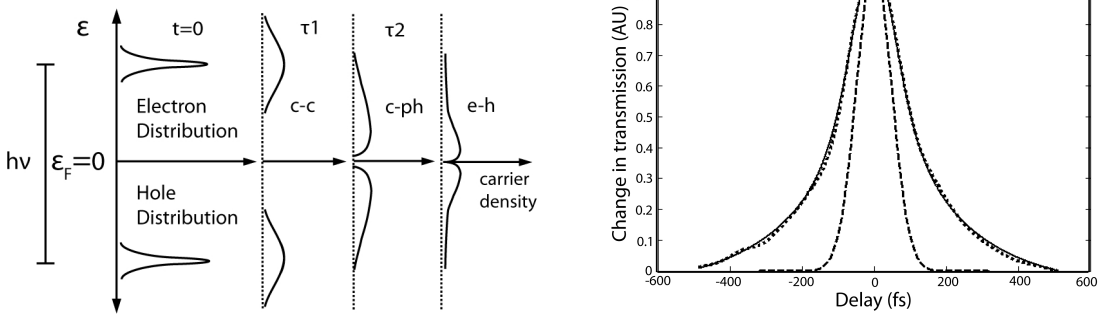

(a) Cartoon schematic illustrating the different relevant relaxation times involved, and the physical meaning of each relaxation process.

(b) An equal pulse correlation trace of the relaxation processes in FLG is shown.

Figure 4.2: Relevant relaxation time constants in FLG

Ability to 'Heavily Saturate'

SESAMs damage according to the fluence (J/m^2) incident on the device but, for pulses of temporal duration longer than the relaxation time of the device, saturate according to the saturation intensity W/m^2. This means that if an incident

intensity is required to be at least 10 times larger than the saturation intensity and the incident pulse is approximately ten times longer than the relaxation time of the device, the total 'equivalent' fluence incident on the device would be 100 times the saturation fluence. Because SESAMs typically can only handle pulse fluences which are 20-30 times the saturation fluence before damaging, it is unrealistic for commonly designed SESAMs to be able to tolerate the design criteria required for self similar formation. Furthermore, SESAMs do not perfectly reproduce the transmission profile of an ideal saturable absorber. For high intensities, the device begins to experience two photon absorption. This phenomena results in a roll over in the transmission profile for high intensities instead of maintaining the nearly flat transmission profile common to ideal saturable absorbers at high intensities. Experiments mode locking solid state lasers with SESAMs, as well as discussions with leading experts who regularly fabricate these devices, have confirmed that without addressing these fundamental issues in design, SESAMs will not be able to match the design criteria required for passive self similar propagation in solid state resonators.

For one test of this conclusion, an all normal dispersion Cr^{4+}:Forsterite chirped pulse oscillator was constructed and the pulse shape and spectrum were categorized. The 7.1 picosecond pulses could be de-chirped outside of the resonator with a grating pair by nearly a factor of fifteen to 450 fs. The temporal shape of the chirped pulse was measured with a cross correlation of the chirped and de-chirped pulses and matched the theoretically expected Hyerbolic secant pulse shape, formed with a saturable absorber displaying the characteristics of being weakly saturated.

The Cr:Forsterite laser in this experiment was inside of an X cavity. Fig 4.3

depicts a schematic of the cavity. The standing wave resonator consisted of only the gain medium and the semiconductor saturable absorbing mirror (SESAM). The presence of mode locking was determined by monitoring the pulse train on a fast photodiode. The cavity remained mode locked irrespective of cavity stability ranges consistent with SESAM mode locking. The characteristics of the SESAM were unknown, as the absorber was found unlabeled in a drawer. However, the insertion of the SESAM did not lead to a significant reduction in output power which suggests that it had a modulation depth of less than a couple percent (similar to the 2 % output coupler).

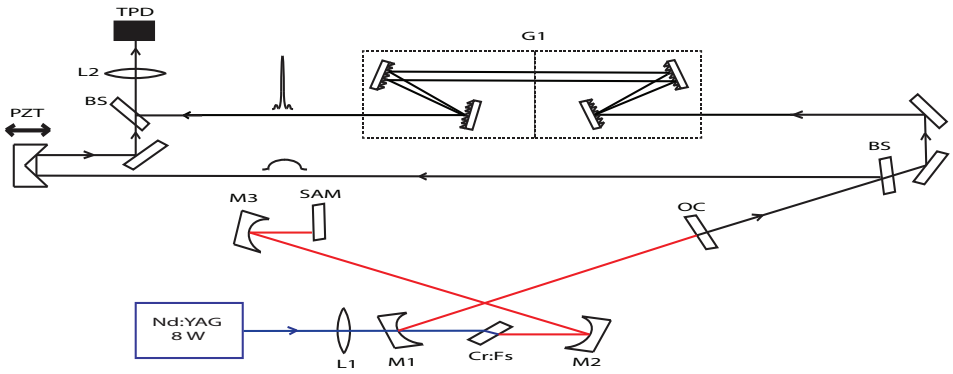

Figure 4.3: Schematic of the resonator; L1-L2: focussing lenses; M1-M3: 10cmCC focussing mirrors; CrFs: 10mm CrForsterite crystal; OC: 2% output coupler; BS: beam splitter; SAM: saturable absorbing mirror; PZT: piezoelectric transducer; TPD: two photon detector; G1: grating pair retroreflector

The output power of the resonator was 280 mW with a 2% output coupler. A 10cmCC spherical mirror was employed to tightly focus the resonator mode onto the SESAM. ABCD analysis predicts a spot size of 40 μm incident on the SESAM. Adjusting the SESAM position relative to the focus of the mirror did not cause noticeable changes to the autocorrelation of the pulse.

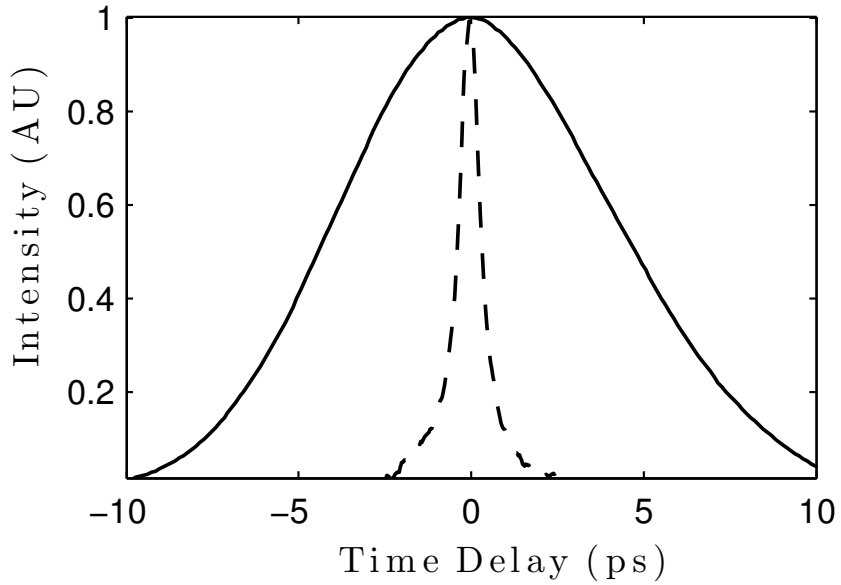

Figure 4.4: The autocorrelation of the chirped pulse with itself (solid line) and the de-chirped pulse with itself (dashed line) are shown on a normalized scale for comparison.

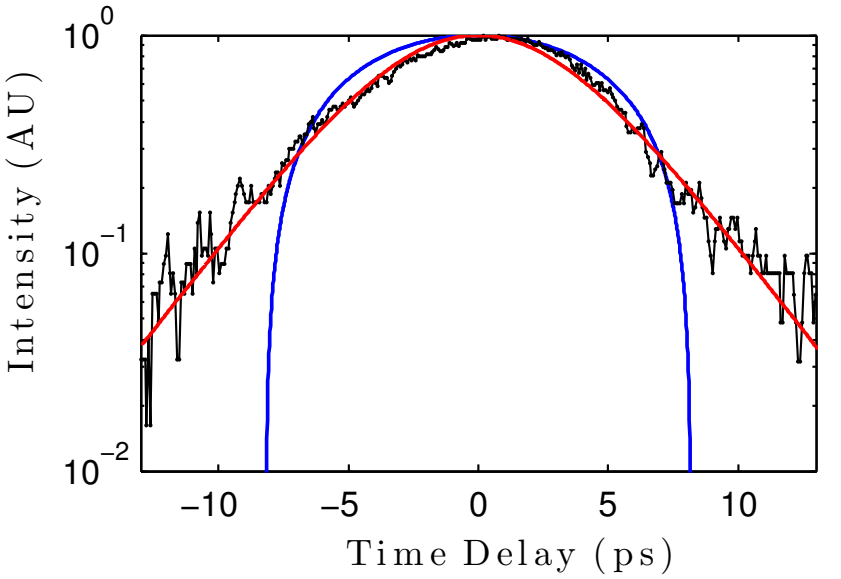

Figure 4.5: The cross correlation between the chirped and de-chirped pulse shows (black line) is shown on a logarithmic scale alongside a parabolic pulse (blue line) and a hyperbolic secant squared pulse (red line) for comparison

Fig 4.4 shows an autocorrelation of the chirped pulse and an autocorrelation of the dechirped pulse. The ability to temporally 'dechirp' a pulse outside of a resonator while maintaining high energy inside the resonator is show in this figure and is representative of a pulse evolution formed within the net normal dispersion regime. This is a benefit which a self similar evolution would extend even further than a dissipative soliton evolution (as depicted here) due to the increased linearity of the chirp function. Fig 4.5 shows a cross correlation of the chirped and de-chirped pulse which gives a measure of the chirped pulse shape. The pulse shape, as expected from SESAM mode locking where the SA can only realistically operate in a weakly or lightly saturated regime, is hyperbolic secant shaped. This shape is characteristic of a chirped soliton or dissipative soliton evolution.

4.1.2 Kerr Lens Modelocking

Another method of mode locking commonly used in solid state lasers is called Kerr lens mode locking. This method utilizes the phenomena of self focussing which occurs when a mode propagates through a medium possessing a self focussing nonlinearity. Each infinitesimal temporal slice of the pulse sees a different power. Each power slice sees a phase profile which matches the spatial distribution of the beam, while the magnitude of the phase shift is determined by the power of that segment of the pulse. In this way, an effective power dependent lens is created in the resonator. Proper design of a laser cavity can ensure that high intensity modes can propagate through the cavity with lower losses than continuous wave or low intensity modes. In this way, an 'artificial' saturable absorber is created. Two of the ways of utilizing the Kerr effect to initiate

and sustain the mode locking process are called 'hard aperture Kerr lens mode locking' and 'soft aperture Kerr lens mode locking', depending on the manner in which the high intensity light is favored within the cavity.

Soft Aperture Kerr Lens Modelocking

Soft aperture Kerr lens mode locking refers to the mode locking process in which lasers are designed so that a high intensity cavity mode sees a better spatial overlap with the pump beam than a low intensity cavity mode, consequently seeing higher overall gain. With this method of mode locking there are two points which must be considered when deciding whether it is a suitable technique for practically generating a 'heavily saturated' effective saturable absorber profile. First, in order for the laser to provide reasonable output powers, the overlap between the pump and both the linear and nonlinear modes must be reasonable. Second, the phenomenon of gain saturation, which results in a roll over in the effective transmission profile of the mode locking process, must be considered. The equation for the saturated gain of a laser can be written as,

$$g = \frac{g_0}{1 + I/I_{sat}}. \tag{4.1}$$

Self focussing causes g_0 to increase with increasing peak power as $g_0 \propto 1/(\omega_p^2 + \omega(P)^2)$ where ω_p is the spot size of the pump beam and $\omega(P)$ is the power dependent spot size of the laser mode. However, as g_0 increases as a result of $w(P)$ decreasing, the intensity I also increases, and the overall gain g reduces. Thus, keeping the mode intensity small enough that the reduction in gain from gain saturation does not overshadow the increase in gain from a shrinking mode size, is necessary. Additionally, in order to keep the discrimination between the

linear and nonlinear modes large while not allowing a roll over from gain saturation, requires that the spot size of the pump beam needs to be made very small. This means that the overlap between the pump and laser modes are very poor and the output power of the laser would suffer, either from poor mode overlap, or from pump saturating effects. As one of the purposes of self similar mode locking is to enable the capability of high average power mode locking, it follows that soft aperture mode locking techniques are not practically suited for generating such a heavily saturated absorber profile. This does not mean that such a profile could not be generated from soft aperture mode locking, it just means that soft aperture more locking would not be a natural, or efficient technique for doing so.

Hard Aperture Kerr Lens Mode Locking (HAKLM)

Hard aperture mode locking refers to lasers which are designed so that a high intensity cavity mode possesses a smaller spot size than a lower intensity cavity mode at a point outside of the gain medium. Generally, this point lies at an end mirror where both the linear and nonlinear spot sizes are at a focus. The insertion of a physical aperture at this location will preferentially select the high intensity radiation from the low intensity radiation, and favor pulse formation.

In order to quantify the difference between the linear and nonlinear mode sizes at a specific point within a cavity, a figure of merit n is introduced. Here, $n = \omega_l/\omega_{nl}$, where ω_l is the spot size of the linear or CW mode and ω_{nl} is the spot size of the mode formed by the highest intensity segment of the pulse within the cavity. In order for the 'hard aperture' to provide the desired flat top heavily saturated characteristics for self similar mode locking, n must, as seen from simula-

tion, be larger than approximately 1.5. Additionally, the aperture width (which transforms this spatial mismatch into intensity dependent transmission)must barely trim the outer Gaussian tails of the linear cavity mode. Hard aperture mode locking is the most promising candidate for initiating passive self similar mode locking in solid state gain media and simulations suggest that self focussing utilized in this manner can mirror the characteristics of an ideal heavily saturated absorber.

4.2 Cavity Design Considerations

Cavity designs which exploit self focussing in order to utilize hard aperture Kerr lens mode locking are now considered in this section. First, an overview of the numerical procedure used to pinpoint cavity configurations of interest is presented. Next, a more in depth analysis of the viability of hard aperture KLM self similar mode locking in an all normal dispersion and in a dispersion managed resonator is presented.

4.2.1 ABCD Analysis of Kerr Lensing

For monitoring how resonator modes were influenced by a self focussing nonlinearity, a nonlinear ABCD analysis was made. Each material possessing a self focussing nonlinearity was divided into thin segments where each segment was considered to have a constant spot size within that section. This allowed calculation of an ABCD matrix for each slice of each Kerr medium within the cavity. To initialize the simulation the linear spot sizes within each slice were

used. After one round trip through the cavity, a unique nonlinear ABCD matrix for each slice of each medium in the forward and reverse directions was defined. Before beginning the next iteration, the spot sizes within each slice of each Kerr medium were re-evaluated and used to define the nonlinear ABCD matrices for the next round trip. This process was repeated until beam convergence was reached. By cycling through different values of the nonlinear crystal stability range and position of the passive nonlinear crystal relative to each of its focussing mirrors, the spot size variation n between the linear and nonlinear beams at certain points of the cavity was tabulated. This information allowed for pinpointing cavity configurations where Kerr lensing was strongest.

Near the edges of the linear stability ranges, the addition of a strongly nonlinear medium shifts the cavity stability regions substantially and, for high peak powers, the nonlinear beam can 'skip' into the second stability region if operating near the edge of the first linear stability region. Because this only happens for large nonlinearity, lasers operating near the edge of the first stability region will drive themselves into the unstable region between the first and second stability zone for moderate amounts of nonlinearity and into the second stability zone for large amounts of nonlinearity. This type of mode locking has been called 'virtual Kerr lensing' as a cavity can be designed so that it is not stable for CW low intensity cavity modes but is stable for high intensity cavity modes [51]. The low intensity unstable region still supports laser action, but it incurs significant round trip diffraction losses. This method does not exclusively rely on either a hard or soft aperture but does make use of both of these principles for operation.

By shifting the linear cavity design so that the laser is operating near the in-

nermost edge of the second stability region, highly nonlinear beams will shift their stability regions towards larger values of the separation between the two focussing mirrors so that at the second innermost edge of the linear stability region, the nonlinear stability region will be defined continuously for large peak powers, allowing for the possibility of mode locking. This means that the nonlinear lens which each peak power of the pulse induces on itself, shifts the location of the linear stability region, but nevertheless keeps the resonator in a stable configuration. As the mechanics of mode locking which this type of self focussing creates is relatively well understood (where all modes are stable modes and where all modes are of the same structure), we will primarily concentrate on this type of configuration in this work (and not 'virtual' Kerr lens mode locking).

The utility of using ABCD matrices to pinpoint stability regions susceptible to large discriminations between linear and nonlinear spot sizes lies in the computation speed. However, it must be mentioned that the ABCD matrix analysis is an approximation based on the assumption that the Kerr lens can be modeled as parabolic in shape, for the purpose of calculating the nonlinear lens strength. In reality, the Kerr lens will reflect the shape of the cavity mode. Furthermore, an ABCD analysis assumes that the cavity modes remain Gaussian in structure as they undergo self focussing. Both of these assumptions are valid to first order with small amounts of a self focussing nonlinearity within the cavity. However, as we shall see in the next section, the ABCD analysis overestimates the lens strength by a factor of 2-5 when compared to an exact analytic treatment, and the assumption that the modes remain Gaussian is not strictly true. Thus, the ABCD analysis is used primarily to pinpoint stability regions of interest where subsequent analysis is performed by an exact treatment of self focussing and

diffraction.

4.2.2 Self Similar Mode Locking with Additional Nonlinearity

In order to achieve an intensity dependent transmission profile which mimics that of a heavily saturated ideal absorber we require a large discrimination between linear and nonlinear cavity modes. A practical way to achieve this is to insert an additional nonlinear medium into the laser resonator. An arbitrary figure of merit for categorizing the strength of self focussing within the resonator is introduced here with the parameter n which is defined by ω_L/ω_{NL}. In order to attain a transmission profile which mimics an ideal heavily saturated absorber with a large enough modulation depth to initiate and sustain mode locking a value of n =1.5 or greater must be realized within the resonator.

Considerations which are addressed within this section are:
(1) n(P) must be defined and increase continuously and preferably linearly for all powers up to P_{peak} so that the conversion between space and intensity is meaningful.
(2) Results obtained from the simplified ABCD analysis (defined below) must be related to an exact numerical treatment of a modified Helmholtz equation in order to accurately model a highly nonlinear resonator.

A simple mathematical model describing the transmission profile created by the insertion of a physical aperture into a resonator supporting both linear and nonlinear modes can be expressed as,

$$T[\omega(P)] = \frac{\int_{-a}^{a} exp(-r^2/\omega(P)^2)}{\int_{-\infty}^{\infty} exp(-r^2/\omega(P)^2)} = erf(a/\omega(P)); \tag{4.2}$$

where $\omega(P)$ is the power dependent spot size of the laser beam at a given location within the resonator and a is the half width of the aperture. Assuming a linear variance of spot size with peak power P we can rewrite the spot size $\omega(P)$ as

$$\omega(P) = -\omega_L \frac{n(P_{peak}) - 1}{n(P_{peak})} \frac{P}{P_{peak}} + \omega_L \tag{4.3}$$

with ω_L and n(P_{peak}) defined above.

The choice of a nonlinear medium is tricky as a suitable balance between GVD and SPM must be attained. If the GVD is too small, wave breaking occurs at lower peak powers than with larger values of dispersion. Furthermore, materials with large nonlinear indices and relatively large values of GVD around 800 nm exhibit unwanted phenomena such as changes in the sign of the nonlinear index, slow relaxation times, and the onset of linear absorption. As a further complication, very long dielectric media will not be homogenous throughout, and scattering losses can obscure the desired process. Thus, we search for a material with a reasonably large value of n_2 to lessen the amount of material needed to acquire the desired nonlinear phase shift, as well as a modestly large value of GVD to prevent wave breaking during the initial pulse evolution when the pulse is not parabolic. For these reasons, SF-11 was chosen as it provides a suitable compromise between a suitably large value of n_2 and GVD, while not exhibiting other potentially deleterious effects.

Simulations in this section were performed on a Ti:Sapphire laser operating

at 800 nm. Simulations were run assuming access to a nominal 15 W pump at 532 nm and a 10mm long .15% weight doped Ti:Sapphire rod (E3), as well as a 10mm thick piece of SF-11 AR coated glass (E7).

Table 4.1: Properties of Nonlinear Media at 800 nm

Type	n_0	n_2 (m^2/W)	GVD (fs^2/mm)
Sapphire	1.76	3E-20	70
ZnSe	2.524	5E-19	1020
CS2	1.63	5E-19	220
SF-11	1.76	4.1E-19	180

As an example, the right trace of Fig 4.6 shows a cavity mode plot of the linear beam and the highest expected peak power nonlinear beam for a linear cavity designed around the innermost second stability region. In this simulation, the focussing mirrors all had 10 cmCC. The numbers at the top represent distinct cavity elements within the resonator. Elements 2-4 represent the two focussing mirrors enclosing the gain medium (E2=51.8mm, E3=10mm, E4=45.95mm) while elements 6-8 (E6=45mm, E7=10mm, E8=51mm) represent the two focussing mirrors enclosing the additional nonlinear medium. Elements 1 (E1=60cm) and 9 (E9=25cm) represent the end arms of the cavity and element 5 is the cavity space between the gain medium and the additional nonlinear medium (E5=60cm).

Addressing consideration (1), we note that in the left trace of Fig 4.6 the discrimination between linear and nonlinear beams increases continuously as peak power is increased, and that n(P) increases more or less linearly. A well defined relationship between peak power and spot size gives the ability to intelligently transmute the spatial effect of self focussing into an intensity dependent effec-

tive 'saturable absorber' which acts on the temporal pulse.

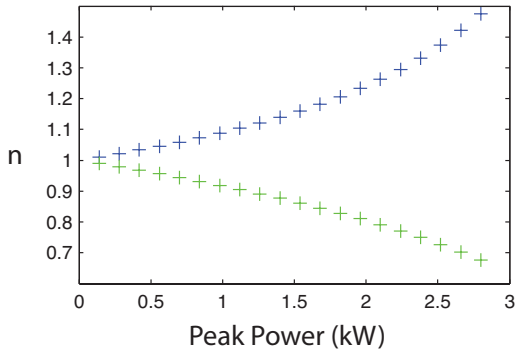

(a) The figure of merit $n(P)$, representing the change in mode size between linear and nonlinear beams is calculated for powers leading up to a given expected maximum peak power. The (blue crosses) represent $n(P)$ at cavity position 1 while the (green crosses) represent $n(P)$ at cavity position 9.

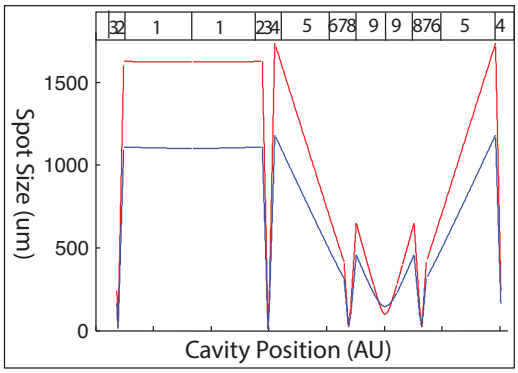

(b) The ABCD solution for spot sizes of the linear (red) and nonlinear (blue) modes at different points within the resonator is shown. The numbers at the top of the figure are to guide the eye and represent different cavity elements.

Figure 4.6: Results of ABCD spatial analysis of an all normal dispersion self similar laser

As mentioned in the beginning of the section, the nonlinear ABCD analysis is useful for pinpointing cavity configurations of interest, but ultimately must be confirmed with a more exact model. To more accurately model the spatial evolution of a mode in a resonator with gain and a self focussing nonlinearity we numerically solve Eq 4.4,

$$\frac{\partial A(x,y,z)}{\partial z} = [i\frac{\nabla_T^2}{2k_0 n(z)} + i\gamma(z)|A(x,y,z)|^2 + g(x,y,z) - l(z) + F(z)]A(x,y,z) \qquad (4.4)$$

where ∇_T is the transverse Laplacian, k_0 is the spatial frequency in vacuum and $n(z)$ is the refractive index of the medium the beam is traveling within. γ(z) is the nonlinear parameter and is given by $k_0 n_2(z)$ where $n_2(z)$ is the nonlinear index of the medium at location z. $g(x,y,z)$ is the saturated gain which includes

the shape and the absorption of the Gaussian pump beam. $l(z)$ represents output coupling which is only nonzero at the output coupler. F(z) is an operator representing the effect which spherical mirrors in the cavity have on beam propagation. Within the nonlinear elements, Eq (4.4) is solved with a standard split step algorithm, dividing the relevant linear and nonlinear operators of Eq (4.4) into individual computational steps in either the spatial frequency or spatial domains. In order to save computation time, a 1-D spatial analysis is utilized so that we are only considering the mode evolution in the x dimension, or about the y=0 point. This assumption is well formed for peak powers which are below the critical value of beam collapse.

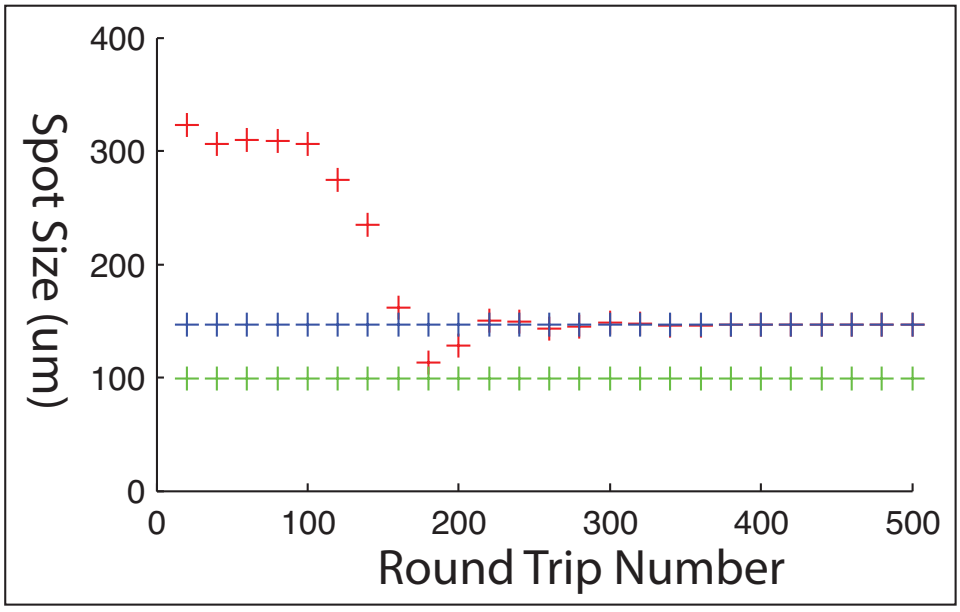

Figure 4.7: The spot size at an end mirror of the resonator (Location 9) is considered. The split step mode (red) at peak power 9kW is compared against the nonlinear ABCD mode (blue) at peak power 2.8 kW and the linear ABCD mode (green) at peak power 0 kW as the mode from the split step evolves from noise.

As discussed above, Fig 4.7 shows that the split step method yields the same results as the nonlinear ABCD analysis once the peak power is adjusted appro-

priately.

The following two tables tabulate the results of three different simulations. Table 4.5 compares results obtained with the nonlinear ABCD matrix approach to results obtained by numerically solving Eq (4.4). As was mentioned above, the ABCD analysis overestimates the amount of self focussing when compared against the modified Helmholtz equation. In order to achieve the same value of n for both simulations the peak power in the Helmholtz analysis needed to increase from 2.8 kW to 8.98 kW.

Table 4.2: Spatial Simulation Parameters

Parameter	Value
ABCD Analysis	
Linear Stability	-0.9997
Nonlinear Stability	-0.9984
P_{peak}	2.8 kW
n	1.5
Helmholtz Analysis	
E_p	11.56 nJ
P_{avg}	1.18 W
P_{peak}	8.98 kW
τ_p	64.38 ps
t_{round}	9.78 ns
ω_{gain}	40 μm
n	1.5

Table 4.3 takes the spot sizes in the forward and reverse directions within

the gain medium and segment of SF-11, as shown in Fig 4.8, to calculate the SPM in the temporal domain. The gain in increased until the peak power of the temporal analysis matches the peak power of the Helmholtz treatment. The effect of the hard aperture in the temporal analysis was computed with the value of n obtained from the Helmholtz treatment in Table 4.5 and Eq (4.3).

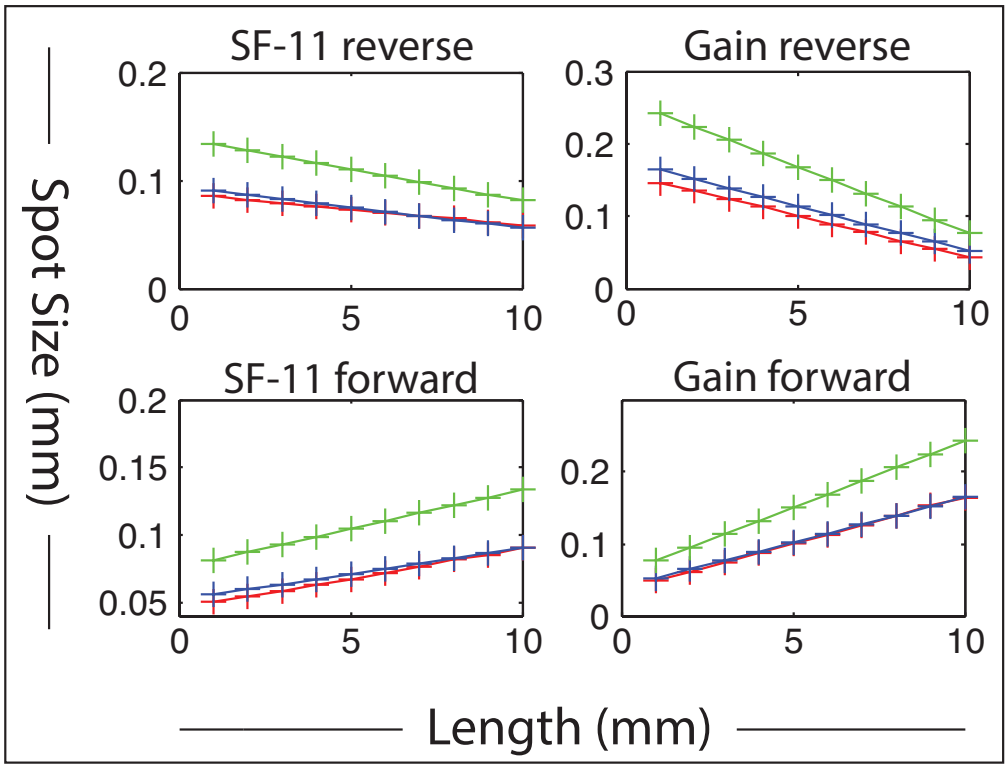

Figure 4.8: A comparison of the nonlinear ABCD mode (blue) and nonlinear split step mode (red) to the linear ABCD mode (green) within the gain medium and piece of SF-11 in the forward and reverse directions of propagation is made.

Table 4.3: Temporal Simulation Parameters

Parameter	Value
Gain Medium	Ti:Sapphire
Length	10 mm
g_0	29 1/m
n_0	1.76
n_2	3E-20 m^2/W
GVD	70 fs^2/mm
Passive Nonlinear Medium	SF-14
Length	10 mm
n_0	1.76
n_2	4.1E-19 m^2/W
GVD	180 fs^2/mm
Saturable Absorber	Hard Aperture
a	2 w_L
n	1.5
Mod Depth	.5 %
Pulse Characteristics	
Chirped τ_p	64.38 ps
Chirped P_{peak}	8.916 kW
E_p	10.9 nJ
De-chirped τ_p	0.80 ps
GDD	9.16 ps^2
FWHM $\Delta\lambda$	2 nm
M	0.053

As can be seen, the peak powers and pulse energies of the temporal and spatial simulations closely match. The average power required to obtain such energies was kept to a value achievable with the nominally 15 W pump laser we have in the laboratory. The M parameter of 0.053 is slightly larger than 0.04, the expected value of a parabola but still makes a compelling argument towards self similar evolution when compared to an M parameter of 0.19, which represents the commonly observed Sech value.

The temporal analysis predicts that the chirped pulse is 81 times broader than the de-chirped pulse which is quite significant.

Further analysis would consider the affects of the gain medium and nonlinear elements at Brewster's angle and the affect of astigmatism on the spatial analysis. A complete treatment would also include a full spatio-temporal model but the changes in spot sizes seen within the nonlinear elements for different peak powers is small enough that it is safe to consider the spatial and temporal evolutions separately.

4.2.3 Dispersion Managed Self Similar Mode locking

At modest average powers, the addition of anomalous dispersion into the resonator, can dramatically increase the peak power of a circulating pulse. This increase in peak power creates nonlinear phase shifts large enough to generate enough self focussing to produce the required mismatch between linear and nonlinear modes for self similar mode locking. Furthermore, with a dispersion managed system, the added alignment complications of inserting an additional nonlinear element into the cavity can be sidestepped. As long as the net dis-

persion in the cavity is normal, and the pulse bandwidth is not large enough to encounter strong filtering from the gain medium, self similar evolution can be achieved with anomalous dispersion within the cavity.

Similar to the simulations run in the previous section for an all normal dispersion self similar resonator, this section presents results of simulations which demonstrate the viability of a dispersion managed self similar resonator. Results from typical simulated experiments in Ti:Sapphire and Cr:ZnSe are tabulated below in Tables 4.4 and 4.5.

Table 4.4: Parameters for Cavity Design

		Ti:Sapphire	Cr:ZnSe
Number	Element	Value	Value
1	Free Space	40 cm	40cm
-	FM	10 cmCC	10cmCC
2	Free Space	5.55 cm	5.55 cm
3	Gain	1 cm	1cm
4	Free Space	4.64 cm	4.79 cm
-	FM	10cmCC	10cmCC
5	Free Space	39.5 cm	39.5 cm

Table 4.5: Temporal Simulation

	Ti:Sapphire	Cr:ZnSe
Parameter	Value	Value
Lxtal	10 mm	10mm
P_{peak}	165.5 kW	17.6kW
T_{round}	6 ns	6ns
E_{pulse}	8.7 nJ	2.35 nJ
g_0	90 1/m	25 1/m
OC	4%	4%
Chirped τ_p	2.78 ps	7.2ps
De-chirped τ_p	85 fs	163 fs
Number Times Dechirped	32.6	44.2
GDD to Dechirp	.054 ps^2	.254 ps^2
M	0.039	0.036
Normal GDD	1400 fs^2	4600 fs^2
Amomalous GDD	-1372 fs^2	-4508 fs^2
n	1.66 @ 140 kW	1.59 @ 17.5 kW
a	2.1 w_0	2.1 w_0

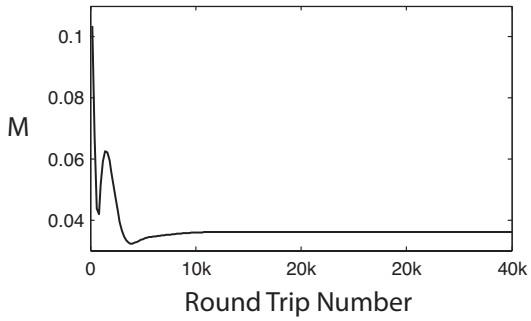

(a) M evolution of Cr:ZnSe

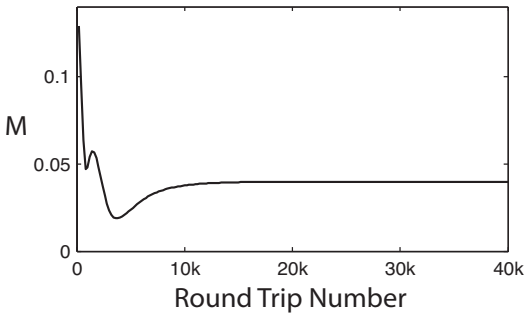

(b) M evolution of Ti:Sapphire

Figure 4.9: Evolution of the pulse shape in Cr:ZnSe and Ti:Sapphire dispersion managed self similar resonators

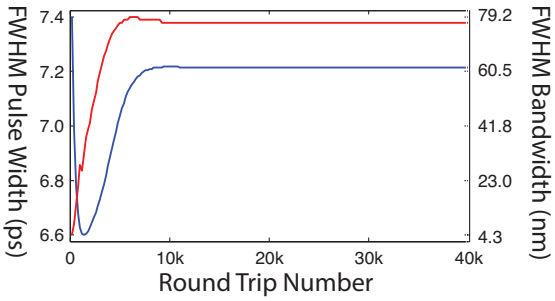

(a) FWHM bandwidth (red) is shown alongside the FWHM temporal width (blue) for self similar evolution in a Cr:ZnSe resonator.

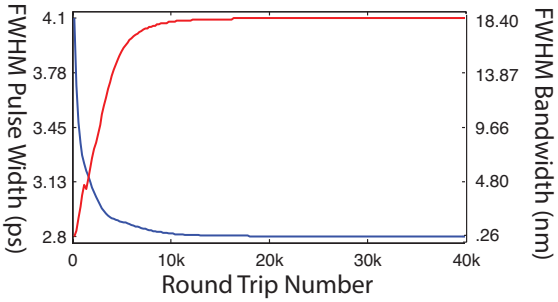

(b) FWHM bandwidth (red) is shown alongside the FWHM temporal width (blue) for self similar evolution in a Ti:Sapphire resonator.

Figure 4.10: Evolution of the temporal and spectral characteristics in Cr:ZnSe and Ti:Sapphire dispersion managed self similar resonators

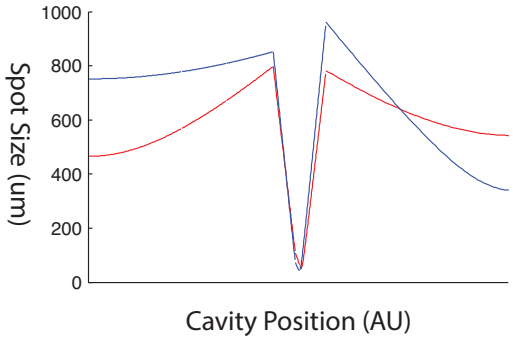

(a) Spatial evolution in Cr:ZnSe. The linear mode (red) is shown alongside the peak nonlinear mode (blue). The ABCD peak power is 7 kW.

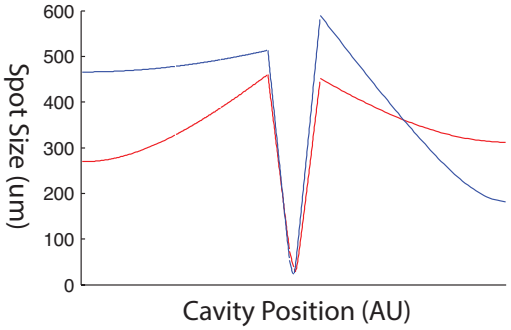

(b) Spatial evolution in Ti:Sapphire. The linear mode (red) is shown alongside the peak nonlinear mode (blue). The ABCD peak power is 70 kW

Figure 4.11: Spatial evolution in Cr:ZnSe and Ti:Sapphire dispersion managed self similar resonators.

Experimental efforts which tried to replicate the results of these numerical experiments were made but were inconclusive. Despite the strong theoretical and numerical evidence for such an evolution, translating this developed framework into experiment was particularly challenging. Kerr lens mode locked lasers with high efficiency are difficult to build due to alignment sensitivity. Furthermore, for a particular cavity configuration, the large aperture width required to produce the SA profile needed for self similar evolution provides much less nonlinear loss than typically used aperture widths. Couple this to the fact that the amount of peak power required for self focussing pushed our pump source to its maximum output levels, and required operating the laser on the very edge of stability within a small window, the experiment was difficult from the beginning.

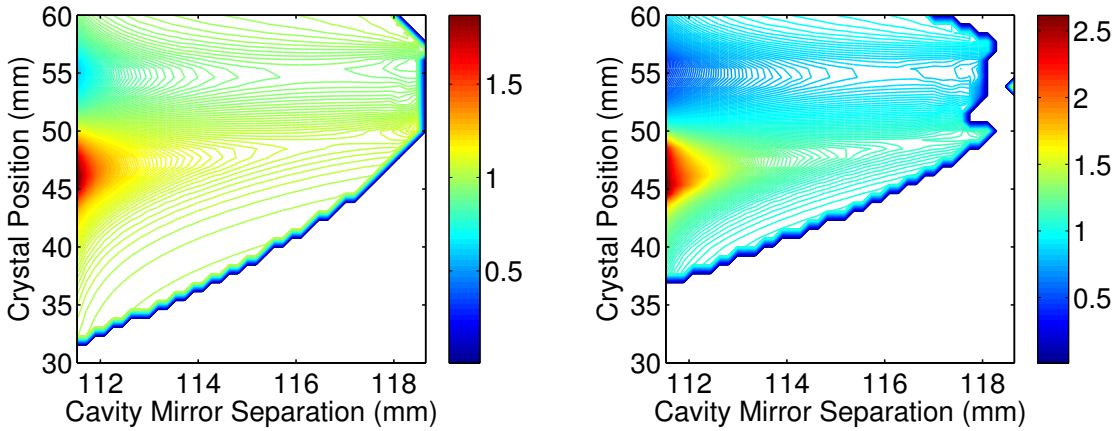

(a) Contour plot of KLM strength n as a function of cavity configurations for 70 kW peak power ABCD pulse.

(b) Contour plot of KLM strength n as a function of cavity configurations for 140 kW peak power ABCD pulse.

Figure 4.12: Contour plot of KLM sensitivity as a function of cavity configuration.

The left plot in Fig 4.12 shows a contour plot of the Kerr lens strength of the simulated Ti:Sapphire dispersion managed self similar laser (with 70 kW of peak power for the ABCD analysis) for a variety of different cavity configura-

tions. The plot displays the sensitivity as a function of the focussing mirror separation, and the position of the gain medium. As the left plot of Fig 4.12 shows, locations with large discrimination between linear and nonlinear modes, designated by a large n, are small and found only near the edge of the stability region. As an example, in the left trace of Fig 4.12, the most stable mirror separation which produces an n larger than 1.5 (minimum required for desired SA profile) occurs at 111.9 mm whereas the edge of stability for the cavity is 111.53 mm. Locating and maintaining a .37 mm precision in a cavity this close to the edge of stability is very difficult experimentally. However, with a higher peak power pulse (which corresponds to both a higher energy pulse and a higher power pump source), the experiment would become much easier, and the practical benefits of self similar evolution would become more obvious. From the right trace of Fig 4.12 we see that when the peak power of the pulse is doubled, the cavity configurations for which self similar mode locking becomes accessible (n>1.5), increases dramatically. For example, the furthest separation between the mirrors the resonator can be operated and still maintain a large enough n to generate self similar pulses through hard aperture KLM, occurs at 112.44 mm, whereas the edge of stability is at 111.53 mm. This means that if the resonator focussing mirrors can be situated anywhere within one mm of the edge of stability, the cavity can produce a large enough discrimination between linear and nonlinear modes. This is certainly within the range of experimental feasibility.

At the power levels available to us, the output energy of the self similar pulses was on the same order of magnitude as typical DM soliton pulse energies. The experimental efforts were aimed towards a proof of concept, which proved very difficult in the low power regime we were trying to operate the laser within. Experiment taught us that this evolution is a natural candidate for

high energy propagation but is not easily accessible in the low power regime. To state this another way: The higher the energy of the output pulse is, the more nonlinear phase accumulation available to the pulse, and the easier it is to implement a 'heavily saturated' absorber by utilizing self focussing. The easier it is to implement a heavily saturated absorber, the easier it is to tune the pulse to the self similar regime, which is naturally suited to tolerate the increased nonlinear phase accumulation. In certain respects, the process represents a type of positive feedback loop.

CHAPTER 5

SELF SIMILARITY IN OPTICAL PARAMETRIC OSCILLATORS

The difficulty of experimentally realizing a saturable absorber profile which displayed the characteristics of being heavily saturated led us to examine other methods for generating self similar pulses which could approach the problem from a different perspective. This consideration led us to examine optical parametric oscillators and the role of the parametric gain profile in shaping a specific pulse evolution. Generating self similar pulses from an optical parametric oscillator (OPO) would produce high energy ultrafast pulses tunable throughout large regions of the electromagnetic spectrum. Generally, when an OPO is synchronously pumped by a mode locked train of pulses, the pulses from the oscillator have a similar temporal duration as the pump source generating them. This means that the temporal characteristics of the OPO signal wave is similar to that of the pump wave but with a reduced pulse energy corresponding to the conversion efficiency of the system. Because the commonly chosen pump source for OPOs (dispersion managed soliton mode locked lasers) must themselves balance a compromise between pulse energy and pulse duration within the cavities supporting their initial evolution, one must choose to optimize either the energy or the temporal width of the pump source. The results of this compromise necessarily determine whether the OPO which this source pumps, generate high energy or ultrafast pulses.

This observation is primarily because of the soliton-like pulse evolutions employed within OPO systems. Because the pulse resonant within the OPO is not heavily chirped, the output pulse more or less mirrors the characteristics of the intra-cavity pulse, and also the pump pulses which generated it. By shaping the

temporal profile of a mode locked pump source, self similar pulses can be generated within the resonator. Due to the linear chirp of the resultant pulses, and the large bandwidth available to sources exhibiting parametric amplification, ultrafast high energy pulses could be generated from pump sources of much longer temporal duration. Essentially, the highly linearly chirped nature of self similar evolution helps to decouple the one-to-one correspondence between pump and signal pulse energy and pump and signal temporal width (after dechirping the output of the OPO). This allows the designer to choose longer pulse width and higher energy pump sources to generate higher energy parabolic pulses which can be de-chirped to short temporal duration outside of the oscillator. Figure 5.1 shows a cartoon schematic of the proposed idea. Here *PS* denotes 'pulse shaper', or an element which can restructure the temporal envelope of the pump pulse.

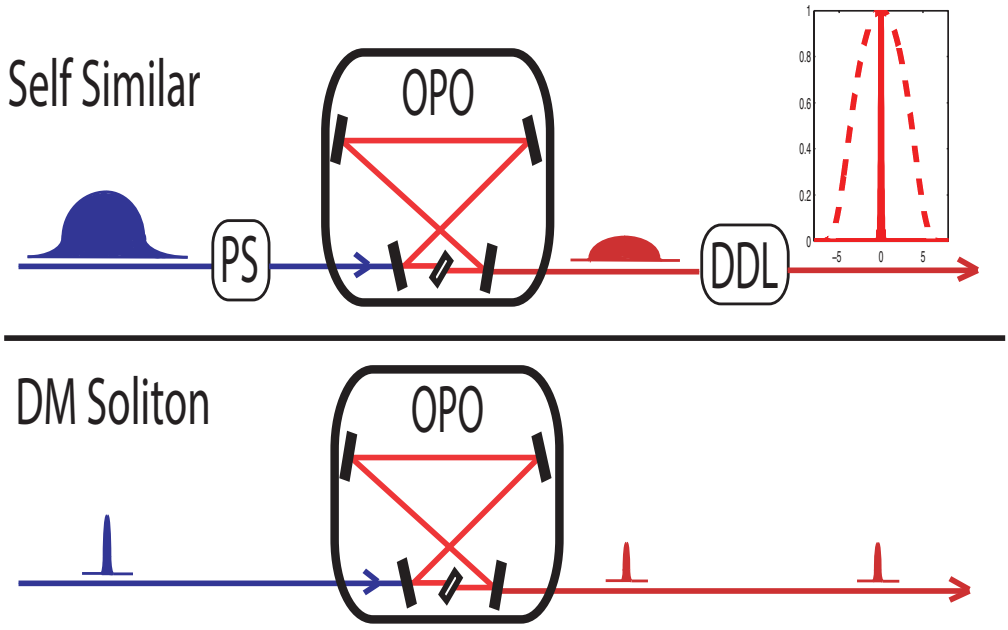

Figure 5.1: Cavity Schematic

Although this investigation is in its primary stages, realizing such a pulse

evolution within an OPO could potentially offer the following benefits:

(1) Relax the requirements on the temporal width of the pump pulse. This could potentially allow for high energy, hundreds of picosecond AO mode locked sources to pump and generate equivalently high energy, hundreds of picosecond parabolic OPO pulses. These highly linearly chirped pulses could then be de-chirped to the femtosecond regime outside the OPO while maintaining the high energy conversion efficiency from the original pump source.
(2) Increase the stability of ultrafast OPO systems. Because the intra-cavity pulse would be heavily chirped, it would generally possess longer temporal durations than conventional soliton mode locked sources. Longer duration intracavity pulses correspond to increased alignment stability, particularly in the longitudinal direction, which requires precise temporal overlap between the pump and signal waves.
(3) Increase the directly generable pulse energies of ultrafast OPOs achievable before wavebreaking.
(4) Reduce the cost of the pump source (AO mode locked compared to DM mode locked)
(5) Reduce the complexity of the OPO by not requiring dispersion management.

Issues which would need to be thoroughly examined in future work and which are not considered in this chapter would be:
(1) How the bandwidth of the pump pulse influences the evolution and the efficiency of parametric conversion.
(2) If the role of gain saturation affects the necessary pulse shape for self similar evolution.
(3) How to shape the pump pulse so that it would efficiently generate the re-

quired parametric gain profile.

5.1 Derivation of Theoretical Model

Following an almost equivalent theoretical approach as we followed in Chapter 3, this section begins by considering the nonlinear Schrodinger Equation with loss and an arbitrary gain profile $g(t)$. Bandwidth filtering is again not included in the model and its removal from the equation follows the same justifications as detailed in Chapter 3. Note that the parametric gain $g(t)$ is now a function of time due to its ability to respond nearly instantaneously to the pump source. Parametric gain $g(t)$ in the OPO replaces the intensity dependent saturable absorption required in a laser system due to the generally long relaxation time of the gain medium (relative to the pulse inside the cavity).

$$i\frac{\partial A(z,t)}{\partial z} = [\frac{\beta}{2}\frac{\partial^2}{\partial t^2} - \gamma|A(z,t)|^2 + i(g(t) - l)]A(z,t) \tag{5.1}$$

Searching for spatially stationary solutions of the form A(z,t)= f(t)exp(i ϕ(t) + i η z) where $f(t)$ represents the real field amplitude of the pulse, η represents the linear phase shift of the pulse acquired through a round trip passage of the oscillator, and the temporal phase $\phi(t)$ is assumed quadratic and of the form $\phi(t) = \alpha t^2$, we can divide Eq (5.1) into its real and imaginary components.

$$-ilf(t) + i\alpha\beta f(t) + if(t)g(t) + 2it\alpha\beta\frac{d}{dt}f(t) = 0 \tag{5.2}$$

$$\frac{1}{2}\beta\frac{d^2}{dt^2}f(t) - 2t^2\alpha^2\beta f(t) + \eta f(t) - \gamma f(t)^3 = 0 \tag{5.3}$$

Considering Eq (5.3), we note that for no dispersion mapping, the temporal duration T of the pulse will be much larger than the spreading resulting from the group velocity dispersion β in one round trip. That is to say for $\beta << T^2$ the adiabatic approximation calls for the term $\frac{d^2}{dt^2}f(t) \to 0$.

With this approximation we can write down an expression for the field envelope of the pulse as

$$f(t) = \sqrt{\frac{\eta - 2t^2\alpha^2\beta}{\gamma}}. \tag{5.4}$$

Now inserting Eq (5.4) into (5.2) we solve for the gain profile $g(t)$ required to satisfy Eq (5.2).

$$g(t) = \frac{(2l\alpha^2\beta - 6\alpha^3\beta^2)t^2 + (\alpha\beta\eta - l\eta)}{2t^2\alpha^2\beta - \eta} \tag{5.5}$$

Parametric gain responds on the timescale of the electronic nonlinearity χ^2 which is generally on the order of a few femtoseconds. As such, there is essentially no energy storage in an optical parametric oscillator so that if the gain $g(t)$ vanishes then so too must the field amplitude of the pulse. This condition will allow us to find an expression for the chirp parameter α.

As we consider the gain profile we see that $g(t)$ approaches negative infinity as the field amplitude approaches zero. This means that negative pumping is required for the outermost wings of the pulse. Although not physically viable, the resultant shaping mechanism of the pulse is consistent with ideas put forth in [6, 7]. In order to find an approximate expression for α we Taylor expand the expression for the gain in Eq (5.5) to fourth order and then impose the condition

that the resultant expression must vanish at time T, or the pulse width of the field amplitude. This yields an expression for the chirp parameter α,

$$\alpha \simeq -\frac{l}{3\beta} \tag{5.6}$$

which only differs from the temporal dependence of the chirp parameter found in [14] by a factor of two.

The field envelope $f(t)$ in Eq (5.4) can now be rewritten as

$$f(t) = A\sqrt{1 - \frac{t^2}{T^2}} \tag{5.7}$$

where the pulse width T is given as $\sqrt{\frac{\eta}{2\alpha^2\beta}}$ and the amplitude A as $\sqrt{\frac{\eta}{\gamma}}$. This allows us to write down an energy area theorem to describe the relationship between pulse width T and energy E as a function of system parameters.

$$\frac{E}{T^3} = \frac{4l^2}{9\beta\gamma} \tag{5.8}$$

where energy E is defined as $2A^2T$.

5.2 Temporally Shaping the Pump Pulse: Theory and Simulation

As the shape of the gain profile $g(t)$ is important for this evolution, it is considered below in more detail. Similar to the derivation in Chapter 3 where the saturable absorber displayed 0% transmission in the low intensity wings due to

the residual effect of approximating $\lim_{\frac{\beta}{T^2}\to 0} \frac{d^2}{dt^2} f(t) = 0$ in the low intensity wings of the pulse, the observation of $g(t)$ approaching negative infinity as the field amplitude approaches zero is also due to this approximation. This approximation is valid for the majority of the pulse envelope, but does begin to break down in the outermost wings. A consequence of this assumption breaking down is that in order to solve the equation exactly, another term must compensate for the impact the second derivative term had in the low intensity pulse wings. This term is the gain profile $g(t)$ which we derived. Thus, in modifying $g(t)$ so that it represents a physically realizable gain profile, we are also correcting for an artifact of one of our original assumptions. Luckily, as the break down of the assumption is confined to the lower intensity wings of the pulse, it does not alter any of the quantitative conclusions derived by the model. The slight modification to the wings of $g(t)$ will only affect the wings of the pulse within the oscillator; the majority of the temporal span of the pulse will see an essentially constant gain and remain parabolic.

We begin by rewriting $g(t)$ in Eq (5.5) as,

$$g(t) = \frac{2l \times (t^2/T^2 - 2/3)}{(t^2/T^2 - 1)} \tag{5.9}$$

where we have used the expression for α and T defined in Eq (5.6) and Eq (5.7), respectively. Having determined an approximate expression for α, if we want the gain profile to always vanish at T but still maintain a similar shape as the original $g(t)$ we can write a new electric field transmission gain profile $g_T(t)$ by simply adding 1 to $\exp[g(t)]$ so that we have,

$$g_T(t) = 1 + g_{sat} \times \exp(g[t]z) \tag{5.10}$$

where g_{sat} provides a for gain saturation and g_T represents the actual gain of

the system (no longer the gain coefficient). In this section we are using the simplest possible model which does not account for the relationship between the bandwidth of the pump source and the parametric gain coefficient, or how gain saturation is a dynamic process which occurs during the parametric conversion process.

The simulation was designed for an OPO resonant at 1064 nm pumped by a 2 picosecond wide gain profile. The specifics of how pulse shape exactly transforms into parametric gain was not included. The pulse output from the OPO had an M value of 0.021, and the 2.68 ps FWHM very parabolic pulses could be de-chirped outside of the resonator to 83 fs. The pulse quality of the de-chirped pulse was determined by dividing the peak power of the output pulse to the peak power of a Gaussian pulse with the same energy and FWHM temporal width. For this definition of pulse quality, the de-chirped pulse had a slightly better than Gaussian quality, possessing a number of 0.99. The output pulses were 11.9 nJ in energy. The numerical experiment was not run with spectral filtering, and further work is required before definitively identifying whether it will be practical to implement this evolution within a resonator, but the general principle is demonstrated by this simple analysis. That is, by temporally shaping the pump pulse we can shape the parametric gain profile. The parametric gain profile causes an evolving pulse to adapt its evolution inside the resonator into a self similar steady state solution which produces pulses that can tolerate high energies and be de-chirped outside of the resonator to a significant degree. The shape of the parametric gain profile is alone not sufficient to guarantee a self similar evolution. The shape of the parametric gain profile *and* the relationship between the pump pulse energy and pump pulse width also plays an important role.

In order to experimentally realize such a profile, several options are available. Adaptive pulse shaping with programmable wavelength filters exist which could produce the temporal profiles of interest. Splitting and recombining a seed pulse could also conceivably function as an option for temporal shaping. However, both of the above methods would incur significant losses during the shaping process. A third option, which would induce negligible losses is to propagate the pump pulse through a segment of fiber possessing self focussing nonlinearity and normal GVD. For appropriate ratios of characteristic dispersion and nonlinear lengths, the injected pulse smoothly adapts to a temporal square wave. The downside of this technique lies in the fact that the bandwidth of the pump pulse increases during the temporal reshaping process. Whether or not the larger bandwidth would significantly impede the efficiency of the self similar evolution is an open question.

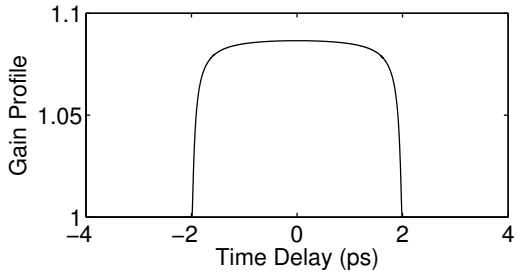

(a) The electric field transmission of the parametric gain profile $g_T(t)$ is shown as a function of temporal delay.

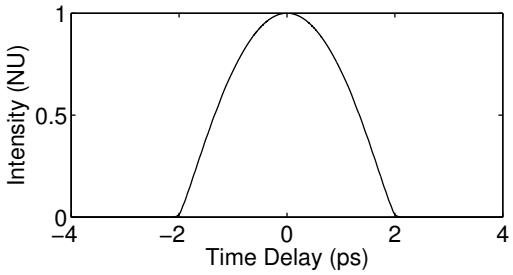

(b) The normalized temporal envelope of the parabolic output pulse is shown.

Figure 5.2: This trace shows how shaping the temporal profile of the gain transmission helps determine the evolution of the pulse.

In Fig 5.2, the gain profile was determined by setting the pump pulse width T to 2 ps and a power output coupling of 15 %.

Although a full exploration of this topic has not been made, it is the author's hope that this chapter provides a useful foundation for future work. Future re-

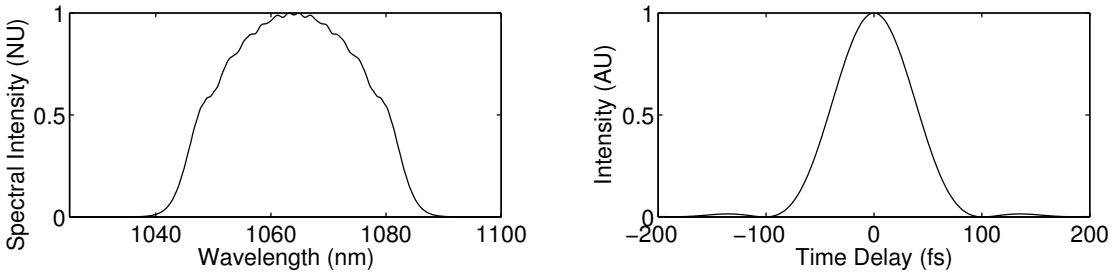

(a) The spectrum of the output pulse is depicted as a function of wavelength.

(b) De-chirped pulse profile.

Figure 5.3: The spectrum and de-chirped pulse profile from the basic simulation modeling the OPO is shown.

search aimed towards understanding how shaping of the parametric gain profile can positively influence direct energy scaling, is interesting and potentially fruitful. To the author's knowledge, this topic has not been considered in detail before now so the question is largely unexplored and undeveloped.

CHAPTER 6

SELF SIMILARITY WITH INCREASING NONLINEARITY

So far this work has only discussed self similar evolution in the presence of gain, nonlinearity, and dispersion. However, there are self similar solutions to other equations which are relevant for ultrafast pulse propagation. Besides the amplifier self similar solution (NLSE with gain) derived by Fermann [14] which this thesis has so far referred to, an alternative mathematically equivalent self similar solution has been derived for a nonlinear element with decreasing dispersion (NLSE with decreasing dispersion [20]). Furthermore, a number of self similar solutions which are not mathematically equivalent to the original amplifier solution, but which exist in the presence of some combination of distributed gain, nonlinearity, dispersion, and additional terms, have also been derived [35, 9]. The self similar solution to the NLSE with distributed dispersion is attractive because the pulse may form within a passive nonlinear element which does not suffer from the bandwidth limitations like a gain medium. Furthermore, this self similar solution is still temporally parabolic, still has has a quadratic temporal phase, and still increases exponentially in bandwidth as it propagates.

This chapter derives a self similar solution which exists in the presence of constant dispersion and increasing nonlinearity. Although the derived solution is seemingly a simple generalization of the results discussed above, to the author's best knowledge, this is the first exploration of this solution in this isolated context. Observing that a self similar solution could exist with distributed gain, distributed dispersion, and distributed nonlinearity, and also that a mathematically equivalent self similar solution to the amplifier solution could exist with

decreasing dispersion, suggests that distributed nonlinearity alone should also possess a mathematically equivalent solution to the amplifier solution. Close analysis of previous work suggest that the mathematical equivalence of the NLSE with distributed dispersion with the amplifier solution is perhaps not due to the decreasing dispersion alone but to the relationship between the dispersion and nonlinearity. Thus, one should be also be able to obtain the same mathematically equivalent solution with some to-be-determined function of distributed nonlinearity.

This chapter will first introduce a theoretical model to confirm this hypothesis, and will then discuss the practical applications of the solution for pulse compressors and ultrafast laser systems. Such an approach could be especially attractive for solid state systems because free space focussing could provide for a variance of nonlinearity, making the solution theoretically easy to experimentally implement.

6.1 Derivation of Theoretical Model

Writing the NLSE with a positionally dependent nonlinearity parameter $\gamma(z)$ we see that,

$$\frac{\partial A(z,t)}{\partial z} = \left[-i\frac{\beta}{2}\frac{\partial^2}{\partial t^2} + i\gamma_0\eta(z)|A(z,t)|^2\right]A(z,t), \tag{6.1}$$

where β is the group velocity dispersion, $\eta(z)$ is an to be determined positionally dependent function which describes the variance of the nonlinearity γ_0 which is assumed to be the nonlinearity at position $z = 0$.

Rewriting the equation in terms of a new field amplitude $f(z,t) = A(z,t)\sqrt{\eta(z)}$ we can rewrite Eq (6.1) as,

$$\frac{\partial f(z,t)}{\partial z} = \left[\frac{1}{2\sqrt{\eta(z)}}\frac{d\eta(z)}{dz} - i\frac{\beta}{2}\frac{\partial^2}{\partial t^2} + i\gamma_0|f(z,t)|^2\right] f(z,t) \tag{6.2}$$

Now, if we require that $\frac{1}{2\sqrt{\eta(z)}}\frac{d\eta(z)}{dz}$ equals a constant $g_0/2$, the equation reduces to the well-known NLSE with gain, of which we know that an asymptotic parabolic self similar solution exists [14]. For this to be the case, we require $\eta(z) = \exp(g_0 z)$, which represents an exponentially increasing nonlinearity profile.

Thus, we may write

$$A(z,t) = \frac{f(z,t)}{\sqrt{\eta(z)}} = \frac{A_0(z)}{\sqrt{\eta(z)}}\sqrt{1 - [\frac{t}{T(z)}]^2}\exp(j\phi(z,t)) \tag{6.3}$$

$$A_0(z) = \frac{1}{2}(g_0 E_{in})^{1/3}(\gamma_0\beta/2)^{-1/6}\exp(g_0 z/3) \tag{6.4}$$

$$T(z) = 3(g_0)^{-2/3}(\gamma_0\beta/2)^{1/3}E_{in}^{1/3}\exp(g_0 z/3) \tag{6.5}$$

$$\phi(z,t) = \phi_0 + \frac{3\gamma_0}{2g_0}A_0^2(z) - \frac{g_0}{6\beta}t^2 \tag{6.6}$$

$$\eta(z) = \exp(g_0 z) \tag{6.7}$$

where A_0 is the initial peak of the pulse field envelope, E_{in} is the input pulse energy, and g_0 is equivalent to the gain coefficient in the amplifier self similar solution.

Next, we confirm through numerical simulation that this solution in indeed mathematically equivalent to the solution to the NLSE with gain (apart from an

amplitude scaling coefficient [$1/\sqrt{\eta(z)}$]). As can be seen in Fig 6.1, the two solutions are equivalent to each other apart from an amplitude scaling factor. Thus, we have demonstrated that an equivalent solution to the amplifier similariton also exists for systems with constant dispersion and exponentially increasing nonlinearity.

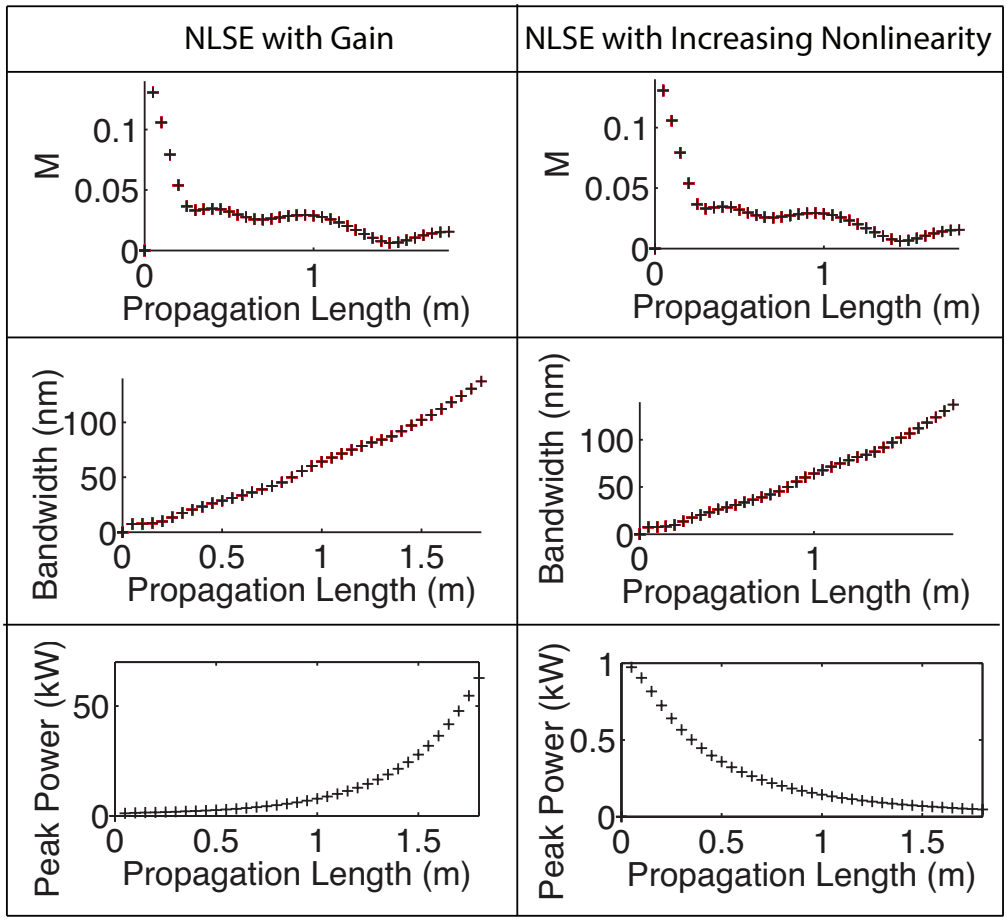

Figure 6.1: Comparison of characteristics of the derived self similar solution generated with increasing nonlinearity (right) with characteristics of the amplifier self similar solution to the NLSE with gain (left). g_0 =4 1/m, $\beta = 23 fs^2/mm$, $\gamma_0 = .0058\ (m \cdot W)^{-1}$

6.2 Discussion of Applications

6.2.1 Laser

The difficulty in experimentally realizing a saturable absorber profile which displays the characteristics of being heavily saturated have already been discussed

and explored. As discussed in Chapter 3, to generate a passive self similar pulse in the solid state laser, one must consider the correlation between the nonlinear loss of a resonator and the degree of saturation of the saturable absorber sustaining the mode locking process. As shown in the left trace of Fig 3.4, the smaller the nonlinear loss, the more saturated the absorber must be to generate the desired pulse. Equivalently, it may be said that the more saturated the absorber is, the less tendency the pulse has to breathe. Thus, if a large breathing potential was made available to a pulse within a solid state resonator (from an element outside of the gain medium so that bandwidth restrictions did not become an issue), a self similar pulse could theoretically be generated with a saturable absorber profile which was not heavily saturated. That is, if the breathing potential of a solid state resonator could be increased by means of passive elements outside the gain medium, then commonly used weakly saturated absorbers such as SESAMs or standard KLM could be used to arrive at the desired solution.

This concept would necessarily draw on a wealth of different ideas, ranging from nonlinear pulse evolution to passive spectral compression. Future work which explores how to increase the breathing capacity in solid state resonators would be useful for other pulse evolutions besides self similar ones. The author believes that this effort would be a next natural step in ultrafast resonator design. The ability to use a combination of free space focussing and self focussing to create an environment which displays increasing nonlinearity is attractive for self similar generation in solid state lasers.

6.2.2 Pulse Compressor

One of the most natural systems suited to make use of this evolution is a pulse compressor. Within a pulse compressor, an input pulse is injected wherein it accumulates some degree of nonlinear phase shift and increases in bandwidth. The output pulse from the system is then de-chirped to obtain a pulse which can be substantially shorter than the input pulse.

The benefit of a passive self similar pulse compressor is that as a self similar pulse propagates, it increases in bandwidth without encountering wave breaking, while maintaining a quadratic temporal phase. This means that the bandwidth of some input pulse could theoretically be increased to the edges of the transparency range of the material it was propagating within.

Simulations have shown that the distance required for an input pulse to attract to a self similar solution is dependent on both the magnitude of the overall nonlinearity and the variance in that nonlinearity throughout propagation. The larger the overall or baseline nonlinearity, the faster a pulse will evolve to a self similar solution. Similarly, the larger the variance in the nonlinearity is, the faster the pulse will evolve to the desired solution. This makes sense when we consider that the baseline nonlinearity, which generates the bandwidth, can be thought of as generating the breathing capacity of the pulse. The variance in that baseline nonlinearity attracts that breathing pulse to the desired solution. However, the baseline nonlinearity plays an important role. For a large variance in nonlinearity, but for a small value of baseline nonlinearity, an input pulse does not have the bandwidth necessary to adapt or change itself into that desired solution.

Dispersion decreasing self similar solutions have been considered in fiber pulse compressors and operate under a similar principle [15]. The baseline dispersion sets the approximate length scale over which the evolution can happen, and the variance in the dispersion determines whether that evolution will happen in that length scale. Self similar pulses generated with increasing nonlinearity have the advantage that in certain environments nonlinearity is easier to control than dispersion.

CHAPTER 7

NONLINEAR-DISPERSIVE SELF SIMILAR LASER

Recently, one of the main thrusts in the development of ultrafast fiber lasers has been to increase the bandwidth of pulses circulating within such systems. Pulse evolutions which are capable of handling nonlinear phase shifts large enough to put fiber lasers in direct competition with solid state lasers in terms of output energy have been developed. However, the gain bandwidth of most fiber lasers is significantly smaller than many solid state systems. For example, Yb:fiber has a gain bandwidth of 40 nm, while Ti:Sapphire has a nearly 300 nm gain bandwidth. Thus, research efforts aimed towards extending the bandwidth generation capabilities of ultrafast fiber lasers have attracted attention recently. For reasons discussed above, these efforts have naturally focussed on increasing the bandwidth of the laser in passive segments of fiber which, for practical pulse powers, do not impose a spectral filter on the pulse. For example, one natural choice for such an extension involved splicing highly nonlinear photonic crystal fiber after a segment of gain fiber to extend the self similar solution within the gain medium [11]. This laser succeeded in increasing the bandwidth of the system to near 200 nm and and generating de-chirped pulse widths as short as 21 femtoseconds. However, the pulse energy of this evolution was limited to 1 nJ so extensions of this concept which could support pulses of even higher energy would be welcomed.

7.1 Conceptual Explanation

In this chapter, a new pulse evolution which is capable of increasing the bandwidth of a fiber laser at larger pulse energies is presented. The proposed res-

onator could best be described as supporting a pulse evolution which is essentially a 'pulse compressor' inside of a laser cavity. More specifically, the proposed laser supports a nonlinear-dispersive self similar evolution within a long segment of passive fiber [53]. This design offers the possibility of high energy, linearly chirped pulses which are competitive with amplifier self similar and dissipative soliton pulse evolutions. Instead of focussing on a specific evolution within the gain medium, and trying to extend this specific evolution to some element after the gain medium (which has been the motivation so far), this method concentrates on exploiting an evolution within the single mode passive fiber succeeding it.

This laser is based around an understanding of the mode locking mechanism as a balancing act between various nonlinearly attracting solutions. Although for the sake of convenience and scientific presentation, labeling mode locking states is useful, practically, the environment within which a pulse forms is much more complicated. For example, by simply varying the initial conditions of the noise profile in certain resonators, either an amplifier self similar or a dissipative soliton pulse may form. Further support of the complexity of this point is the report of a soliton-similariton laser in which two locally nonlinearly attracting solutions were found to exist independently of each other within discrete segments of the same laser resonator [37]. Taking a step backward from these two extremes (the simultaneous potential for one of two solutions versus the discrete appearance of two solutions), it is reasonable to expect that a whole family of solutions may exist. These solutions would not adequately be described as either a soliton, dissipative soliton, or self similar pulse, but would constitute a balancing act between them.

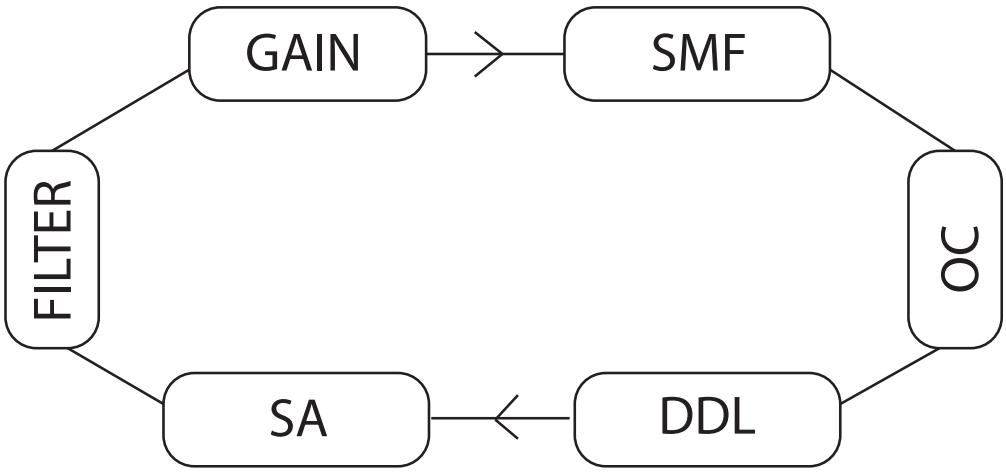

Figure 7.1: Schematic of Triangle Wave Cavity

Considering how we might extend the bandwidth of a fiber resonator with this perspective, we recall that there are pulse evolutions available in passive fiber which are generally not thought of as accessible 'cavity' solutions. This chapter focusses on one such pulse evolution; the normal dispersion pulse compressor which has generally been considered from the perspective of square wave evolution [47]. Of course, within the gain medium, there will still be the typical amplifier self similar attraction. However, by appropriately setting the initial conditions at the entrance to the SMF fiber, we can ensure that the dispersive self similar wave within the passive fiber is the dominant pulse shaping mechanism. As discussed in the previous chapter, a pulse compressor is a system wherein an input pulse accumulates some degree of nonlinear phase shift and increase in bandwidth within a passive segment of normal dispersion fiber. Subsequently, the output pulse from the system is de-chirped to obtain a pulse which can be substantially shorter than the input pulse. In a pulse compressor, the characteristics of the input pulse greatly influence whether or not the pulse evolves into a square wave, breaks apart, or broadens further in the far field into a non parabolic nonlinear-dispersive similariton pulse where the temporal and

spectral profiles of the pulse begin to mirror each other [53].

One key aspect of this evolution is the net anomalous dispersion of the resonator. For small net normal dispersion, the oscillator supports an extended self similar evolution which is known to multi-pulse for moderate to high pulse energies. For increasing amounts of net anomalous dispersion, the gain medium no longer provides a noticeable attraction to the amplifier self similar pulse. In fact, for larger values of net anomalous dispersion, spectral and temporal compression occur within the gain medium. Both of these characteristics are not indicative of an amplifier self similar solution. The spectral and temporal compression within the gain medium minimizes the chirp of the pulse and increases its peak power as it traverses the gain medium. Then, at the entrance of the SMF fiber, the pulse is near transform limited and is not a heavily chirped parabolic pulse like we generally expect. For pulses with characteristics like these, it is very easy to stimulate a nonlinear-dispersive self similar evolution.

As a nonlinear-dispersive self similar pulse propagates, it generates bandwidth up until a point of maximum compressibility. This point can be identified by the square-like shape of the temporal profile of the pulse. After moving through the point of maximum compressibility, the bandwidth of the pulse does not increase significantly. The temporal wings begin to linearize and spread as the center of the pulse maintains a flat top. The spectrum begins to adapt itself as it evolves into this mid field expression by beginning to mirror the temporal pulse. Eventually, in the far field, the temporal pulse resembles a shape somewhere between a triangular and parabolic pulse, depending on the net anomalous dispersion in the cavity, and it continues to temporally broaden. In the far field, the temporal pulse is governed completely by dispersive effects and the

spectrum maintains a constant shape and width and mirrors the shape of the temporal pulse nearly perfectly.

7.2 Numerical Confirmation of Proposed Pulse Evolution

7.2.1 Characteristics of the Evolution Phase of the NL-D Similariton Laser

Fig 7.1 shows a cartoon schematic of the proposed fiber laser. In the following simulations the length of the Yb:fiber gain medium is 80 cm, has a gain bandwidth of 40 nm, small signal gain of 30 dB, and E_{sat} of 5 nJ. The SMF spliced after the gain fiber is 33 m, and comprises the majority of the cavity. The length of the SMF can be made longer or shorter than this with similar results as long as the net cavity dispersion remains proportionately anomalous. After the SMF, a proportion of the heavily chirped pulse is output from the resonator and the pulse is sent through a dispersive delay line (DDL). The DDL provides a net anomalous dispersion of -57,500 fs^2 to the cavity and allows the pulse input into the gain medium and SMF to maintain a reasonable peak power. After the DDL, the pulse encounters a saturable absorber (SA), experimentally realized through the use of nonlinear polarization evolution (NPE) turned into an intensity dependent transmission with a combination of quarter and half wave plates. In the simulations, the SA was modeled by writing its intensity transmission as $1-1/(1+|A(z,t)|^2/P_{sat})$ where P_{sat} is .2 kW. After the SA, the pulse is sent through a 4 nm FWHM Gaussian spectral filter, experimentally realized by taking the first order diffraction mode off of a grating and then coupling the dispersing

mode into the gain fiber after a specifically calculated distance. Exiting from the spectral filter, the pulse finishes one round trip, and begins the process again. As long as the SMF is long enough for the majority of the pulse shaping within the cavity happens within it, speaking about a 'pulse compressor' evolution makes sense.

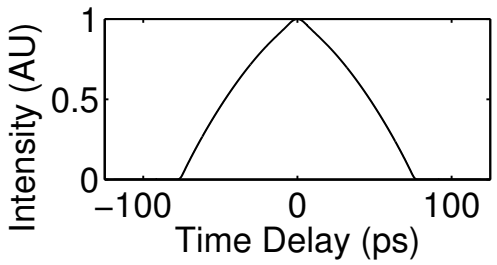

(a) Temporal profile of the steady state pulse

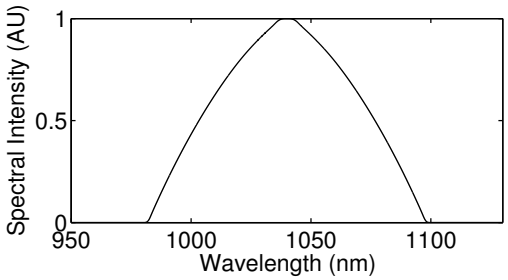

(b) Spectral profile of the steady state pulse

Figure 7.2: The steady state temporal and spectral profiles of the converged pulse are shown after exiting the 30 m segment of SMF

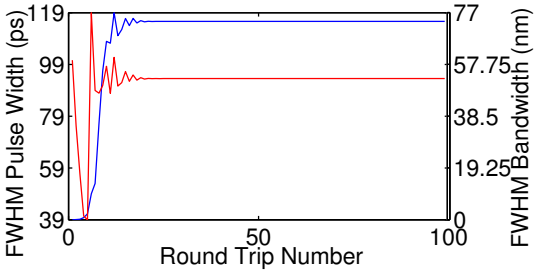

(a) Evolution of the temporal and spectral widths of the pulse as a function of round trip number as it reaches a steady state. The pulse is categorized at the end of the SMF fiber. *Red* is the FWHM temporal width and *Blue* is the FWHM spectral width.

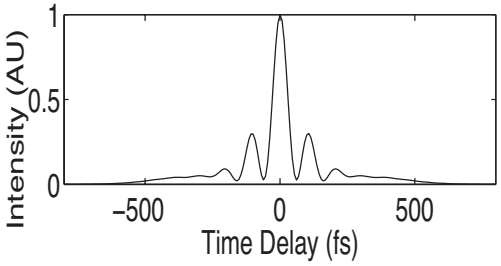

(b) Dechirping the pulse after the SMF fiber. Here requiring -.746 ps^2 of dispersion to dechirp the pulse.

Figure 7.3: The pulse evolution and the quality of the de-chirped pulse of the proposed 'triangle' wave evolution are shown.

The pulse after the SMF fiber can be de-chirped with second order dispersion over 1,756 times from a chirped pulse width of 93 ps to a de-chirped pulse width of 53 fs. The amount of dispersion required to fully de-chirp the pulse was

-0.746 ps^2, and the de-chirped pulse width was 1.4 times larger than the zero-phase spectral transform limit of 38 fs. Comparing the peak power of the de-chirped pulse to the peak power of a Gaussian pulse with the same energy and FWHM pulse duration, we see that the de-chirped pulse from simulation has peak power 2.22 times smaller than a Gaussian pulse. This gives us a metric of the de-chirped pulse quality by revealing how much energy is contained in secondary structure. The simulations shown in this section were seeded with a temporally long Gaussian pulse with microWatt peak power. However, the evolution is still accessible when the simulations are started from noise. The pulse energy output from the 70% output coupler is 8.7 nJ, which corresponds to a 75 mW output power, well within the achievable limits of a Yb:fiber laser. The output energy and average power can be scaled to even higher values with this evolution by increasing the pump power.

As can be seen from Fig 7.2, the temporal and spectral shapes of the pulse are somewhere between a parabola and a triangle wave. The spectrum does not reflect what is generally thought of as a dissipative soliton, which is generally categorized by sharp points on the spectral edges. The temporal shape is not parabolic and a self similar parabolic evolution would not be expected to be an attractor or solution at the end of 30m of SMF.

7.2.2 Characteristics of the Steady State NL-D Similariton Laser

For this simulation, the net anomalous dispersion of the cavity was increased to -.112585 ps^2. The other parameters in the cavity are the same as in the section above except the length of SMF is 33.5m instead of 33m. This simulation was

run to clearly demonstrate the different parts of this nonlinear evolution. Fig 7.4 shows the FWHM steady state values of the temporal and spectral components of the NL-D similariton pulse at different locations in the cavity.

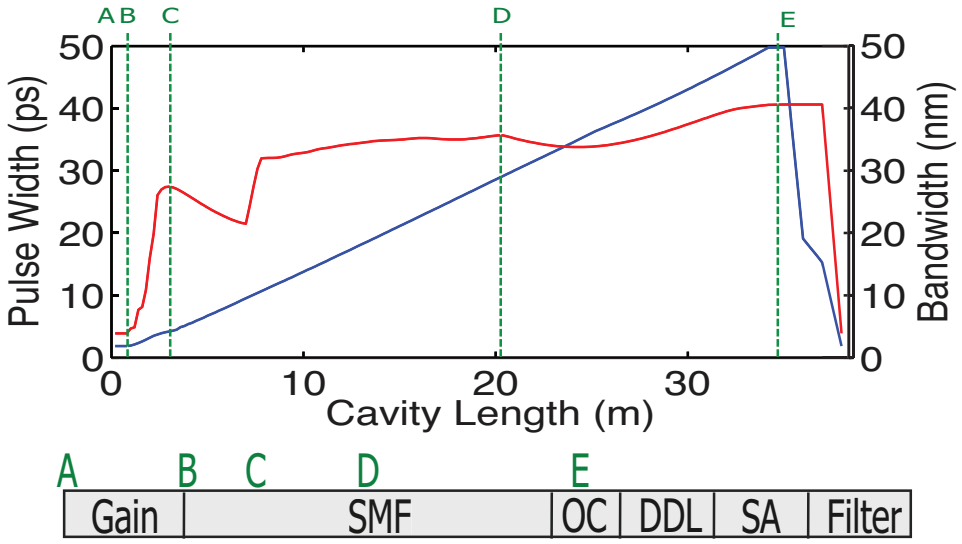

Figure 7.4: Steady state evolution of the temporal and spectral FWHM values of the pulse. (Red) is the spectral component and (Blue) is the temporal component.

Fig 7.5 depicts the evolution of the pulse within the gain segment of the resonator. As clearly shown in the figure, the pulse remains up-chirped throughout its traversal of the gain medium. As we expect from an up-chirped pulse, the pulse undergoes spectral compression due to the combination of the up-chirp and self phase modulation. The pulse duration remains nearly the same throughout the gain medium. Both of these points demonstrate that the pulse is not attracting to the amplifier self similar solution within the gain medium.

The up-chirped pulse which exits the gain medium, which still has a significant peak power, is next input into a long segment of SMF fiber. Fig 7.6 shows the NL-D similariton as it evolves through the point of maximum compressibility and into the near field of its evolution. At the point of maximum

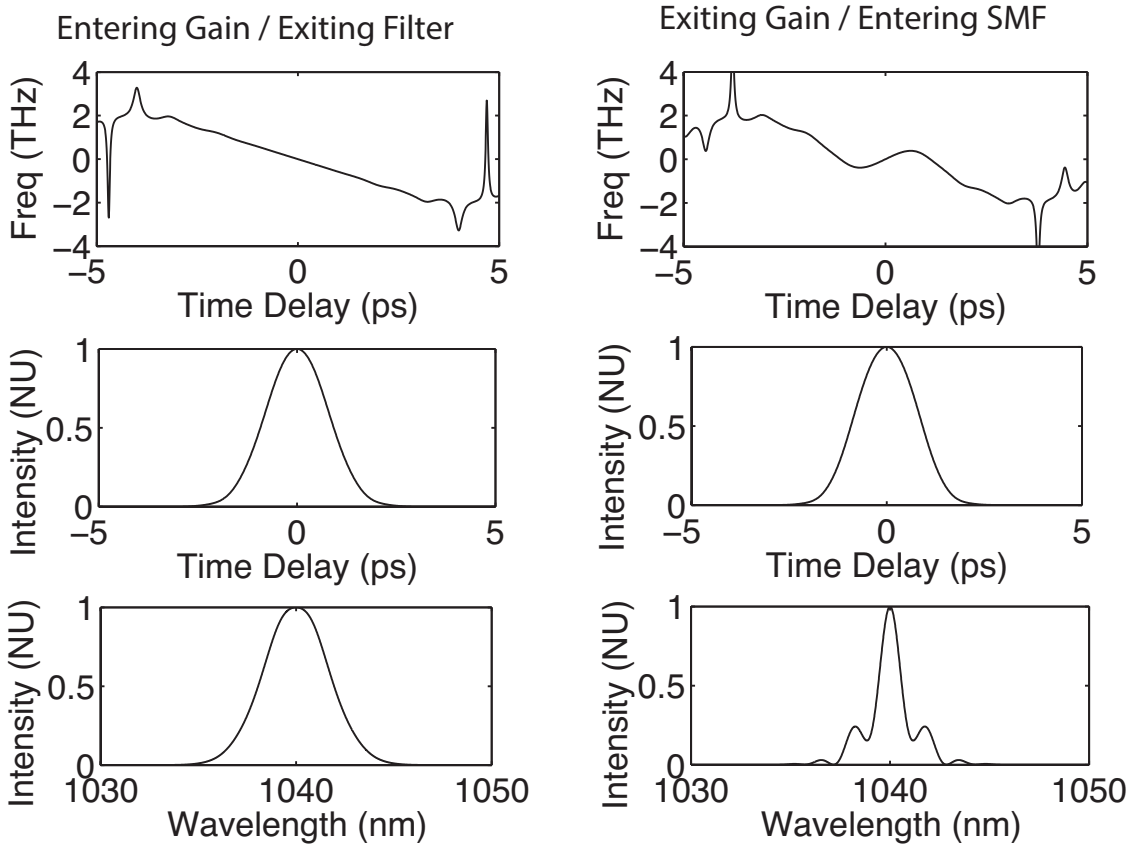

(a) Location A. NL-D similariton entering the gain medium after the spectral filter.

(b) Location B. NL-D similariton exiting the gain medium before entering the SMF.

Figure 7.5: NL-D similariton evolution within gain medium.

compressibility we see that the pulse resembles a square wave, with a flat top and steep sides. After this point, the bandwidth of the pulse does not increase substantially. In the mid-field evolution, the pulse spectrum begins to mirror the temporal profile of the pulse which has begun to evolve self similarly at this point. The chirp of the pulse is now down-chirped, and the increased propagation moving into the mid-field linearizes the chirp.

The mid-field pulse approaches the far field when the spectral and temporal profiles mirror each other and when the spectral profile no longer changes. At this point, the temporal profile of the pulse evolves self similarly due to the

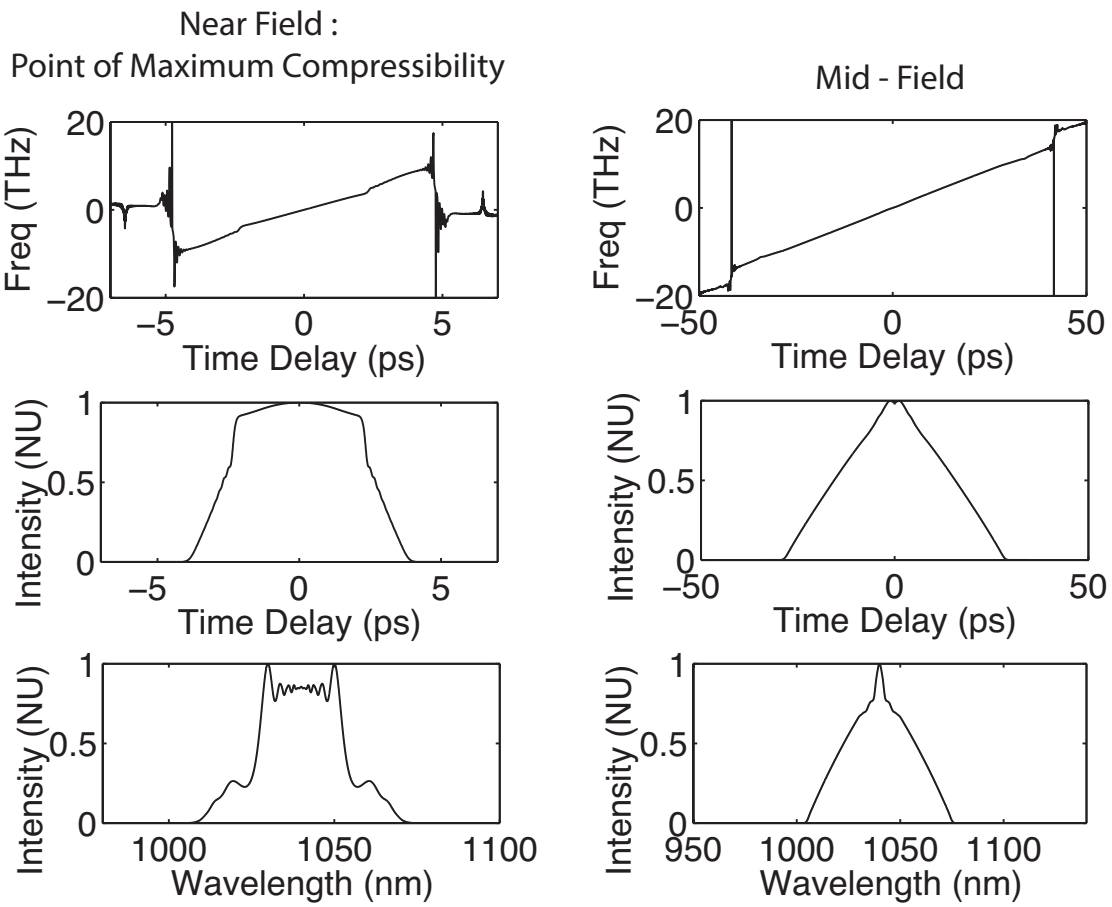

(a) Location C. In the SMF, the NL-D similariton evolution in the near field, at the point of maximum compressibility, is shown.

(b) Location D. In the SMF, the NL-D similariton evolution in the mid-field is depicted.

Figure 7.6: NL-D similariton evolution at the near and mid-field points.

nearly perfect linearity of the chirp and GVD. At this point in the evolution, the peak power of the pulse is low enough that SPM does not play any significant role in pulse formation. The right trace of Fig 7.7 shows the de-chirped version of the far field pulse shown in the left trace of the figure. As seen, the pulse de-chirps significantly, from a nearly 60 ps pulse width to less than 80 fs. The pulse energy is 9 nJ.

The author believes that this pulse, categorized by the spectral and temporal resemblance to a triangle wave, is representative of a new pulse evolution

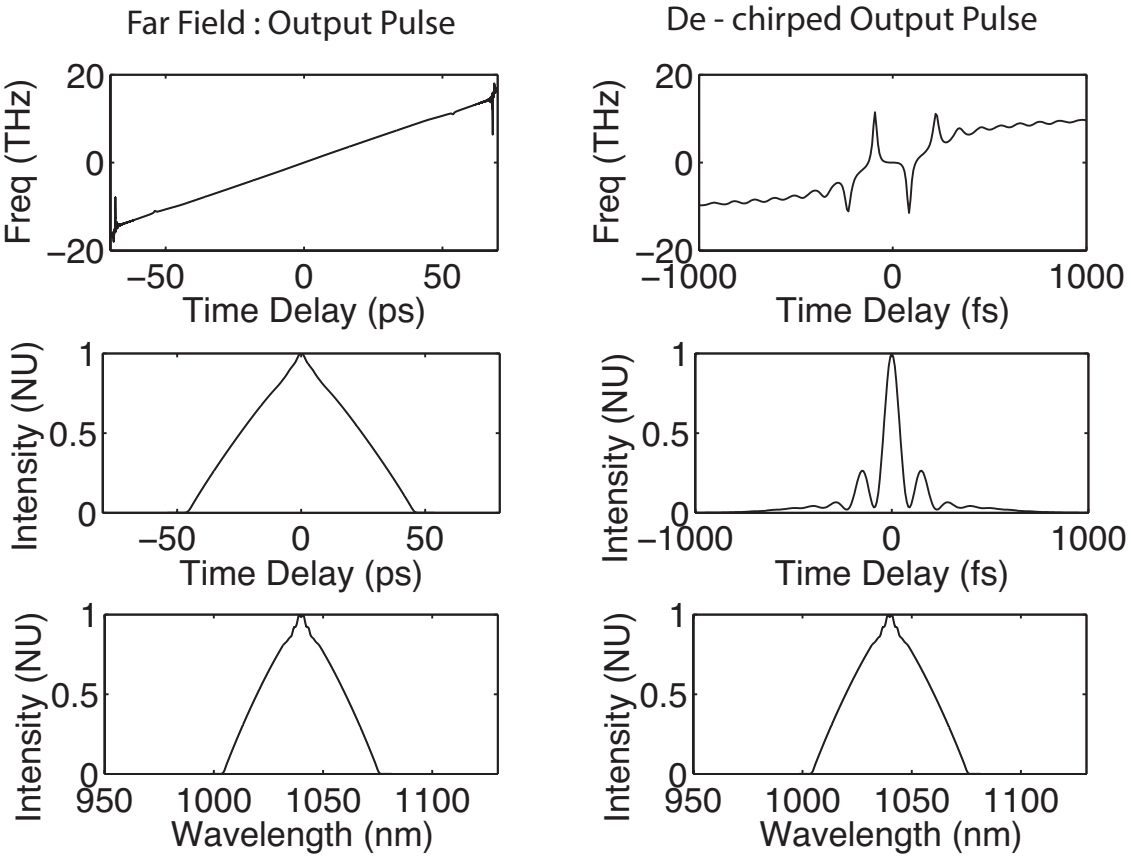

(a) Location E. In the SMF, the NL-D similariton evolution in the far field where the spectral and temporal profiles mirror each other.

(b) The NL-D similariton output pulse (far field) is de-chirped.

Figure 7.7: NL-D similariton evolution at the far field and de-chirped pulse characteristics.

within an ultrafast laser and best described by Ref [53]. The ability to de-chirp the pulse from around 100 ps nearly over 1000 times to less than 100 fs is unique in and of itself, and the pulse energy is on par with outputs from self similar and dissipative soliton fiber lasers. The evolution could find application in seed lasers for chirped pulse amplification, perhaps replacing giant chirp oscillators in some circumstances. Simulations suggest that stable 'cavity solutions' can be realized by considering pulse evolutions which are not generally considered within the context of a fiber laser. These simulations suggest that by balancing

the relative influences of the different relevant attracting solutions present in the cavity, the pulse solution can be tuned to new regimes of operation.

CHAPTER 8

CONCLUSIONS AND FUTURE WORK

In conclusion, this work has developed and explored a variety of different nonlinear pulse evolutions. In the first two chapters, a framework for understanding passive self similar pulse evolution in solid state resonators was developed both numerically and theoretically. The third chapter explored what was necessary to apply this developed framework to experiment. It was concluded that hard aperture Kerr lens mode locking offered the greatest potential for serving as a saturable absorber for the self similar evolution. Practical difficulties in demonstrating this pulse evolution experimentally were due to both the experimental difficulty, as well as the limitations on pump power: This evolution is really best suited for propagation at higher energies and its efficiency and ease of implementation scales with its output energy. Future work would consider applying the numerical experiments detailed in these three chapters to a solid state resonator capable of producing output pulses with higher energies.

After the discussion of how to implement self similar pulses into solid state lasers, the next chapter explored the first steps of how one might generate self similar pulses in optical parametric oscillators. The chapter found that by controlling the shape of the parametric gain profile one could tune the pulse within the oscillator to a self similar evolution. Both theoretical and numerical evidence of this evolution was presented. Extending the range of pulse evolutions within such systems offers benefit not only to the characteristics of the output pulses, but also to the pump pulses driving the parametric conversion. Future work on this experiment would include a detailed investigation of how the finite acceptance bandwidths of the signal and pump beams affect the pulse evolution.

Also, a detailed analysis of the dynamic nature of parametric gain saturation is required before implementation. Both of these questions need to be answered before choosing which method of pump shaping is most practical and efficient.

The fifth chapter presented a derivation of a self similar solution to the NLSE with increasing nonlinearity. This solution was shown to be mathematically equivalent (apart from a scaling factor) to the amplifier similariton and NLSE similariton with decreasing dispersion solutions. A discussion of how this solution could be used in pulse compressors was presented. Additionally, a discussion of the promise the solution offers in solid state laser systems where increasing nonlinearity can be realized with free space focussing, was made. Future work on this experiment would consider how one could practically employ this evolution within a solid state laser, and how to passively control the bandwidth growth which accompanies this solution.

In the last chapter we proposed a novel ultrafast evolution for a laser resonator which can support high energy pulses as well as extend the bandwidth available to ultrafast fiber laser systems. This laser can best be described as a pulse compressor inside of a resonator. Specifically, the evolution may called a nonlinear-dispersive self similar pulse. The primary pulse shaping within the laser occurs within a long segment of passive normal dispersion fiber. The output pulses could be de-chirped to below 100 fs and could support greater than 10 nJ of energy. Future work involves exploring how TOD from the DDL line influences the pulse evolution, as well as how other nonlinear effects like Raman amplification affect the NL-D similariton pulse evolution.

BIBLIOGRAPHY

[1] N. Akhmediev, J. M. Soto-Crespo, and G. Town. Pulsating solitons, chaotic solitons, period doubling, and pulse coexistence in mode-locked lasers: Complex ginzburg-landau equation approach. *Phys. Rev. E*, 63:056602, Apr 2001.

[2] D. Anderson, M. Desaix, M. Karlsson, M. Lisak, and M. L. Quiroga-Teixeiro. Wave-breaking-free pulses in nonlinear-optical fibers. *J. Opt. Soc. Am. B*, 10(7):1185–1190, Jul 1993.

[3] Cristian Antonelli, Jeff Chen, and Franz X. Kartner. Intracavity pulse dynamics and stability for passively mode-locked lasers. *Opt. Express*, 15(10):5919–5924, May 2007.

[4] Qiaoliang Bao, Han Zhang, Yu Wang, Zhenhua Ni, Yongli Yan, Ze Xiang Shen, Kian Ping Loh, and Ding Yuan Tang. Atomic-layer graphene as a saturable absorber for ultrafast pulsed lasers. *Advanced Functional Materials*, 19(19):3077–3083, 2009.

[5] V. Bucklew, B. Wysocki, and C. Pollock. Femtosecond carrier dynamics in photoexcited highly ordered pyrolytic graphite films. *Optical Materials*, 34:1299–1302, June 2012.

[6] Victor G. Bucklew and Clifford R. Pollock. Realizing self-similar pulses in solid-state laser systems. *J. Opt. Soc. Am. B*, 29(11):3027–3033, Nov 2012.

[7] Victor G. Bucklew, William H. Renninger, Frank W. Wise, and Clifford R. Pollock. Average cavity description of self-similar lasers. *J. Opt. Soc. Am. B*, 31(4):842–850, Apr 2014.

[8] J. R. Buckley, F. W. Wise, F. Ö. Ilday, and T. Sosnowski. Femtosecond fiber lasers with pulse energies above 10 nj. *Opt. Lett.*, 30(14):1888–1890, Jul 2005.

[9] Shihua Chen and Lin Yi. Chirped self-similar solutions of a generalized nonlinear schrödinger equation model. *Phys. Rev. E*, 71:016606, Jan 2005.

[10] A. Chong, H. Liu, B. Nie, B. G. Bale, S. Wabnitz, W. H. Renninger, M. Dantus, and F. W. Wise. Pulse generation without gain-bandwidth limitation in a laser with self-similar evolution. *Opt. Express*, 20(13):14213–14220, Jun 2012.

[11] A. Chong, H. Liu, B. Nie, B. G. Bale, S. Wabnitz, W. H. Renninger, M. Dantus, and F. W. Wise. Pulse generation without gain-bandwidth limitation in a laser with self-similar evolution. *Opt. Express*, 20(13):14213–14220, Jun 2012.

[12] Andy Chong, Joel Buckley, Will Renninger, and Frank Wise. All-normal-dispersion femtosecond fiber laser. *Opt. Express*, 14(21):10095–10100, Oct 2006.

[13] P. B. Corkum. Plasma perspective on strong field multiphoton ionization. *Phys. Rev. Lett.*, 71:1994–1997, Sep 1993.

[14] M. E. Fermann, V. I. Kruglov, B. C. Thomsen, J. M. Dudley, and J. D. Harvey. Self-similar propagation and amplification of parabolic pulses in optical fibers. *Phys. Rev. Lett.*, 84:6010–6013, Jun 2000.

[15] D. Ghosh, M. Basu, and S. Sarkar. Generation of self-similar parabolic pulses by designing normal dispersion decreasing fiber amplifier as well as its staircase substitutes. *Lightwave Technology, Journal of*, 27(17):3880–3887, Sept 2009.

[16] S. Hädrich, M. Krebs, J. Rothhardt, H. Carstens, S. Demmler, J. Limpert, and A. Tünnermann. Generation of μw level plateau harmonics at high repetition rate. *Opt. Express*, 19(20):19374–19383, Sep 2011.

[17] Akira Hasegawa and Frederick Tappert. Transmission of stationary nonlinear optical pulses in dispersive dielectric fibers. i. anomalous dispersion. *Applied Physics Letters*, 23(3):142–144, 1973.

[18] H. A. Haus, J. G. Fujimoto, and E. P. Ippen. Structures for additive pulse mode locking. *J. Opt. Soc. Am. B*, 8(10):2068–2076, Oct 1991.

[19] C. Hernández-García, J. A. Pérez-Hernández, T. Popmintchev, M. M. Murnane, H. C. Kapteyn, A. Jaron-Becker, A. Becker, and L. Plaja. Zeptosecond high harmonic kev x-ray waveforms driven by midinfrared laser pulses. *Phys. Rev. Lett.*, 111:033002, Jul 2013.

[20] Toshihiko Hirooka and Masataka Nakazawa. Parabolic pulse generation by use of a dispersion-decreasing fiber with normal group-velocity dispersion. *Opt. Lett.*, 29(5):498–500, Mar 2004.

[21] Nicholas G. Horton, Ke Wang, Demirhan Kobat, Catharine G. Clark,

Frank W. Wise, Chris B. Schaffer, and Chris Xu. In vivo three-photon microscopy of subcortical structures within an intact mouse brain. *Nat Photon*, 7(3):205–209, 03 2013.

[22] F. Ilday, F. Wise, and F. Kaertner. Possibility of self-similar pulse evolution in a ti:sapphire laser. *Opt. Express*, 12(12):2731–2738, Jun 2004.

[23] F. Ö. Ilday, J. R. Buckley, W. G. Clark, and F. W. Wise. Self-similar evolution of parabolic pulses in a laser. *Phys. Rev. Lett.*, 92(21):213902, May 2004.

[24] Fatih Ö. Ilday, Joel R. Buckley, and Frank W. Wise. Self-similar evolution of parabolic pulses in a fiber laser. In *Nonlinear Guided Waves and Their Applications*, page MD8. Optical Society of America, 2004.

[25] Christian Jirauschek and F. Omer Ilday. Semianalytic theory of self-similar optical propagation and mode locking using a shape-adaptive model pulse. *PHYS.REV.A*, 83:063809, 2011.

[26] T. Juhasz, F.H. Loesel, R.M. Kurtz, C. Horvath, J.F. Bille, and G. Mourou. Corneal refractive surgery with femtosecond lasers. *Selected Topics in Quantum Electronics, IEEE Journal of*, 5(4):902–910, Jul 1999.

[27] V. L. Kalashnikov. *Solid State Laser*. ISBN 978-953-51-0086-7. In Tech, 2012.

[28] V. L. Kalashnikov and A. Apolonski. Chirped-pulse oscillators: A unified standpoint. *Phys. Rev. A*, 79:043829, Apr 2009.

[29] V L Kalashnikov, E Podivilov, A Chernykh, S Naumov, A Fernandez, R Graf, and A Apolonski. Approaching the microjoule frontier with femtosecond laser oscillators: theory and comparison with experiment. *New Journal of Physics*, 7(1):217, 2005.

[30] V.L. Kalashnikov, E. Podivilov, A. Chernykh, and A. Apolonski. Chirped-pulse oscillators: theory and experiment. *Applied Physics B*, 83(4):503–510, 2006.

[31] Vladimir L. Kalashnikov. The unified theory of chirped-pulse oscillators. pages 73540T–73540T–12, 2009.

[32] Vladimir L. Kalashnikov and Alexander Apolonski. Energy scalability of mode-locked oscillators: a completely analytical approach to analysis. *Opt. Express*, 18(25):25757–25770, Dec 2010.

[33] U. Keller, K.J. Weingarten, F.X. Kartner, D. Kopf, B. Braun, I.D. Jung, R. Fluck, C. Honninger, N. Matuschek, and J. Aus der Au. Semiconductor saturable absorber mirrors (sesam's) for femtosecond to nanosecond pulse generation in solid-state lasers. *Selected Topics in Quantum Electronics, IEEE Journal of*, 2(3):435–453, Sep 1996.

[34] Guy M Kezirian and Karl G Stonecipher. Comparison of the intralase femtosecond laser and mechanical keratomes for laser in situ keratomileusis. *Journal of cataract and refractive surgery*, 30(4):804–811, 04 2004.

[35] V. I. Kruglov, A. C. Peacock, and J. D. Harvey. Exact self-similar solutions of the generalized nonlinear schrödinger equation with distributed coefficients. *Phys. Rev. Lett.*, 90:113902, Mar 2003.

[36] S. Namiki and H. Haus. Noise of the stretched pulse fiber laser. i. theory. *Quantum Electronics, IEEE Journal of*, 33(5):649–659, 1997.

[37] B. Oktem, C. Ulgudur, and F. Ilday. Soliton-similariton fibre laser. *Nat Photon*, 4(7):307–311, May 2010.

[38] W. H. Renninger, A. Chong, and F. W. Wise. Dissipative solitons in normal-dispersion fiber lasers. *Phys. Rev. A*, 77:023814, Feb 2008.

[39] William H. Renninger, Andy Chong, and Frank W. Wise. Area theorem and energy quantization for dissipative optical solitons. *J. Opt. Soc. Am. B*, 27(10):1978–1982, Oct 2010.

[40] William H. Renninger, Andy Chong, and Frank W. Wise. Self-similar pulse evolution in an all-normal-dispersion laser. *Phys. Rev. A*, 82:021805, Aug 2010.

[41] William H. Renninger, Andy Chong, and Frank W. Wise. Amplifier similaritons in a dispersion-mapped fiber laser. *Opt. Express*, 19(23):22496–22501, Nov 2011.

[42] Thomas Schreiber, Bülend Ortaç, Jens Limpert, and Andreas Tünnermann. On the study of pulse evolution in ultra-short pulse mode-locked fiber lasersby numerical simulations. *Opt. Express*, 15(13):8252–8262, Jun 2007.

[43] Alan Sugar. Ultrafast (femtosecond) laser refractive surgery. *Current Opinion in Ophthalmology*, 13(4), 2002.

[44] W. D. Tan, C. Y. Su, R. J. Knize, G. Q. Xie, L. J. Li, and D. Y. Tang. Mode locking of ceramic nd:yttrium aluminum garnet with graphene as a saturable absorber. *Applied Physics Letters*, 96(3):–, 2010.

[45] A.J. Taylor, D.J. Erskine, and C.L. Tang. Equal pulse correlation technique for measuring femtosecond excited state relaxation times. *Applied Physics Letters*, 43(11):989–991, Dec 1983.

[46] Nikolai Tolstik, Evgeni Sorokin, and Irina T. Sorokina. Graphene mode-locked cr:zns laser with 41 fs pulse duration. *Opt. Express*, 22(5):5564–5571, Mar 2014.

[47] W. J. Tomlinson, R. H. Stolen, and C. V. Shank. Compression of optical pulses chirped by self-phase modulation in fibers. *J. Opt. Soc. Am. B*, 1(2):139–149, Apr 1984.

[48] F.W. Wise, A. Chong, and W.H. Renninger. High-energy femtosecond fiber lasers based on pulse propagation at normal dispersion. *Laser & Photonics Reviews*, 2(1-2):58–73, 2008.

[49] F.W. Wise, A. Chong, and W.H. Renninger. High-energy femtosecond fiber lasers based on pulse propagation at normal dispersion. *Laser & Photonics Reviews*, 2(1-2):58–73, 2008.

[50] C. Xu and F. W. Wise. Recent advances in fibre lasers for nonlinear microscopy. *Nat Photon*, 7(11):875–882, 11 2013.

[51] Shai Yefet and Avi Pe´er. A review of cavity design for kerr lens mode-locked solid-state lasers. *Applied Sciences*, 3(4):694–724, 2013.

[52] V. E. Zakharov and A. B. Shabat. Exact theory of two-dimensional self-focusing and one-dimensional self-modulation of waves in nonlinear media (Differential equation solution for plane self focusing and one dimensional self modulation of waves interacting in nonlinear media). *Sov. Phys*, 34(3):62–69, January 1972.

[53] A. Zeytunyan, G. Yesayan, L. Mouradian, P. Kockaert, P. Emplit, F. Louradour, and A. Barthélémy. Nonlinear-dispersive similariton of passive fiber. *Journal of the European Optical Society - Rapid publications*, 4(0), 2009.